AN ABSTRACT OF THE THESIS OF

Jamie M. Lescinski for the degree of Master of Ocean Engineering in Ocean Engineering presented on September 14, 2004.

Title: Nearshore Hydrodynamic Model Comparison and Predictions of Bathymetric Evolution

Redacted for privacy

Abstract approved: _____
H. Tuba Özkan-Haller

The surf zone exhibits large energetic signals from wave shoaling and subsequent dissipation due to breaking, forcing circulation. The bathymetry responds to the wave and wave-induced circulation with the growth, transport, and destruction of large scale bathymetric features, such as mega ripples and sand bars. There is an obvious fluctuation of energy, which results in the continual change of the coastline, indicating a need for a predictive tool that includes a feedback between the hydrodynamics and morphology.

Modeling of the nearshore environment has been of active interest to the engineering and oceanographic research community for close to a century. Wave and circulation prediction have improved dramatically since the advent of coastal modeling, and has reached a point in the modern day where the solution of the full Navier Stokes equation is in the foreseeable future. However, the computational expense associated with these highly skilled predictions of waves and currents are not always suitable for practical application in the field of coastal engineering. Therefore, in practice, engineers must compromise between computational efficiency and prediction skill of a model. A comparison of various model prediction skills and further discussion of such practical applications will occur in this manuscript.

In contrast to the highly evolved wave and current models presently available, bathymetric evolution modeling is still in its infancy and has more recently become a primary focus of the nearshore researching community. The success of sediment transport predictions, and subsequent morphological evolution predictions, among other things, are

dependant upon the included physics of the model, quality of input data, and stability of the modeling routines.

In this study, hydrodynamic models were compared based upon their skill exhibited when predicting cross-shore profiles of nonlinear wave and wave velocity properties: skewness and asymmetry. These nonlinear characteristics have proven to be challenging to predict in a variety of hydrodynamic climates in combination with variable water depths. Predictions of skewness and asymmetry by three types of models were compared, which ranged dramatically in computational expense and complexity. The more complex models were derived using the physics-based governing equations of fluid systems, where the less complex and extremely computationally efficient models are empirically developed based on physics of the nearshore system. The most complex wave evolution model used in this study was FUNWAVE, which is a fully nonlinear Boussinesq wave model (Wei *et al.*, 1995). The nonlinear, phase-resolving, fully dispersive wave model of Kaihatu (2001), in which the evolution of the waves is governed by the parabolic approximated mild-slope equation, is the second complex wave evolution model. Wave and velocity skewness and asymmetry are thus computed from the predicted time series from each of the two nonlinear wave models. The third type of model was empirical formulations developed to predict wave velocity skewness and asymmetry. Two of these empirical models were used in this study; the Doering and Bowen (1995) formulations, which were derived through bispectral analysis of wave evolution, and the Doering *et al.* (2000) formula, which was generated using an evolutionary algorithm. These empirically-derived expressions are currently being utilized, but have not been thoroughly testes, hence our comparisons of nonlinear wave characteristics between multiple model predictions and observations.

Predictions of skewness and asymmetry were used to gauge the skill of these models. The quantity of wave skewness and asymmetry changes vertically in the water column, due to effects by the bathymetry in the wave boundary layer versus the free streaming flow. The characteristics of the nearshore flow field have been of interest to the engineering community because of the vital role these nonlinear quantities play in predictions of the morphologic evolution. Hence, our investigation of the quality of predictions of nonlinear wave properties by these three types of predictive tools.

Another focus of coastal modelers is to ably simulate the hydrodynamics and subsequent morphodynamics of the nearshore using a complete feedback system; i.e. the predicted bathymetry after a pre-defined time step would be used as the initial bathymetry

for the following time step and so on. A full feedback model of this sort is afflicted with issues ranging from model validity to stability. Also, there are currently few data sets available which contain all the necessary measurements required to thoroughly test such a proposed set of models. In the second half of this study a model series was implemented, using a feedback system, to simulate the 1DH (1-dimensional-horizontal), cross-shore evolution of sand beaches for a lab and a field experiment. The nonlinear, fully dispersive wave model of Kaihatu (2001) was used to predict the cross-shore evolution of wave field. A Bailard (1981) sediment transport model was used to predict the local cross-shore change of the bathymetry, as a function of time, from which the new cross-shore profile was predicted, and subsequently used as the initial bathymetry for the following time step.

The overall goal of this study is to make progress in the direction of building community models, in which compatible wave, circulation, and transport models of differing degrees of complexity can be used in combination for simulating the nearshore environment. It is hopeful that in the near future we will be capable of simulating long term coastal evolution in real time, therefore, providing the ultimate modeling tool for the researching and practicing engineering community.

Nearshore Hydrodynamic Model Comparisons and Predictions of Bathymetric Evolution

by
Jamie M. Lescinski

A THESIS

submitted to

Oregon State University

in partial fulfillment of
the requirements for the
degree of

Master of Ocean Engineering

Presented September 14, 2004
Commencement June 2005

Master of Ocean Engineering thesis of Jamie M. Lescinski presented on September 14, 2004.

APPROVED:

Redacted for privacy

Major Professor, representing Ocean Engineering

Redacted for privacy

Head of the Department of Civil, Construction, and Environmental Engineering

Redacted for privacy

Dean of the Graduate School

I understand that my thesis will become part of the permanent collection of the Oregon State University libraries. My signature below authorizes release of my thesis to any reader upon request.

Redacted for privacy

Jamie M. Lescinski, Author

TABLE OF CONTENTS

TABLE OF CONTENTS (Continued)

LIST OF FIGURES

LIST OF FIGURES (Continued)

LIST OF FIGURES (Continued)

LIST OF FIGURES (Continued)

LIST OF TABLES

LIST OF TABLES (Continued)

Chapter 1

INTRODUCTION

The nearshore region can be defined as the area which ranges from 10 meters and less of water depth to the farthest extent which is affected by run-up due to extreme spring tides and storm surges. The processes in this region are dynamic, and consequently fluctuate on time scales ranging from O(1/100 seconds) for turbulent processes to O(months) for development and growth of large-scale bathymetric features. The coastal domain is continually morphologically evolving as a result of the ever-changing hydrodynamics and atmospheric processes which govern the local systems. In general, erosive (accretive) beach processes are associated with highly (weakly) energetic hydrodynamic forcing, which tend to fluctuate seasonally. The dominant coastal hydrodynamic characteristics and morphological features such as longshore currents, undertow, presence of headlands, dominant grain diameters all play a vital role in shaping the dynamic nearshore system.

The surf zone exhibits large energetic signals from wave shoaling and subsequent dissipation due to breaking. The bathymetry responds to the waves and wave-induced circulation with the growth, transport, and destruction of large scale bathymetric features, such as mega ripples and sand bars. There is an obvious significant fluctuation of energy, which results in the continual change of the coastline, indicating a need for a predictive tool that includes a feedback between the hydrodynamics and morphology.

Modeling of the nearshore environment has been of active interest to the engineering and oceanographic research community for close to a century. Wave and circulation prediction have improved dramatically since the advent of coastal modeling, and has reached a point in the modern day where the solution of the full Navier Stokes equation is in the foreseeable future. However, the computational expense associated with these highly skilled predictions of waves and currents are not always suitable for practical application in the field of coastal engineering. Therefore, in practice, engineers must compromise between computational efficiency and prediction skill of a model. A comparison of various model prediction skills and further discussion of such practical applications will occur in this manuscript.

In contrast to the highly evolved wave and current models presently available, bathymetric evolution modeling is still in its infancy and has more recently become a primary

focus of the nearshore researching community. The success of sediment transport predictions, and subsequent morphological evolution predictions, among other things, are dependant upon the included physics of the model, quality of input data, and stability of the modeling routines.

1.1 Relevant History of Hydrodynamic Modeling of the Nearshore

A number of successful techniques have been developed to modeling the evolution of a wave field. With modern day capabilities of computing power, many historically computationally expensive models have become commonly used by the engineering and scientific community. Two such nonlinear wave evolution modeling techniques solve the shallow water wave equations or the mild-slope Equation

Basco (1983) commented on the potential of Boussinesq models to "*eventually raise the fundamental knowledge of coastal hydrodynamics to a higher level.*" The Boussinesq (shallow water) wave models have made advances in the last two decades since the development of this contemporary modeling approach. The extended domain models have led to generation of the current operational Boussinesq models used in, but not limited to, simulations of wave evolution, current generation and interaction, and wave structure interaction.

The Boussinesq models can be solved in the time domain or the frequency domain. Almost all shallow water wave models are derived assuming incompressible, inviscid flow, and use the non-dimensional parameters μ and δ to describe dispersion and nonlinearity, respectively. The designation *weakly dispersive* refers to $\mu<<1$, while *weakly nonlinear* refers to $\delta<<1$. The full linear problem follows the linear wave dispersion relationship given by

$$\sigma^2 = gk \tanh kh \tag{1.1}$$

where k is the wavenumber, g is the acceleration due to gravity, and σ is the angular wave frequency. In the limit of $\mu<<1$, $\tanh(kh)$ will approach kh, where the waves will be nearly non-dispersive. The implementation of an assumption of $\mu<<1$ will severely limit the validity of the model results in variable water depths. Due to this implication, the modern Boussinesq models are derived as to result in an approximation of the linear dispersion relationship which is fairly robust over a range of water depths and peak wave frequencies, therefore, extending outside the limit of $\mu<<1$.

The constraints by the water depth were proven to be quite limiting, therefore,

generating a concerted effort to extend the range of the validity of the Boussinesq wave evolution models for larger μ. McCowan and Blackman (1989), Madsen *et al.* (1991), and Nwogu (1993) were some of the first researchers to perform this task of extending the validity of the Boussinesq wave models beyond shallow water. These types of models were collectively referred to as the 'extended' Boussinesq models. Madsen *et al.* (1991) added terms to the classical Boussinesq momentum equations which were multiplied by a spatially varying free parameter, which was zero in shallow water. The parameter was calibrated using Páde approximations so that the new dispersion relationship would compare favorably with the linear wave dispersion relationship in a wide range of the water depths. Next, varying bathymetry was accounted for by Madsen and Sorensen (1992). The equations of Madsen *et al.* (1991) have been analyzed extensively (Schäffer and Madsen, 1995; Madsen and Schäffer, 1998; Madsen and Schäffer, 1999), and many nonlinear and dispersion enhancements have been made (Eldeberky and Battjes, 1996; Kofoed-Hansen and Rasmussen, 1998; Becq-Girard *et al.*, 1998).

In contrast to Madsen *et al.* (1991), Nwogu (1993) defined a reference elevation, z_α, located within the water column, and re-expressed the velocity potential equation in terms of the values at z_α. The velocity potential equation was solved using the bottom boundary condition, and truncating the resulting series expansion after $O(\mu^2)$, gave a dispersion relationship of

$$\sigma^2 = ghk^2 \frac{1-(\alpha+1/3)(kh)^2}{1-\alpha(kh)^2} \tag{1.3}$$

where

$$\alpha = \frac{1}{2}\left(\frac{z_\alpha}{h}\right)^2 + \frac{z_\alpha}{h} \tag{1.4}$$

α=-1/3 results in the classical Boussinesq dispersion relationship based on depth-averaged velocity. Nwogu (1993) found α=-0.39 minimized the phase speed error over a range of kh values by best-fitting the linear wave dispersion relationship (Figure 1.1).

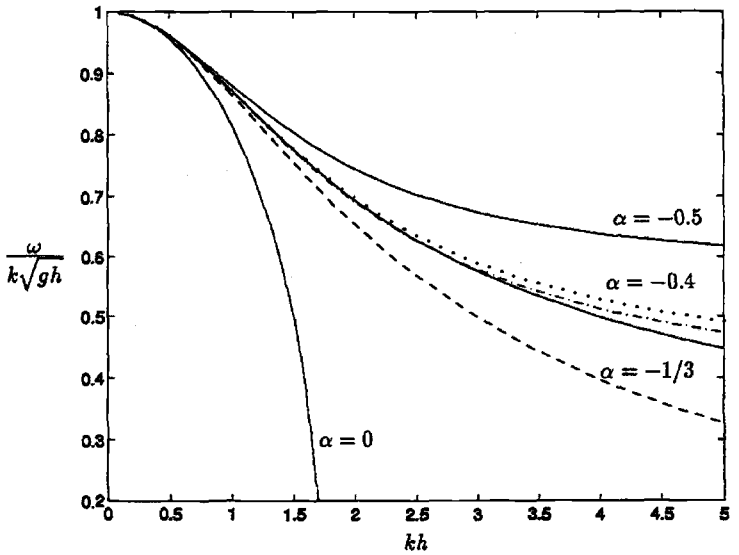

Figure 1.1. Comparison of linear dispersion relations between the exact solution (middle solid line) and those of Nwogu's equations for several values of α: α=-0.5 (-), α=-0.4 (...), α=-0.39 (-.-), α=-1/3 (---), α=0 (-) [adapted from Wei and Kirby (1998)].

Wei *et al.* (1995) developed an extended Boussinesq model which was fully nonlinear and has truncation errors one order higher than the $O(\mu^2)$ dispersive terms. They also used the extended Boussinesq equations of Nwogu (1993), but in the form of horizontal velocity at the reference elevation ($\mathbf{u}_\alpha$) and water surface elevation (η). This was preferred for practical purposes when modeling breaking, frictional and mixing effects (Kirby, 2003). Wei and Kirby (1995) used a non-staggered grid approach, with $\mathbf{u}_\alpha$ and η defined at the same location. Shi *et al.* (2001a) utilized a staggered grid approach and found the results to be less sensitive to the treatment of the boundary conditions.

The $O(\mu^2)$ models described above has proven to be limited in their range of application for values of μ far smaller than implied by the limitations of the accuracy of the dispersion relationship (Kirby, 2003). The model tends to break down in its predictions of wave-induced near bed horizontal velocities. The quality predictions of kinematics become terribly important when attempting to calculate rates local sediment transport. To provide a more accurate means for predicting the near bed kinematics, higher-order approximations in the Boussinesq models have been developed [Gobbi *et al.* (2000) and Agnon *et al.* (1999)]. Gobbi *et al.* (2000) and Gobbi and Kirby (1999) increase the accuracy of the extended Boussinesq model to $O(\mu^4)$ for the vertical structure of the velocity potential, providing a

dramatic improvement of the resulting predictions of velocity components. Agnon *et al.* (1999), and continued work by Madsen *et al.* (2003), also increased the accuracy of the extended Boussinesq equations which are correct to $O(\mu^8)$. The approach taken was to describe the problem in terms of the identity of the horizontal velocity **u** and vertical velocity *w*, where the two velocities are related through the bottom boundary condition. Madsen *et al.* (2003) went on to further improve the predictions of the vertical profile of the horizontal velocities, rather than the dispersion relationship. Kirby (2003) provides a comprehensive review of these two modeling approaches for developing higher-order approximations in the Boussinesq models.

A second present-day technique for modeling nonlinear wave evolution is solving the mild slope equation, which simulates wave refraction, shoaling and diffraction over mildly-varying bathymetry. The linear mild-slope equation (Berkhoff, 1972; Smith and Sprinks, 1975) is an elliptical equation, therefore, requiring knowledge of all boundary conditions prior to solving for the interior domain. For most modeling applications in the nearshore coastal environment, the required knowledge of all boundary conditions is not practical, therefore, approximations can be made to the full equation to reduce the required initial boundary information. The derivation of the parabolic approximation to the mild-slope equation (Radder, 1979; Lozano and Lui, 1980) has considerably increased the applicability of the modeling approach. The parabolic approximation requires knowledge of the lateral boundary conditions and a small angle of wave incidence. The parabolic approximation also requires the model to simulate forward propagating waves, therefore, reflection is not included. A graphical analysis of the parabolic approximations used by various models is shown in Figure 1.2. The elliptic model should be viewed as the benchmark and the others compared to it. From this illustration, one can see that the wide angle parabolic approximation model (Kaihatu and Kirby DSO, 1995) appears to compare well with the elliptic solution, especially $0<k_y/k<0.7$.

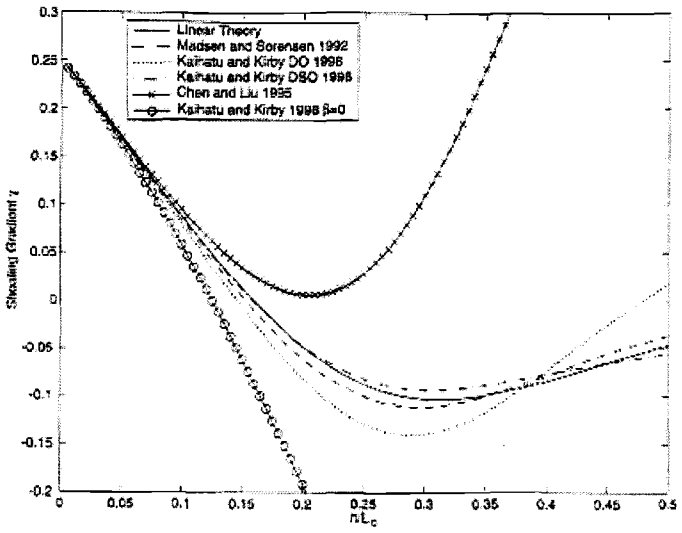

Figure 1.2. Visual comparison of shoaling gradients of various parabolic approximation models and an elliptic model (which is held as true). h/L0 is plotted versus the shoaling gradient (γ) [adapted from Kaihatu (2003)].

A relevant model to the current study is the Kirby and Kaihatu (1995) parabolic approximation fully dispersive wave model. The model was developed from the boundary value problem for water waves, with the free surface expanded to the 2nd-order in wave amplitude. It is first assumed the velocity potential solution can be expressed as a superposition of waves, where each contributing complex velocity potential is frequency component-specific and contains phase information. The model dispersion is dictated by linear wave theory (Equation 1.1). Resonant triad interaction theory is utilized to generate a time-periodic velocity potential evolution equation as a function of frequency. Kirby and Kaihatu (1995) then assumed a propagating wave, which is derived from the 1st-order dynamic free surface boundary condition

$$\hat{\phi}_n = -\frac{ig}{\sigma_n} A_n e^{i\int k_n dx} \tag{1.5}$$

where g is the acceleration due to gravity, k_n is the wavenumber, A_n is the complex amplitude, and σ_n is the angular frequency for the nth frequency component. The velocity potential (Equation 1.5) and its conjugate are substituted into the time-periodic equation for the velocity potential and then the parabolic approximation is made to justify neglecting the 2nd derivatives of the complex amplitude, A_n, with respect to x. Equation 1.5 also is a transformation from amplitudes of velocity potential to those of the free-surface elevation. The transformation is 1st order and subsequently does not include nonlinear terms inherent in

the dynamic free surface boundary condition. Eldeberky and Madsen (1999) determine neglecting these nonlinear terms led to the under prediction of the nonlinear energy transfer. Tang and Oulette (1997) also took 2^{nd}-oder terms into account, but using a different approach than Eldeberky and Madsen (1999).

Kaihatu (2001) derived the required correction to make the model consistent. The correction was derived from the 2^{nd}-order dynamic free surface boundary condition. He also extended the parabolic fully dispersive wave model to include wide-angle propagation terms, which are essentially those of Kirby (1986a). The wide angle enhancement markedly improved the resulting predictions of wave evolution (Chawla *et al.*, 1998).

1.2 Relevant History of Sediment Transport Modeling of the Nearshore

The 1960's marked the development of a method for modeling sediment transport using an energetics-based approach (Bagnold, 1963). Also beginning around this time was the development of bottom boundary layer–based sediment transport predictions (Madsen and Grant, 1976). These two approaches have received much attention and development amongst nearshore researchers. With the increased knowledge of nearshore fluid dynamics and subsequent sediment transport effects, bathymetric evolution modeling has begun a steady evolution towards the inclusion of most applicable physics. There are also continued attempts to approach this problem using empirical methods for parameterizing sediment transport. The empirical methods lack the physics of the complex nonlinear transport models, but provide an efficient method to estimate local volumetric change of the bathymetry as a function of time and space.

In the current study, an energetic-type sediment transport model, following Bailard (1981), is used to predict the morphological evolution. The parameterization of fluid acceleration effects in addition to Bailard (1981) transport models has been shown to be successful at predicting onshore bar movement, and have consequently received much attention in recent years. However, these models approach the inclusion of applicable physics (the fluid acceleration effects) empirically. In contrast, the bottom boundary layer models tend to be more inclusive of the underlying physics, but have proven to be somewhat computationally expensive and complex. A brief review of the relevant history of these three types of sediment transport models is given below.

1.2.1 Energetics-Type Sediment Transport Models

Work (W_b) done by a fluid in the form of bottom shear stress (τ_b), for the purpose of transporting sediment as bed load , can be simply defined as $W_b = \tau_b * U_b$, where U_b is the time averaged velocity of the grains being transported. The bottom shear stress is commonly expressed as $\tau_b = \rho c_f |U_b| U_b$ (ρ is the fluid density and c_f is a friction coefficient for the bed). The fluid power expended in transport as bed load can be expressed as the dynamic (or immersed weight (i)) transport rate multiplied by the difference in the local bed slope and sediment angle of repose [$P_b = i_b(\tan\phi - \tan\beta)$]. If we then assume that the total amount of power expended by the fluid is W, then we can also assume a certain percentage, ϵ_b, of that power will be utilized to transport sediment as bed load (Equations 3.14)

$$i_b = W \frac{\varepsilon_b}{(\tan\phi - \tan\beta)} \tag{1.6}$$

It is important to note that the unidirectional mean flow induced transport is thus far only a result of the work done by the fluid against bottom stress, and therefore, does not yet include any influence on the fluid velocities from wave breaking. It is also important to notice that when the bed slope is equivalent to the sediment angle of repose, the immersed weight transport rate will predict infinite transport, which can be physically interpreted as 'avalanching' of the bed.

Similarly, an expression can be generated for the transport of a suspended load, taking in to account the sediment fall velocity, w, through a body of fluid which is moving in one direction at a mean velocity, U_s. The resulting expression for the immersed weight suspended sediment transport rate is

$$i_s = W \frac{\varepsilon_s(1-\varepsilon_b)}{(w/U_b) - \tan\beta} \tag{1.7}$$

where ϵ_s is the suspended sediment efficiency factor, which dictates the fraction of total power utilized to transport sediment as suspended load. The total immersed weight transport rate, assuming energy dissipation in a unidirectional stream occurs through shear stress at the bed, and that a fraction of the total power is used to move sediment, is (Bagnold, 1963):

$$i = i_b + i_s = \omega\left[\frac{\varepsilon_b}{(\tan\phi - \tan\beta} + \frac{\varepsilon_s(1-\varepsilon_b)}{(w/\bar{u}) - \tan\beta}\right] \tag{1.8}$$

where $\bar{u}$ is the mean free stream velocity and

$$\omega = \tau_b \overline{u} = \rho c_f |\overline{u}|^3 \tag{1.9}$$

Energetic-type sediment transport models are primarily based upon Bagnold (1963 and 1966). The models he developed are adapted from stream flow sediment transport models. Bagnold's physics-based energetics model assumes transport occurs in distinct modes: as bed load and as suspended load. These two modes differ in the mechanism by which the grains are supported as they are being transported. Material transported as bed load is supported by the grain-to-grain interactions under the force of the near-bottom flow. According to Bailard (1981), the suspended load transport is supported by the stream fluid through the process of turbulent diffusion throughout the water column.

Bagnold proposed that a fraction of the total power of the stream was utilized to transport sediment as either bed load or suspended load. The coefficients used to define the fraction of total power expended on sediment transport as bed load or suspended load are the efficiency factors, ϵ_b and ϵ_s, which are discussed above. Bagnold (1966) found that for stream flow conditions above a certain power threshold, $0.11 \leq \epsilon_b \leq 0.14$ and $\epsilon_s = 0.01$.

Bagnold (1963) developed a related sediment transport expression for oscillatory flows, such as found in the nearshore. Bagnold reasoned that the distance sediment moved back and forth due the oscillatory wave motion is directly proportional to the local rate of energy dissipation. No net transport would occur due to this process, but time-averaged transport would occur when a current was superimposed on the oscillatory wave motion. The transport would occur in the direction of the superimposed current. The result of this conceptual model for the current-directed, immersed weight transport, i_θ, is

$$i_\theta = K' \omega \frac{u_\theta}{u_m} \tag{1.10}$$

Where K' is a dimensionless constant, ω is the local rate of energy dissipation, u_m is the magnitude of the oscillatory water velocity, and u_θ is the steady current in the θ direction.

One criticism of Bagnold's expression for transport by currents superimposed upon oscillatory wave motions was that it predicted total load (Equation 1.10) transport, as opposed to his unidirectional steady flow model (Equation 1.8), which broke the transport into the bed load and suspended load contributions. Another criticism was that Bagnold's transport expressions did not include incurred transport due to the bed slope. Bailard and Inman (1981) and Bowen (1981) attempted to remedy Bagnold's equations by differentiating between transport as suspended load and as bed load within the surf zone, as well as including

transport effects from the bed slope. From Bagnold's stream-based model, Bailard and Inman (1981) derived a bed load expression valid in the surf zone, for an arbitrarily oriented sloping bed. Their bed load expression model reduces to Bagnold's bed load expression in the case of unidirectional stream flow. From data comparisons with the Bailard and Inman (1981) bed load transport model, they found that Bagnold's expression (Equation 1.8) is only valid for weak longshore currents and near normal wave incidence (neglecting suspended transport effects).

Bowen (1981) applied Bagnold's total load sediment transport equation to model the cross-shore directed transport on beaches with normally incident waves. He assumed only cross-shore oriented currents, therefore, neglecting longshore currents. Bowen (1981) used second-order Stokes's waves and Longuet-Higgins bottom streaming solutions to solve for the equilibrium profile of a natural beach. From this study, Bowen (1981) validated the observations that steeper beaches are characterized by coarse grains, while flat beaches are characterized by fine grains. His study also supported the observation that shorter period waves caused beaches to erode and longer period waves induced accretion of beaches.

Bailard (1981) went on to derive a total load sediment transport model based on Bagnold's unidirectional flow equation (Equation 1.8). This model is quite similar to the Bagnold (1963) transport equation in that the expression for the local sediment transport rate is composed of separate suspended load and bed load components. The derived-equation also applies to the surf zone, therefore, including transport due to oscillatory and steady near-bottom flows. In the Bailard (1981) formulations, the near-bed flows used to drive the model are defined as velocities within the region where the velocity distribution is nearly logarithmic. More specifically, Grant and Madsen (1979) define this region to be the entire bottom boundary layer, with a vertical extent off the bed defined by $(u^*)_m/\sigma$, where $(u^*)_m$ is the magnitude of the oscillatory shear velocity and σ is the angular wave frequency. More specifically, the Bailard (1981) model utilizes nonlinear combinations of the near-bed velocity field, which are direction functions of wave skewness only. A time series which contains a high degree of skewness if comprised of very large, peaked crests, and long, shallow troughs. Typically, in the nearshore environment, a skewed velocity field is observed when the waves are shoaling, and reaches a maximum degree of skewness near the wave breaking location.

The Bailard (1981) expression also includes a bed slope term, similar to the Bailard and Inman (1981) equation. In general, Bailard's model is applicable to idealized surf zone

conditions, with steady longshore and cross-shore currents in addition to oscillatory wave velocities. The model additionally takes into consideration the local wave angles and the local bed slope. The Bailard model does not resolve the vertical distribution of the sediment flux, because it is derived from vertically integrated equations. Another problem with predicting the sediment transport rate using an energetics approach is that the sediment is assumed to respond instantaneously to the imposed near-bed velocities. This assumption is reasonable when studying bed load transport rates because the bed load layer tends to be rather thin and likely responds rapidly to the bed shear stress. This assumption tends to become invalid for suspended load transport because of the large vertical distribution of the suspended sediment, hence, a delay is to be expected in response to the bottom shear stress. Measurements of suspended sediment flux in the field (Hanes, 1990) showed the quantity of suspended sediment tended to be rather sporadic, instead of quasi-steady, suggesting that the suspension processes are markedly more complex than the Bailard (1981) transport equation.

Thornton *et al.* (1996) utilized measured water velocities from the Delilah field experiment to drive the Bailard (1981) transport rate equation. The measurements were taken in mid-water column. The short wave velocities were then corrected to the bed-level using linear wave theory, which offers a good approximation (Guza and Thornton, 1980). Thornton *et al.* (1996) justified their use of the corrected short wave velocities, which have under estimated turbulent velocities, by stating that in the surf zone short wave velocities tend to be an order of magnitude larger than the turbulent velocity intensities (George *et al.*, 1994). Their intent was to model the erosion and accretion events observed at Duck Beach, NC during the DELILAH experiment. Thornton *et al.* (1996) was successful at predicting the observed formation and offshore migration of a longshore parallel sand bar during the two large storm events. The trough depth was under predicted, and the predicted bar crest was slightly offshore of its observed location. Roelvink and Stive (1989) found similar differences in their profile predictions using Bailard's (1981) formulation to model a laboratory experiment, where they used approximations for the nonlinear velocity quantities that drive the Bailard (1981) model. They did not have measured velocity time series, hence, their development and implementation of the approximated nonlinear quantities of velocity. Thornton *et al.* (1996) found that the model failed to predict the observed minor erosion and accretion events which occurred in between the two large storm events. He attributed this discrepancy to the short wave asymmetry term under estimating the onshore transport over the bar and/or the over estimated offshore transport via the undertow past the bar. Thornton *et al.*

(1996) also found that the computed suspended load was an order of magnitude larger than the bed load during the DELILAH experiment because of the low fall velocity of the fine grain sediments. During the large storms, the strength of the longshore current alone was significant enough to keep the fine grain sediment in suspension. This contributed to the predictions that more than half the total transported sediment was directly due to suspension by the mean longshore current coupled with the transport by undertow.

Gallagher *et al.* (1998) had similar results to Thornton *et al.* (1996) when trying to predict the DUCK94 observed bar migration events. The more current study also utilized velocity measurements made by the mid-water level current meters, but did not use a linear wave theory conversion to approximate the near-bed velocities. In contrast to the study performed by Thornton *et al.* (1996), Gallagher *et al.* (1998) used a cross-shore variable fall velocity to better represent the observed distribution of grain sizes, which ranged from 0.15 mm to 0.3 mm. Gallagher *et al.* (1998) modeled the bathymetric evolution of four observed bar movement events, as well as a 60-day period initiated near the beginning of the experiment. The predictions of the storm-induced offshore bar movement events compared well with the observations, especially when a strong undertow was also observed. The cross-shore gradients of the suspended sediment transport term contributed greatly to the predicted offshore bar migration. The onshore bar migration event was not predicted well using the Bailard (1981) formulation. Similar to others (Roelvink and Stive, 1989; Thornton *et al.*, 1996), Gallagher *et al.* (1998) stated a potential fault with the model as the assumed instantaneous suspended sediment response to bed shear stress (therefore, a phase lag is excluded), which could contribute to the poor onshore bar movement predictions. Gallagher *et al.* (1998) also attributed some of the poor predictions of shoreward bar movement to the observed bed forms (such as the mega ripples) and the exclusion of effects from fluid accelerations, which could all be rather important when oscillatory wave velocities dominate the flow (primarily the undertow) in the surf zone. Overall Gallagher *et al.* (1998) found that the model predicted the cross-shore profile evolution of the energetic, stormy 2-month period well.

1.2.2 Empirical Acceleration-Based Sediment Transport Models

In recent years, onshore bar movement has gained a significant amount of attention by the nearshore modeling community. Gallagher *et al.* (1998) demonstrated that the Bailard

(1981) sediment transport model was unable to predict the observed onshore bar migration during the DUCK94 field experiment. One explanation offered by Gallagher *et al.* concerning the poor predictions by the energetics model during periods of accretion was the exclusion of effects from fluid accelerations. When the wave is shoaling and commences breaking, the associated velocity time series is very asymmetric, representing the forward-pitching of the waves. The velocity acceleration time series of an asymmetric velocity time series has a high degree of skewness, because of the large accelerations of the fluid velocities near the front of the wave.

Cox and Kobayashi (2000) showed that sediment transport at the instant of strong acceleration is potentially related to the flow suspension in front of the wave crest from wave breaking-generated turbulence. Drake and Calantoni (2001) simulated sediment particle flow on a micro-scale, and their research led to the development of an acceleration term, commonly referred to as 'a-spike' in the literature, which has been used to enhance the Bailard transport formulation by parameterizing fluid acceleration contributions. From measurements taken at DUCK94, Elgar *et al.* (2001) offered supporting evidence that onshore-directed sediment transport is in part related to fluid accelerations.

Hoefel and Elgar (2003) implemented the parameterization of fluid acceleration effects using 'a-spike' in addition to the Bailard (1981) sediment transport formulation which they drove with measured velocity time series. They successfully predicted the DUCK94 onshore bar movement event observed in late September. They were also able to successfully predict one of the offshore bar movement events observed at DUCK94, but were unsuccessful when attempting to predict a second observed offshore bar migration. Long and Kirby (2003) also employed 'a-spike' in combination with the Bailard (1981) transport formulation. In contrast to previous efforts, they drove the transport model with predicted velocity time series by the Boussinesq wave model of Wei *et al.* (1995) and Chen *et al.* (2000), which was extended to calculate the wave breaking-induced undertow through a simple mass transport balance. Long and Kirby (2003) had similar success when predicting the onshore bar migration observed at DUCK94. Long and Kirby (2003) employed a Boussinesq wave model, FUNWAVE, to predict the cross-shore evolution of the wave field, and a simplistic undertow computation to obtain the mean cross-shore flows. The hydrodynamics were predicted using the measured bathymetry, which they utilized to drive the sediment transport model. Predictions of the bathymetric evolution by Hoefel and Elgar (2003), Henderson *et al.* (2003) and Long and Kirby (2003) were all made for the instrument locations.

The parameterization of the fluid acceleration through a simplistic addition to the Bailard transport formulation (Hoefel and Elgar (2003); Long and Kirby (2003)) has proven somewhat successful when attempting to predict the qualitative evolution of the nearshore bathymetric profile, primarily during accretion events. It is agreed that fluid accelerations play a role in the evolution of the nearshore bathymetry. However, the proposed techniques for including acceleration effects are not universally agreed upon, and are to date an area of active research.

1.2.3 Physics-Based Boundary Layer-Influenced Sediment Transport Models

An alternative, physics-based approach to modeling nearshore sediment transport is the use of bottom boundary layer flow characteristics to drive transport models. Trowbridge and Young (1989) suggested that nonlinear bottom boundary layer processes potentially play an important role in the mechanisms causing onshore bar migration.

The bottom boundary layer is typically thought to extend 5-10cm off the bed, and is generated due to the influence of viscous effects from the bottom boundary. The boundary layer flow is rotational and assumed to possess a logrithmic vertical velocity profile. The shear stress in this friction-affected region has been observed to be approximately 45° out of phase with the flow velocities for laminar flow. For turbulent flows, the phase shift is approximately 20°-30°, which is postulated to lead to significant transport effects that are often neglected by commonly applied quasi-steady transport models. It has been shown that shoreward propagating waves carry a vertical flux of shoreward directed momentum in the wave boundary layer. The variations in time of this shoreward momentum flux leads to boundary layer streaming (Longuet-Higgins, 1953). Trowbridge and Madsen (1984) state that under non-sinusoidal waves, a covariance between eddy viscosity and velocity shear could exert a mean stress that modifies the boundary layer streaming. Trowbridge and Young (1989) demonstrated that the wave-generated momentum flux into the wave boundary layer has a local maximum over a sand bar, making implications of a shoreward directed transport mechanism. Trowbridge and Young (1989) were able to successfully model the onshore migration of a sand bar, using predicted boundary layer flow characteristics. They neglected undertow effects, thereby resulting in failed offshore bar migration predictions.

Nielsen (1992) proposed that transport under waves with skewed accelerations can be predicted from the bed shear stress, assuming weak undertow. Nielsen (1992) hypothesized

that transport under asymmetric waves was due to the negative correlation of shoreward water velocities and boundary layer thickness; hence, a thinner boundary layer is associated with higher water velocity, and increased sediment transport. Nielsen and Callaghan (2003) suggest that Nielsen (1992) might include effects from pressure gradients and boundary layer thickness. They also found that the Meyer-Peter-Müller (1948) approach can be improved by including phase-lag effects in the Shield's parameter calculations.

Henderson *et al.* (2003) proposed modeling suspended sediment transport using boundary layer streaming forced by wave-generated momentum flux. 2^{nd}-order wave-generated advection is included in their sediment conservation equation, thereby simulating Stokes drift generated transport. Henderson *et al.* (2003) successfully predicted the onshore bar movement event observed during DUCK94. They were also able to predict the initial offshore bar movement event observed in early September, but were unable to predict the offshore bar migration in early October. These results are strikingly similar to those of Hoefel and Elgar (2003), possibly suggesting the simulation of similar processes, which have resulted in likewise similar bathymetric evolution predictions, even though different approaches were taken to model the bar migration events.

1.3 Focus of Research

In this study, hydrodynamic models were compared based upon their skill when predicting cross-shore profiles of nonlinear wave and wave velocity properties: skewness and asymmetry. These nonlinear characteristics have proven to be challenging to predict in a variety of hydrodynamic climates in combination with variable water depths. Predictions of skewness and asymmetry by three types of models were compared, which ranged in computational expense and complexity. The more complex models were derived using the physics-based governing equations of fluid systems, where the less complex and computationally efficient models are empirically developed using physics of the nearshore systems. The most complex wave evolution model used in this study was FUNWAVE, which is a fully nonlinear Boussinesq wave model (Wei *et al.*, 1995). It was utilized to make predictions of water surface elevation time series, from which wave velocity time series were calculated using linear wave theory. The nonlinear, phase-resolving, fully dispersive wave model of Kaihatu (2001), in which the evolution of the waves is governed by the parabolic

approximated mild-slope equation, was also used to predict water surface elevation and wave velocity time series. Wave and velocity skewness and asymmetry are thus computed from the predicted time series from each of the two nonlinear wave models. The third type of model was empirical formulations developed to predict wave velocity skewness and asymmetry. Two of these empirical models were used in this study: the Doering and Bowen (1995) formulations, which were derived through bispectral analysis of wave evolution, and the Doering *et al.* (2000) formula, which was generated using an evolutionary algorithm.

Predictions of skewness and asymmetry were used to gauge the skill of these models. The quantity of wave skewness and asymmetry changes vertically in the water column, due to effects by the bathymetry in the wave boundary layer versus the free streaming flow. The characteristics of the nearshore flow field have been of interest to the engineering community because of the vital role these nonlinear quantities play in predictions of the morphologic evolution. Hence, our investigation of the quality of predictions of nonlinear wave properties by these three types of predictive tools.

Another focus of coastal modelers is to ably simulate the hydrodynamics and subsequent morphodynamics of the nearshore using a complete feedback system; i.e. the predicted bathymetry after a pre-defined time step would be used as the initial bathymetry for the following time step and so on. A full feedback model of this sort is afflicted with issues ranging from model validity to stability. Also, there are currently few data sets available which contain all the necessary measurements required to thoroughly test such a proposed set of models. In the second half of this study a model series was implemented, using a feedback system, to simulate the 1DH (1-dimensional-horizontal), cross-shore evolution of sand beaches for a lab and a field experiment. The nonlinear, fully fully dispersive wave model of Kaihatu (2001) was used to predict the cross-shore evolution of wave field. A Bailard (1981) sediment transport model was used to predict the local cross-shore change of the bathymetry, as a function of time, from which the new cross-shore profile was predicted, and subsequently used as the initial bathymetry for the following time step.

The overall goal of this study to make progress in the direction of building community models, in which compatible wave, circulation, and transport models of differing degrees of complexity can be used in combination for simulating the nearshore environment. It is hopeful that in the near future we will be capable of simulating long term coastal evolution in real time, therefore, providing a realistic modeling tool for the researching and practicing engineering community.

Chapter 2

HYDRODYNAMIC MODEL COMPARISON

The hydrodynamic study was performed to assess the skill of nonlinear wave models and the empirical formulations when predicting the nonlinear wave characteristics, skewness and asymmetry. The nonlinear wave models are quite complex and are both computational expensive. For this study, the waves were assumed to propagate shore-normally by both complex nonlinear wave models. The empirical models are computationally inexpensive, but the validity of their predictions is thus far untested, even though the models are currently being utilized. In the nearshore community, computational expense is typically perceived as a tremendous drawback, therefore, the empirical formulations become quite appealing due their computational efficiency.

We intended to provide a comparison of model skill between each of the models to gauge their individual ability to accurately predicted nonlinear quantities of the wave velocities. Quality predictions of velocity skewness and asymmetry are of interest to the modelers of nearshore sediment transport because they are directly related to the morphological evolution. The currently utilized sediment transport formulations are directly functions of skewness and/or asymmetry. In our bathymetric study we employ the Bailard (1981) sediment transport formulation, which is a function of velocity skewness, only. Therefore, in the hydrodynamic study we are mainly concerned with the predictions of the velocity skewness. Subsequently, we weighted our overall assessment of the individual models based on their model skill when predicting velocity skewness.

2.1 Nonlinear Wave Models

There are a number of nonlinear wave models available today for a variety of applications in the dynamic nearshore environment. Even though these types of models tend to be rather computationally expensive, they are valuable for their ability to simulate the nonlinear characteristics of water surface elevation and velocities associated with waves. The higher order nonlinear wave parameters, such as wave skewness and asymmetry play a role in predictions of bathymetric evolution. For example, predictions of onshore sediment transport

by energetics-based sediment transport models is a direct function of wave velocity skewness. As the predictions of higher order moments of wave velocity improve, so will the predictions of morphological evolution, hence, the significant value of wave models which can predict nonlinear quantities of waves.

2.1.1 Nonlinear Parabolic Mild Slope Equation

The nonlinear fully dispersive wave model of Kaihatu and Kirby (1995) solves the parabolic mild slope equation in the frequency domain. The parabolic mild slope equation includes the effects of wave refraction and diffraction, but neglects reflection (Berkhoff, 1972). The model is phase-resolving and fully dispersive, hence dispersion follows the linear dispersion relationship. Kirby and Kaihatu (1995) invoke resonant interaction theory (Phillips, 1980) to select the interacting frequencies of the nonlinear triad, generating a time-harmonic evolution equation for the velocity potential. The resulting 1-D governing equation is

$$A_{nx} + \frac{(kCC_g)_{nx}}{2(kCC_g)_n} A_n + \alpha_n A_n = -\frac{i}{8(kCC_g)_n} \cdot \left[\sum_{l=1}^{n-1} RA_l A_{n-1} e^{i\int (k_l + k_{n-1} - k_n)dx} + \sum_{l=1}^{N-n} SA_l^* A_{n+l} e^{i\int (k_{n+l} - k_l - k_n)dx} \right] \tag{2.1}$$

where C is the wave celerity, C_g is the group wave speed, R and S are complicated interaction coefficients [shown in equations 26 and 27 of Kaihatu and Kirby (1995)], and k is the wave number. α_n is the frequency-weighted dissipation coefficient, and will be further discussed below. A_n is the complex amplitude, which carries phase information, and the surface elevation, η, is defined as:

$$\eta = \sum_{n=1}^{n_{\max}} A_n e^{i\left\{\int k_n dx - \sigma t\right\}} \tag{2.2}$$

The three-wave (triad) interactions are explicit since the solution is in the frequency domain. The model is phase-resolving because the complex amplitude, A_n, retains phase information. Consequently, the wave velocity time series can be reconstructed using a higher-order correction to the transformation from phase velocity to water surface elevation, which was derived from the second-order dynamic free surface boundary condition and added to the model formulation by Kaihatu (2001). The nonlinear fully dispersive wave model is solved

using a fourth-order Runga Kutta technique.

The model uses an input water surface elevation time series as its offshore boundary condition. The bottom boundary is defined by the input bathymetry. The model requires that all energy is dissipated by the wet-dry boundary of the still water level shoreline.

The fully dispersive wave model implements a dissipation model based on Thornton and Guza (1983). The rate of dissipation if a function of frequency (*f*), amplitude (A), *F* (a weighting parameter), and β (which is a wave shape parameter from Thornton and Guza (1983)).

$$\alpha_n = \alpha_{n0} + \left(\frac{f_n}{f_{peak}}\right)^2 \alpha_{n1} \tag{2.3}$$

$$\alpha_{n0} = F\beta(x) \tag{2.4}$$

$$\alpha_{n1} = [\beta(x) - \alpha_{n0}] \frac{f_{peak}^2 \sum_{n=1}^{N} |A_n|^2}{\sum f_n^2 |A_n|^2} \tag{2.5}$$

The weighting parameter, *F*, dictates the split between f^2_n- weighted dissipation and a frequency-independent dissipation. It has a range from 0 to 1, where $F = 0$ allows only f^2_n-weighted dissipation. F=1 allows only for frequency-independent dissipation because α_{n1} goes to zero.

2.1.2 Fully Nonlinear Boussinesq Wave Equation

Fully Nonlinear Boussinesq Wave Equation model (FUNWAVE) is the Boussinesq wave model of Wei and Kirby (1995), which includes an extension to intermediate water depths based on the work of Nwogu (1993). The wave model is dispersive, but does not follow the linear theory dispersion relation. Figure 2.1.1 plots the extent of the Boussinesq wave model validity, as a function of μ^2 and δ, where $\mu=kh$ and $\delta=a/h$. FUNWAVE is phase-resolving, with the governing equations solved in the time domain. It uses a 4th order Adams-Bashforth-Moulton (Press *et al.*, 1992) predictor-corrector solution scheme to step through time.

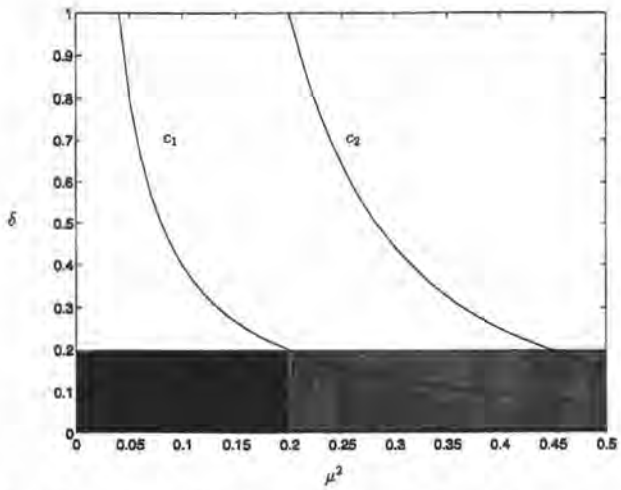

Figure 2.1. Mathematical limits of validity of Boussinesq wave models. Standard Boussinesq models (Dark Gray), region of validity of extended Boussinesq wave model of Nwogu (1993) (Light Gray). Curve c_1 denotes $\delta\mu^2$=0.04. Curve c_2 denotes $\delta\mu^4$=0.04.

Similar to Kaihatu's fully dispersive wave model, Wei and Kirby found it convenient to maintain dimensional variables for the development and application of the numerical model. The dimensional model equations are

$$\eta_t = E(\eta,u) + \gamma E_2(\eta,u) + f(x,t) \tag{2.6}$$

$$[U(u)]_t = F(\eta,u) + \gamma[F_2(\eta,u) + F^t(\eta,u_t)] + F_{br} + F_b + F_{sp} \tag{2.7}$$

where η is the water surface elevation, u is the horizontal velocity in the x direction at depth $z = z_\alpha$, where z_α is defined by Nwogu (1993). The subscript t denotes the partial derivative with respect to time, and γ is a control parameter defining the degree of nonlinearity. For this study γ is set to 1, therefore,making the model fully nonlinear (Wei and Kirby, 1998). The quantities U, E, and F are functions of η and u and defined as:

$$U = u + h[b_1 h u_{xx} + b_2 (hu)_{xx}] \tag{2.8}$$

$$E = -\frac{1}{\kappa}[\Lambda u]_x - \{a_1 h^3 u_{xx} + a_2 h^2 [(hu)_{xx}]\}_x \tag{2.9}$$

$$F = -g\eta_x - uu_x \tag{2.10}$$

where, Λ and κ are functions which modify the mass equation due to the changes presence of slots in the bathymetry, which are used to parameterize run-up. The quantities E_2, F_2, and F^t are higher order dispersive terms which are defined as:

$$E_2 = -\left\{\left[a_1 h^2 \eta + \frac{1}{6}\eta(h^2 - \eta^2)\right](u_{xx})\right\}_x - \left\{\left[a_2 h\eta + \frac{1}{2}\eta(h+\eta)\right][(hu)_{xx}]\right\}_x \tag{2.11}$$

$$F_2 = -\left\{\frac{1}{2}(z_\alpha{}^2 - \eta^2)[uu_{xx}]\right\}_x - \{(z_\alpha - \eta)u(hu)_{xx}\}_x$$
$$-\frac{1}{2}\{[(hu)_x + \eta u_x]^2\}_x \tag{2.12}$$

$$F^t = \left\{\frac{1}{2}\eta^2 u_{xt}] + \eta\left[\left[hu_t\right]_x\right]\right\}_x \tag{2.13}$$

The quantity $f(x,t)$ is the source function term for generating waves inside the computing domain (Wei and Kirby, 1998). F_{br} is a term related to breaking in the x direction. F_b is a bottom friction term and becomes important for run-up simulations. F_{sp} is a sponge layer term. The constants a_1, a_2, b_1, and b_2 are used for the convenience of implementing four different model equations using the same numerical scheme, and are functions of β. $\beta = z_\alpha/h$ = -0.531 is a dimensionless parameter related to the reference water depth z_α at which the horizontal velocity is chosen as a dependant variable.

The offshore boundary is located approximately two offshore wavelengths seawards of the wavemaker. Within the computational domain, the wavemaker is the location of the source region where the waves are generated and where the input water surface elevation time series is used to drive the model. An offshore sponge layer, beginning at the most offshore boundary, typically extends one wavelength shoreward. The onshore sponge layer begins at the onshore boundary and extends approximately ¼ to a ½ of an offshore wavelength seaward into the domain. Slots are placed near the shoreline to handle the moving wet-dry boundary while simulating wave run-up. The slots are around one wavelength in the cross-shore and encompass the wet-dry shoreline boundary.

FUNWAVE implements an energy dissipation model following models of Heitner and Housner (1970) and Zelt (1991), who utilize an eddy viscosity term, ν_b , to account for wave breaking. F_{br}, the breaking term mentioned above, is expressed as

$$F_{br} = (\nu_b u_x)_x \tag{2.14}$$

where the simplified eddy viscosity model is

$$\nu_b = B\delta_b^2(h+\eta)\eta_t \tag{2.15}$$

is shown to perform well when compared with monochromatic and random wave experiments in 1-D simulations. B is a coefficient relating to local wave shape and the corresponding critical value for wave breaking to take place. δ is the coefficient of mixing length, which is

determined empirically, and in this particular model kept a constant with a value of 2. To avoid instability in the numerical computations, which could be caused by sudden changes in the eddy viscosity, the coefficient B is given by

$$B = \begin{cases} 1 & \eta_t \geq 2\eta_t^* \\ \left(\frac{\eta_t}{\eta_t^*} - 1\right) & \text{if} \quad \eta_t^* < \eta_t \leq 2\eta_t^* \\ 0 & \eta_t \leq \eta_t^* \end{cases} \tag{2.16}$$

The parameter η_t determines the onset and cessation of breaking. According to Kennedy *et al.* (2000), the use of η_t to define in this manner ensures the dissipation is concentrated on the front face of the wave. A breaking event begins when η_t exceeds a defined threshold. Breaking will continue even if η_t drops below this threshold. The magnitude of η_t^* will decrease in time from some initial value, η_t^I, to some final value, η_t^F. A simple linear relationship was used to describe this decrease in time of η_t^*. The typical default values used for η_t^I and η_t^F are $0.65\sqrt{(gh)}$ and $0.15\sqrt{(gh)}$, respectively (g is the acceleration due to gravity and h is the local water depth).

The predictions of water surface elevation time series by FUNWAVE are sensitive to many of the input parameters. A few of the primary input parameters which results are sensitive to, are the slot length, temporal filter step and the modeled frequency range. The slot or permeable-seabed technique proposed by Tao (1983, 1984) involves replacing the bottom boundary with a porous bed in areas with very little or no water covers the dry bed in the domain. The replacement porous seabed is composed of slots, ranging in width from 0.01 to 0.001 times the grid size. The slots allow for the modeled water level to exist below the beach elevation during periods when the land surface is dry. The replacement of the solid bathymetry by the slots causes a modification of the mass conservation equation. The resulting run-up predictions were shown to have approximately a 10% error by Madsen *et al.* (1997), who also predicted the wave climate using a Boussinesq wave model. Testing of the slot width and length by Kennedy *et al.* (1999), the results were found to have the best agreement with analytical solutions by Carrier and Greenspan (1958). It was also found by Kennedy *et al.* (1999) that run-up simulations on a steep beach improved with an increase in the slot width.

The model generates higher frequency harmonics as it propagates shoreward. These super-harmonics could have a wavelength that is smaller than the required model minimum of

2 times the grid spacing. These higher harmonics tend to cause instability of the model, therefore, a numerical filter is implemented to smooth the evolving water surface elevation time series. The model user can dictate the filter time step, as well as the beginning and end of the application of the numerical filter. The implemented 4^{th} order filter uses the original values of the 9-adjacent points to determine the new value of the central point.

A large frequency component is indicative of a large wavenumber component. When wave energy is present at high frequencies, there is the potential for $kh>\pi$, which means the spectral component of the wave at this frequency is traveling in deep water. If any portion of the wave energy is in deep water, this violates the shallow water assumptions of FUNWAVE. To avoid this, a maximum modeled frequency can be defined by the user of FUNWAVE.

As a note, this model produces water surface elevation time series that are larger in magnitude than the observations near the wave paddle. The over-estimated magnitude of the water surface elevation is due to the increased variance near the source region to account for waves generated which propagate towards the offshore and onshore boundaries. The nonlinear characteristics of the waves in this region are predicted well, but the magnitude of the water surface elevation is simply larger. The increased variance effects decay 2-3 offshore wavelengths away from the source region. Therefore, water surface elevation predictions by FUNWAVE will not be utilized near the wave paddle to prevent the model skill being affected by the increase variance.

2.1.3 Empirical Models Used to Predict Non-linear Wave Parameters

Nonlinear characteristics of waves are commonly utilized to predict sediment transport rates and the direction of transport. For example, energetic-type sediment transport models, such as Bailard (1981) are typically driven by higher order moments of velocity. Therefore, quality predictions of higher order moments of wave velocity, such as skewness and asymmetry, are necessary to predict sediment transport when utilizing an energetics-type model.

Wave velocity skewness and asymmetry predictions obtained using a nonlinear wave model can be rather computationally expensive. Therefore, predictions of these nonlinear wave parameters made by empirical formulations have the potential to be useful when computational power is limited and one is attempting to predict bathymetric evolution. For example, the available computational power could be exceeded due to a very large

computational domain or a distant prediction horizon. Thus far, most empirical models for predicting velocity skewness and asymmetry were developed using velocity measurements from only a few beaches, from similar geographical locations.

Two existing empirical models for predicting velocity skewness and asymmetry are Doering and Bowen (1995) and Doering *et al.* (2000). Doering and Bowen (1995) used the bispectrum to develop a parameterization for velocity skewness and asymmetry from deep water into the surf zone. Bispectral analysis was chosen because it provided a simple and convenient way to determine wave skewness and asymmetry arising from triad interactions. Their model is strongly dependent upon the Ursell parameter and attempts to describe how bispectra evolve due to wave shoaling. In contrast, Doering *et al.* (2000) developed their empirical model using the evolutionary algorithm (genetic programming) of Keizer and Babovic (1999). Their expression for predicting skewness was based on measurements of wave height, wavelength, bed slope, and near bed wave velocity. Below we review both models in more detail.

Doering and Bowen (1995) developed their empirical model using near bed velocity measurements made from four beaches (Leadbetter Beach, California; Pte. Sapin, New Brunswick; Stanhope Lane, Prince Edward Island; and Queensland Beach, Nova Scotia). These beaches embody a range of bathymetric features from planar to barred profiles. Complex bispectra were generated and analyzed for each of the measured velocity time series. Skewness can be determined by taking the integral of the real part of the bispectrum (Equation 2.17) (Hasselman *et al.*, 1963).

$$S = \frac{\int_{-\infty}^{+\infty}\int \Re\{B(f_1, f_2)\}df_1 df_2}{E[\varsigma^2(t)]^{3/2}} \tag{2.17}$$

where E is the expected value and ς is the integral of the real part of the bispectrum, with respect to the two interacting frequencies, where $f_1 > f_2$.

$$A = \frac{\int_{-\infty}^{+\infty}\int \Im\{B(f_1, f_2)\}\, df_1 df_2}{E[\varsigma^2(t)]^{3/2}} \tag{2.18}$$

Similarly, wave asymmetry can be determined by taking the integral of the imaginary part of the bispectrum (Equation 2.18) (Elgar and Guza, 1985).

The Ursell parameter can be expressed in terms of H_c, which is a characteristic wave height, T_p, the peak period, and h, the local still water depth. Phillips (1960) showed that the nonlinear self-interactions cause the transfer of energy to higher harmonics creating a Stokes wave. Doering and Bowen (1995) reasoned the since the Ursell number is the expansion parameter for a Stokes wave train, that it could also be utilized to parameterize the evolution of the integrated biamplitude arising from peak-peak-harmonic frequency interaction. With this justification, they compared the computed Ursell number (Equation 2.19) and the normalized integrated biamplitude arising from self-self interaction of the peak frequency for each site.

$$Ur = \frac{3gH_cT_p^2}{32\pi^2h^2} \tag{2.19}$$

To determine a parameterization for the biamplitude (B) and the biphase (β), a Least Squares Regression of this data was performed, giving

$$B(f_p, f_p) = 0.42 + 0.27\log(Ur) \tag{2.20}$$

$$\beta(f_p, f_p) = -90°+90°\tanh(0.63 / Ur) \tag{2.21}$$

Other comparisons were made between the normalized integrated biamplitude and the biphase, but they were both found to most strongly depend upon the Ursell number.

Through further analysis concentrating on wind-wave bispectra, parameterized expressions for skewness and asymmetry were derived (Equations 22 and 23, respectively).

$$S_{ww} = [0.8 + 0.62\log(Ur)]\cos\{[-90° + 90°\tanh(0.73/Ur)]\pi/180°\} \tag{2.22}$$

$$A_{ww} = [0.8 + 0.62\log(Ur)]\sin\{[-90° + 90°\tanh(0.73/Ur)]\pi/180°\} \tag{2.23}$$

In contrast to the study of Doering and Bowen (1995), Doering *et al.* (2000) implemented an evolutionary algorithm to determine an expression for wave velocity skewness. The genetic program utilized field measurements from a number of sites (> 55,000 observations). A significant amount of the data came from Terschelling (Netherlands), Duck94 (Duck Beach, North Carolina), Sandyduck97 (Duck Beach, North Carolina), and Egmond (Netherlands). From the available data, only runs longer than 20 minutes were considered. All velocity data were band pass-filtered, with cutoff frequencies of 0.05 Hz and

1 Hz.

A data matrix was constructed containing the following non-dimensional parameters: H_s/h, λ/h, and the surf similarity parameter (ξ). H_s is the local significant wave height, h is the time averaged local water depth, and λ is the wavelength of the peak spectral component wave. The surf similarity parameter is defined as

$$\xi = \frac{\tan\beta}{(H_s / \lambda_0)^{1/2}} \tag{2.24}$$

where β is the mean bed slope over the domain and λ_0 is the deep-water wavelength. The matrix was then used as input to the genetic program, which then developed an initial population of formulae. The performance of the individual formulae is evaluated using two criteria: 1) the correlation between the predicted and observed data, and 2) the size of the formula. Substructures of the population of formulae are randomly combined resulting in a new generation of formulae (which is the same size as the initial population). This new generation is then tested and the process is repeated. The program typically iterates through 20 to 50 generations before deriving the optimal formula.

The optimal expression for skewness produced by the evolutionary algorithm is:

$$S = -14.076[\tanh(1 + a1 + \sqrt{a2 + a3}) + a4] + 14..133 \tag{2.25}$$

where,

$$a1 = \frac{2.582}{\lambda / h} \tag{2.26}$$

$$a2 = |\xi - 0.207| \tag{2.27}$$

$$a3 = \sqrt{\left|-0.22 + \left|\frac{\xi \tanh(Ur) + 2.527}{\lambda / h}\right|\right| + \left(\frac{\lambda / h}{Ur^2}\right)} \tag{2.28}$$

$$a4 = \left|\frac{\lambda / h}{Ur} - 0.218\right| \tag{2.29}$$

$$Ur = \frac{H_s \lambda^2}{h^3} \tag{2.30}$$

The model performed well when comparing the predicted and measured skewness from the utilized data. Doering *et al.* (2000) were able to show that approximately 92% of the variation within the processed data set was explained by the expression. When comparing with the raw data (not band-passed data) sets, the expression was able to still explain approximately 77% of the variation.

2.2 Data Sets Used for Model Comparisons

Two lab data sets and one field data set were utilized for the hydrodynamic model comparisons. The lab cases were the Mase and Kirby (1992) [Cox *et al.*, 1991] experiment and the Large Installation Plan (LIP) 11D experiment. The Mase and Kirby experiment took place in a 20m-long, two-dimensional wave flume in Kyoto, Japan. This experiment was composed of two test cases and was performed to study the evolution of waves from intermediate to shallow water. The LIP11D experiment was performed by a number of researchers in the European Union in a 200m-long 2-D flume. LIP11D took place at Delft Hydraulics (in the Netherlands) and attempted to simulate varying morphodynamic states of a sandy beach (Roelvink. and Reniers, 1995). The field data set was collected during the DUCK94 experiment at Duck Beach, North Carolina (USA). One focus of the experiment was to study the erosive and accretive states of sand bars in nature [Elgar *et al.*, 1997; Gallagher *et al.*, 1998].

2.2.1 Mase and Kirby (1992): Test Case 2

The Mase and Kirby (1992) [Cox *et al.*, 1991] random shoaling wave experiment took place in a two-dimensional wave flume with an immovable bed. The offshore water depth of 47cm was constant for the initial 10m from the wave paddle. The toe of a 1:20 slope began in 47cm of water depth 10m from paddle. A schematic of the flume and the instrument locations is shown in Figure 2.2.1. There were 12 capacitance-type wave gauges located on a cross-shore transect, beginning at the toe of the slope in 47cm of water depth and ending in a water depth of 2.5cm. The water surface elevation was recorded by a digital recorder at the sampling interval of 0.025 seconds for 30 minutes for Test Case 1 and 20 minutes for Test Case 2 [Mase and Kirby, 1992; Cox *et al.*, 1991].

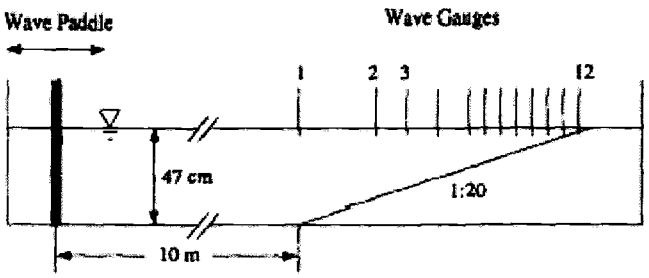

Figure 2.2. Schematic of experimental setup of the Mase and Kirby (1992) [Cox *et al.*, 1991] random wave study (from Wei and Kirby, 1994)

A Pierson-Moskowitz spectrum was used to generate random waves with a peak frequency of 0.6Hz (Test Case 1) and 1.0Hz (Test Case 2). The dominant breaking type was a spilling breaker. The experiment was performed to study the process of shoaling and breaking of random waves where the peak frequency of the spectrum was outside the shallow water range (Kaihatu, 1994). Therefore, this data set provides a means for testing the performance of the wave models in intermediate water depths.

2.2.2 LIP11D: Test Cases 1B and 1C

LIP11D (Large Installation Plan – code number 11D) was a European Union (EU) supported program, under which the Delta Flume experiment of 1993 was performed. The Delta Flume experiment took place in a two-dimensional large-scale wave flume at Delft Hydraulics, which is 233m in length, 7m deep and 5m wide (Figure 2.3). The experiment focused on the bathymetric evolution of a sandy beach, with a grain size of 220μ, due to various hydrodynamic forcing. Two different profile geometries were tested (equilibrium profile of Bruun-Dean-Moore, with and without a berm [Bruun, 1954; Dean, 1977;Moore, 1982]) and three different morphodynamic states were simulated (equilibrium, erosive, and accretive) (Arcilla, A. *et. al.*, 1994). . One goal of the experiment was to simulate a stable wave climate, followed by an erosive and then accretive climate (Roelvink and Reniers, 1995). This sequence was chosen to mimic the natural development of a storm state, followed by a calm, post-storm state. The experiment design followed the work of Kraus, Larson, and Kriebel (1991) to produces these three different morphodynamic states, based on feasible wave heights and water levels in the 2-D wave flume.

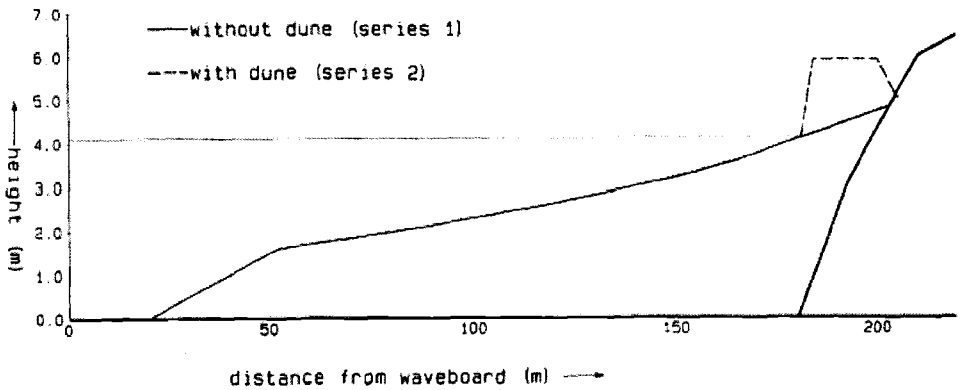

Figure 2.3. Flume geometry of Delta Flume'93 Experiment. The dashed region (---) represents the berm. The mean water level (MWL) for Test Case 1B and 1C was 4.1m.

For the duration of the experiment ten pressure sensors (type PDCR 10/D/F-01, Druck Ltd., Leicester) and five electro-magnetic velocity-meters (type EMF01, Delft Hydraulics) were attached to the walls of the flume. The pressure sensors were mounted to the wall as close to the water surface as possible, make sure they were always below the wave trough level. The current meters were mounted 1/3 of the local water depth above the bed (Fig. 2.4). A roving carriage was instrumented with an automatic sounding system (PROVO), a sediment concentration sampler, five electro-magnetic current-meters, four optical backscatter sensors (OBS), one bottom sediment transport meter (HARK), and one video camera. Three moveable wave gauges were also utilized throughout the experiment (two surface-following wave gauges are located near the paddle, and one resistance gauge type is located near the carriage) (Roelvink and Reniers, 1995). The PROVO system was used to measure the bottom profile (throughout the experiment). The bottom was measured a number of times throughout each test case (somewhat dependant upon the wave climate) and at the end of each test case. The resulting bathymetry after each test case is the initial bathymetry for the following test case, i.e. the final profile of Test Case 1B is the initial profile of Test Case 1C. A layout of the fixed instrument locations is shown in Figure 2.4.

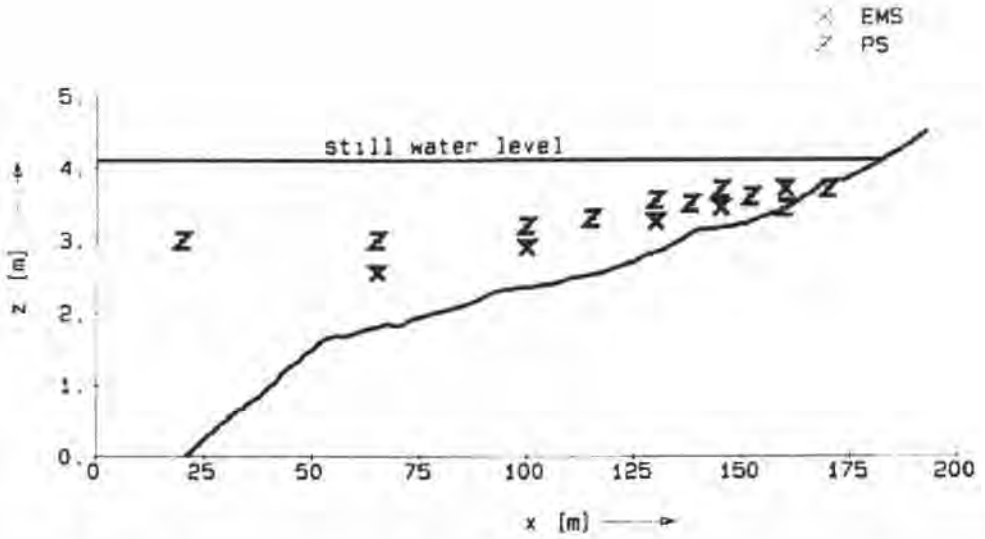

Figure 2.4. Layout of fixed pressure sensor (Z) and velocity-meter sensor (X) locations.

Waves were generated for one hour at a time during each test case. The pressure sensors, velocity and current meters, and the wave gauges were all sampled at 10 Hz for the duration of each hour. The collected time series were low-pass filtered by an analog filter at 5Hz. (The data collected by these three types of instruments were used in the present hydrodynamic study.) In general, narrow-banded waves were chosen such that the wave steepness at the peak frequency in combination with the water level would simulate the desired morphodynamic state, i.e. stable, erosive, or accretive (Roelvink and Reniers, 1995). For the duration of each test case the waves and water level were kept constant.

The two cases used for data comparisons in the present study, Test Case 1B and Test Case 1C, are erosive and accretive simulations, respectively. The mean water level for both test cases was 4.1m. In Test Case 1B the significant offshore wave height was 1.4m, with a peak period of 5s (Roelvink and Reniers, 1995). Few profiles were collected during the latter half of Test Case 1B (18-hrs duration). Therefore, many of comparisons seen throughout the present study will concentrate on the first 10hrs of the experiment. Test Case 1C, the accretive simulation, was characterized by a significant wave height of 0.6m and a peak period of 8s. This case was 13hrs in length, with profiles taken around every three hours throughout the latter half of the experiment.

The time series of water surface elevation measured near the wavemaker (x=20m)

was used to drive the two nonlinear wave models that were tested as part of the present study. The measured pressure (P) time series from the ten spatially fixed pressure sensors were used to generate water surface elevation (η) time series and cross-shore oscillatory velocity (u) time series using linear water wave theory. The converted time series were used for some of the comparison because of a lack of direct measurements of water surface elevation across the tank. The pressure sensors were the most numerous instrument types in the flume, offering more cross-shore locations for model-to-data comparisons.

Errors arise when using linear theory to relate P, u, and η, and considerations based on the Korteweg-deVries equations show that these errors are $O(a/h)$. The size of a/h can be significant; therefore, large errors could be expected when converting P to η, particularly in the higher order harmonics. Guza and Thornton (1980) conducted a study to investigate these errors by comparing velocity and sea surface elevation predictions using linear theory and measurements by pressure sensors, current meters, and wave staffs. Measurements were made in water depths ranging from 0.7m to 10m. Overall, they found the errors in both total variance and energy density for a particular frequency band to be less than 20% throughout the cross-shore and attributed a significant portion of the error to instrument calibration and uncertainties with the experiment, especially associated with the current meters. Their conclusion was that utilizing linear wave theory was sufficiently accurate for situations where random waves were prevalent.

Water surface elevation and wave velocity time series computed from the converted pressure sensor measurements represent the bulk of the data used for the comparisons and were used to compute cross-shore wave height statistics and nonlinear characteristics of the waves (i.e. wave skewness, asymmetry, higher order velocity moments, etc.). Comparisons were also made between the velocity meter measurements, the computed velocity time series from the pressure sensor, and the model predictions to ensure the converted data and model were accurate.

2.2.3 DUCK94

DUCK94 was a field experiment at the Army Corps Field Research Facility (FRF) located on Duck beach on the coast of North Carolina. Duck is located on a barrier island exposed to the Atlantic Ocean. The research site is a nearly long-shore uniform barred-beach.

The beach is typically characterized by a single offshore bar, but it has been observed with multiple well defined offshore sand bars (Lippmann and Holman, 1993).

The experiment was performed between August and October of 1994. Pressure sensors, current meters, and sonic altimeters were used to instrument the nearshore, from about 8m of water depth to the shoreline. CRAB (Coastal Research Amphibious Buggy) surveys were taken by the Army Corp of Engineers during the experiment, though the CRAB could not operate during periods when the significant wave height exceeded 2m (Lee and Birkemeier, 1993). Argus images spanning the length of the field site were also collected by cameras installed on the FRF tower (Holman and Sallenger, 1993).

The SPUV (Sonar altimeter, Pressure sensor, U-velocity meter, V-velocity meter) data set was specifically utilized for the present hydrodynamic and sediment transport studies. The SPUV instrument cross-shore array consisted of nine fixed frames of co-located pressure-sensors, bi-directional Marsh-McBirney electromagnetic current meters, and sonic altimeters, as well as four fixed frames of collocated pressure sensors and current meters. The array was located approximately 400m north of the Field Research Facility (FRF) pier and covered a cross-shore transect of approximately 225m, with an average instrument spacing of 25m (Gallagher *et al.*, 1998). A plot of the cross-shore profile measured by the sonar altimeters compared to the CRAB surveyed profile is shown in Figure 2.5. The plan form locations of the cross-shore SPUV instruments, relative to the FRF pier, are inset in the figure.

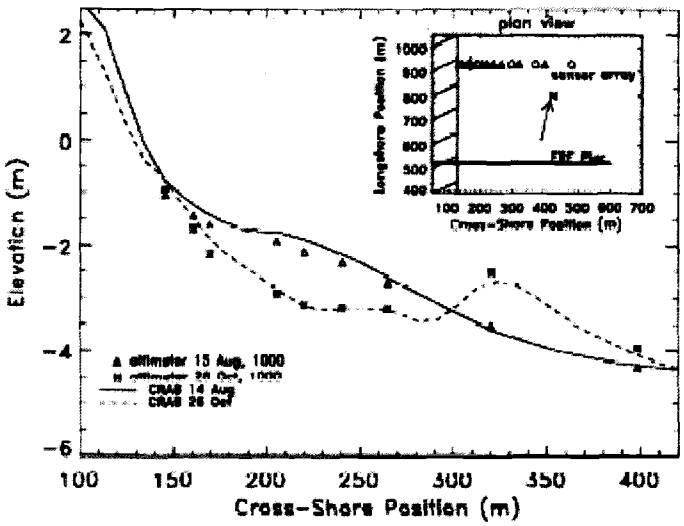

Figure 2.5. Initial profiles on August 15th by the 3-hour averaged sonar altimeter measurements (Δ) and the 14th by the CRAB survey (-). Final profile on the October 26th by the 3-hour averaged altimeter measurements (*) and the CRAB survey (--). The inset is a plan view of the SPUV cross-shore instrument array, relative to the FRF pier: Collocated pressure sensors, current meters, and altimeters (Δ); collocated pressure sensors and current meters (o); a small two-dimensional array of altimeters (+). (Adapted from Gallagher *et al.*(1998))

Gallagher *et al.* (1996) estimated the bed elevation directly under each sonar altimeter by averaging the altimeter data over the approximate six-inch-diameter circular footprint. The initial measured profile from mid-August varies slightly between the sonar altimeter measurements and the CRAB survey over the hump of the bar. The slight variation between the two surveys over the bar crest can also be seen in the final profile from October 26th. These differences can be attributed to the interpolation of the CRAB data to the SPUV instrument locations, different sampling time periods, and possible instrument errors.

The SPUV cross-shore array of pressure sensors, current meters, and sonar altimeters collected data at 2Hz in three-hour spurts for the duration of the experiment. During large bar movement periods some of instruments were buried due to the dynamic bathymetry therefore, instruments were periodically raised and lowered (Gallagher *et al.*, 1998). There were also periods during large storm events when instruments were temporally disabled and were unable to be fixed until after the storm event had passed.

The offshore boundaries of the wave models were co-located with a pressure sensor

and a sonar altimeter. The pressure sensor time series was converted to water surface elevation time series using the same linear conversion routine as described above in section 2.2.2. The converted water surface elevation times series was used to drive the wave models. Ideally the wave models should have been driven with measured water surface elevation time series, but the SPUV cross-shore array did not contain any wave gauges. We note here that driving the wave model with water surface elevation time series that are derived from measured pressure time series potentially introduces errors due to the inaccuracies in the conversion (determined by Guza and Thornton (1980)). Driving the wave model with measured water surface elevation time series would eliminate this inherent error and is therefore, more desirable.

2.3 Mase and Kirby (1992) Comparison: Test Case 2

The Mase and Kirby (1992) [Cox *et al.*, 1991] experiment was performed to test the accuracy of wave models when predicting wave evolution from intermediate to shallow water depths, over a sloping profile. This data set provided a rigorous test for the two nonlinear wave models, FUNWAVE and the NPMSE, when predicting nonlinear wave characteristics. Both models were driven with the measured water surface elevation time series collected by the 1st wave gauge (reference to Figure 2.2), because no wave measurements were taken at the wave paddle location.

Both FUNWAVE and NPMSE have been previously compared with the Mase and Kirby (1992) [Cox *et al.*, 1991] Test Case 2 data set (Wei and Kirby, 1998; Kaihatu, 2001). Our comparisons were made to develop a template for the two models. We intended to obtain a more thorough understanding of the performance of the two models to provide a basis for our other lab and field comparison.

The FUNWAVE domain was approximately 13m in length, with the source region located about 2m shoreward of the offshore boundary. The bathymetric grid had a spatial step of 5cm. The offshore sponge layer extended approximately 1.5m into the domain and the onshore sponge layer began near the still water shoreline and ended at the shoreward boundary. A schematic of the model domain is show in Figure 2.6. The bottom boundary is shown as the solid blue line; the sponge layers are indicated by the large red dots offshore and onshore of the source region (green crosses); the horizontal extent of the slots is shown by the

smaller black dots.

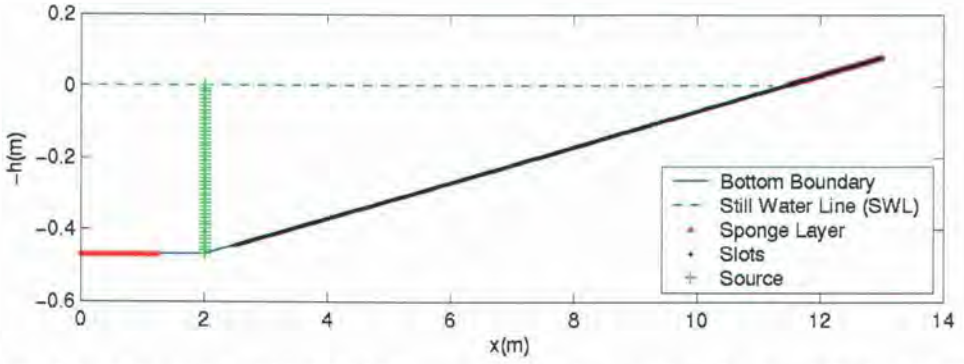

Figure 2.6. Schematic of FUNWAVE cross-shore domain for Mase and Kirby (1992) Test Case 2 simulations. The model input bathymetry is the bottom boundary (blue line).

The Boussinesq model was driven with an input water surface elevation time series 12.5min in length, which had a time step of 0.05s. This time series was broken up into 14 realizations, each 1024 points in length. Within FUNWAVE, the measured input water surface elevation time series was re-sampled at 0.01s, due to the interdependent relationship of the temporal and spatial steps. This interdependent relationship is defined by the Courant condition, where $dt<0.5dx/\sqrt{(gh)}$ (g is the acceleration due to gravity, h is the maximum water depth and a is the wave amplitude).

There were a number of tuning parameters in FUNWAVE which required careful attention. The results were most sensitive to the adjustment of the parameters which related to bottom friction, the eddy viscosity, the slot width and length, and the temporal filter-step. These parameters were set to 0.0, 0.35, 50, 10.5m, and 200 steps, respectively. A more complete discussion of the input parameters and their typical value ranges can be found in Kirby *et al.* (1998).

The NPMSE modeling domain was 9.4 m in length. The bathymetry began at the toe of the slope (corresponding to the 1st wave gauge location) and extended to the still water shoreline. The spatial step was slightly less than 0.3cm. The input time series was 102.4s long, with a temporal step of 0.025s. In contrast to FUNWAVE, the wave measurements and NPMSE model used the same time step, therefore, the input times was taken directly from the measurements and no re-sampling was necessary. 500 frequency components were maintained in the NPMSE model simulation.

Comparisons were also made for FUNWAVE using only 102.4s, and found that the

results were representative of the results shown in Figure 2.7, where FUNWAVE utilizes a 12.5 min input time series. Also, comparisons were made between the measured statistics using the full time series and the one containing only 102.4 seconds. Once again, it was found that the shorter time series was representative of the total measured time series, justifying our use of the shorter time series to drive NPMSE.

Compared to FUNWAVE, NPMSE has few tuning parameters. Also, the predictions by NPMSE were found to be not nearly as sensitive to the required input parameters as the FUNWAVE results. In the dissipation model, B and γ were set to 1.0 and 0.7 respectively.

The wave parameter results of the two nonlinear wave models versus the measurements are shown in Figure 2.7. In this figure, comparisons of root-mean-square wave height (H_{rms}) (upper panel), wave skewness (upper central panel), and wave asymmetry (lower central panel) are shown. The bathymetry is plotted in the lower panel.

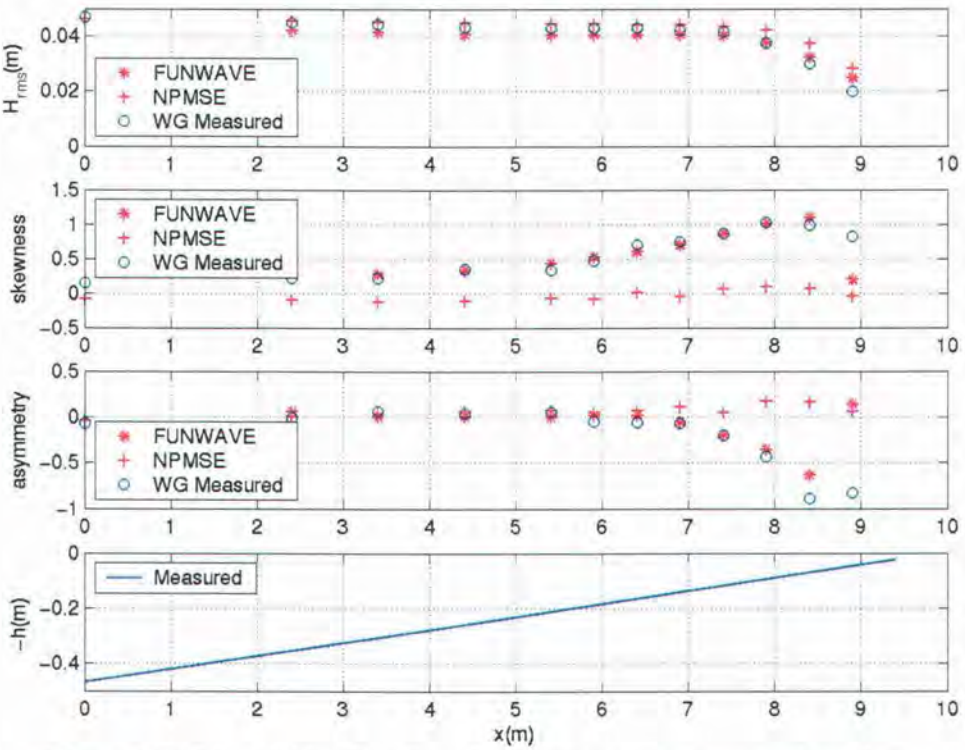

Figure 2.7. Mase-Kirby Test Case 2: Wave parameter comparisons between FUNWAVE (red asterisks), NPMSE (red crosses), and the wave gauge measurements (blue circles); Comparisons of Hrms (upper panel), skewness (upper central panel), and asymmetry (lower central panel). The cross-shore profile is shown in the lower panel.

The models performed quite well at predicting the H_{rms} through the shoaling region.

From the breaking location shoreward, the NPMSE model overpredicted the wave height more so than FUNWAVE. The NPMSE did rather poorly at predicting the wave skewness throughout the domain, where FUNWAVE did very well at predicting both nonlinear quantities (skewness and asymmetry). Skewness is analogous to the degree of nonlinearity of the system. A wave becomes skewed due to nonlinear interactions between wave components at different frequencies, as well as self-self wave interactions. These interactions cause the transfer of energy to higher harmonics producing a system that is increasingly nonlinear. Therefore, to properly simulate a highly nonlinear system the model must be correct in nonlinearity to an order which is significant compared with the observations. The NPMSE solves for the full linear dispersion relationship, therefore, it performs well when predicting effects of dispersion. FUNWAVE, being derived from the shallow water wave equations, is only accurate to the 2nd order in dispersion. In contrast, FUNWAVE is fully nonlinear, hence the superior predictions of nonlinear wave characteristics by FUNWAVE over NPMSE. The water surface elevation skewness and asymmetry skill values, shown in Table 2.1, are thrown off for FUNWAVE by the poor quality prediction at the most onshore gauge location (WG 12). If the predictions by FUNWAVE at this gauge location are not included in the skill computation, the model skill when predicting H_{rms}, skewness and asymmetry are 0.99, 0.95, and 0.99, respectively. Skill values were also computed for FUNWAVE when using on the first 102.4s of the predicted time series (same length as NPMSE predictions) and comparable values were obtained when including and not including the predictions at the most shoreward gauge location.

Table 2.1. Summary of wave model skill (r^2-values) for the Mase and Kirby (1992) [Cox et al., 1991] Test Case 2 data set.

	FUNWAVE	NPMSE	FUNWAVE (WG 1-11)
η Skewness	0.58	0.80	0.95
η Asymmetry	0.30	0.28	0.99
H_{rms}	1.00	0.98	0.99

The NPMSE model did well at predicting wave asymmetry seaward of the surf zone. Within the surf zone, the asymmetry predictions by the NPMSE model became quite poor, therefore, showing no significant skill (r2-value of 0.2810) (Table 2.1). From Figure 2.7, it appears that the model never predicted the forward pitching of the wave in the surf zone,

hence the sign of the predicted asymmetry in this region was positive. NPMSE predictions of asymmetry are consistently quite poor in the surfzone because of the dissipation model. The frequency-weighting parameter, F, can be tuned so that the model better predicts skewness or asymmetry. We were more interested in the skewness predictions, and wanted to maintain a constant F that would be consistent for all our comparisons, so we chose to maintain the suggested F by Kaihatu (2001).

Near the shoreline the magnitude of the nonlinear wave characteristics were consistently under predicted by FUNWAVE, which has been a problem in the past with this model (Kennedy *et al.*, 2000)

2.4 LIP11D: Test Case 1B

LIP11D Test Case 1B was designed to simulate energetic, high-wave hydrodynamic conditions which were representative of storm conditions during which offshore sand bar migration events have been observed (Kraus *et al.*, 1991). In accordance with simulating highly energetic conditions, a large offshore significant wave height of 1.5m and peak period of 5s were chosen. Due to the shallow offshore depth (h~4.1m), the waves began to brake almost immediately off the wave paddle. These observed offshore conditions violate the boundary conditions employed by FUNWAVE. This Boussinesq wave model generates a wave in its source region which is approximately double the energy of the observations, because half of the wave will travel shoreward (which is the wave of interest in the model), while the remaining half of the wave will travel seaward, upon which it will be absorbed by the offshore sponge layer. One of the restrictions of FUNWAVE is that the generated wave at the source location may be no larger than approximately half the local water depth, or the model will be unstable. For Test Case 1B a wave with a height of 3m would need to be generated at the wave paddle (source region), therefore, making this model inoperable when attempting to simulate the observed hydrodynamic conditions.

The NPMSE model was driven with the measured water surface elevation from the wave gauge located at the wavemaker (x~20m) for 2nd, 3rd, 4th, 7th, 8th, and 10th test hours. Other hours from Test Case 1B were excluded since all the required measurements (i.e. measured offshore water surface elevation, bathymetry, and the pressure sensors and current meter data) were not available. The NPMSE modeling domain was approximately 165m in

length. The bathymetry began at the wavemaker and extended to the still water shoreline. The spatial step was approximately 5cm. The input time series was 409.6s long, with a temporal step of 0.1s. The wave model maintained 300 frequency components, giving it a modeled frequency range from 0.002Hz to 0.7Hz. The high frequency limit of the modeled range is approximately 3.5 times the peak frequency. We attempted to choose combinations of time series length and the number of frequency components to obtain a modeled frequency range at least 3-times the peak frequency. It was found that the majority of the energy within the observed system would be contained within these frequency bounds. The wave shape parameters B and γ were set to 1.0 and 0.7 respectively.

The wave parameter results of the NPMSE wave model and the observations are shown in Figure 2.8 and 2.9. The fully dispersive wave model exhibited significant skill when predicting the cross-shore evolution of the H_s with an associated r^2-value of 0.97 (yellow-highlighted line in Table 2.2). The shape of the observed wave height profile is captured by the model through the two breaking locations, which were due to the presence of the bar and the decreasing water depth near the shoreline. The NPMSE did not show skill predicting the wave skewness (r^2-value of 0.26) or asymmetry (r^2-value of 0.35). For all the test hours in Test Case 1B, the model consistently predicted the observed sign (+) of skewness. In contrast, the model did not consistently predict the correct sign of asymmetry, which implies the model was predicting the wave to pitch in the opposite direction of the observations at particular gauge locations. Overall, the wave model did exhibit significant skill when predicting the cross-shore evolution of the wave height, but had a broad range of skill-values when predicting wave skewness and asymmetry for Test Case 1B (Table 2.2)

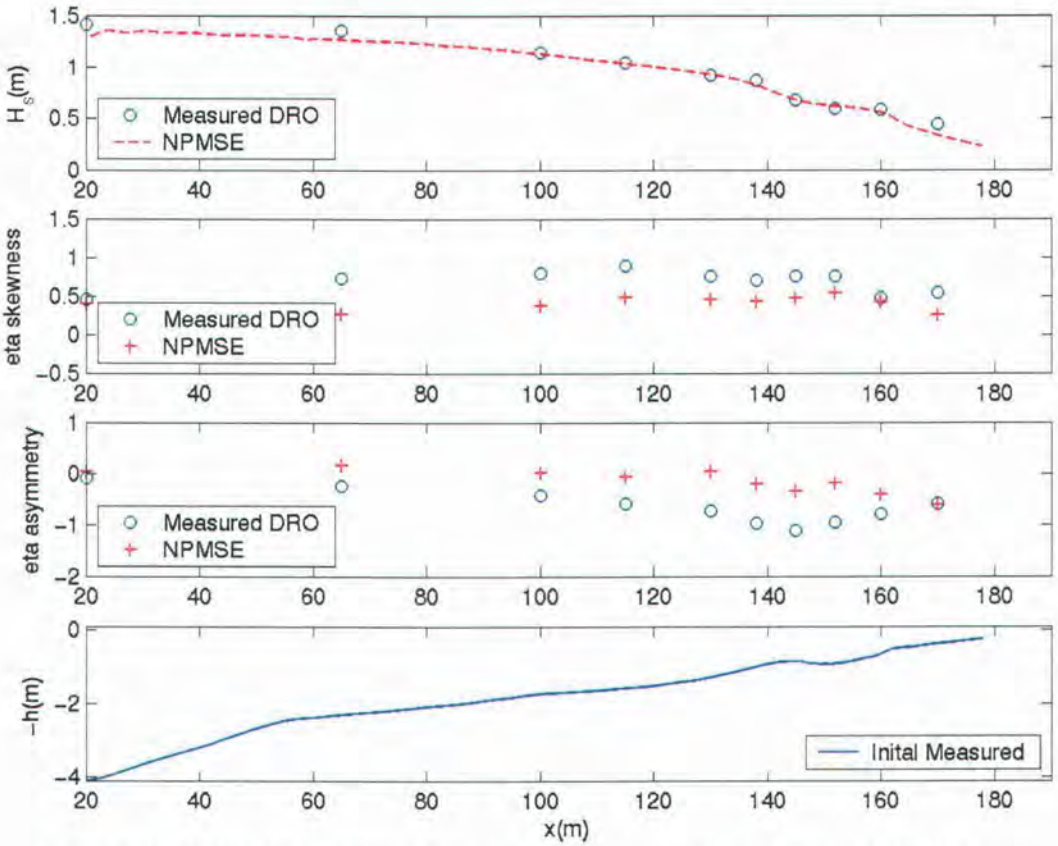

Figure 2.8. LIP11D 1B0304: Wave parameter comparisons between NPMSE (red crosses) and the wave gauge measurements (blue circles); Comparisons of H_s (upper panel), water surface elevation skewness (upper central panel), and water surface elevation asymmetry (lower central panel). The cross-shore profile is shown in the lower panel.

Table 2.2. LIP11D 1B0304: Skill (r2-values) of NPMSE wave model when predicting the water surface elevation. Model-to-data comparisons between wave height (H_{rms}), wave skewness, and wave asymmetry.

Test Hour	H_{rms}	NPMSE skewness	NPMSE asymmetry
1B0213	0.98	0.62	0.52
1B0304	0.97	0.26	0.35
1B0405	0.98	0.47	0.52
1B0707	0.93	0.06	0.33
1B0808	0.97	0.09	0.61
1B1010	0.97	0.26	0.30
Mean	**0.96**	**0.29**	**0.44**
Std. Dev.	**0.02**	**0.22**	**0.13**

The upper and lower central panels of Figure 2.9 are the comparison of velocity

skewness and asymmetry, respectively. The comparisons of skewness are made between the observations from the current meters (EMF) and pressure sensor (DRO), and predictions by the NPMSE, DB1995, and D2000. The respective model skill (r^2) values for skewness are listed in Table 2.3, when comparing observations from the pressure sensors and model predictions with the current meter observations. The asymmetry comparisons are also made between the EMF and DRO measurements, but only by the model predictions by NPMSE and DB1995. The wave velocity asymmetry skill values are listed in Table 2.4.

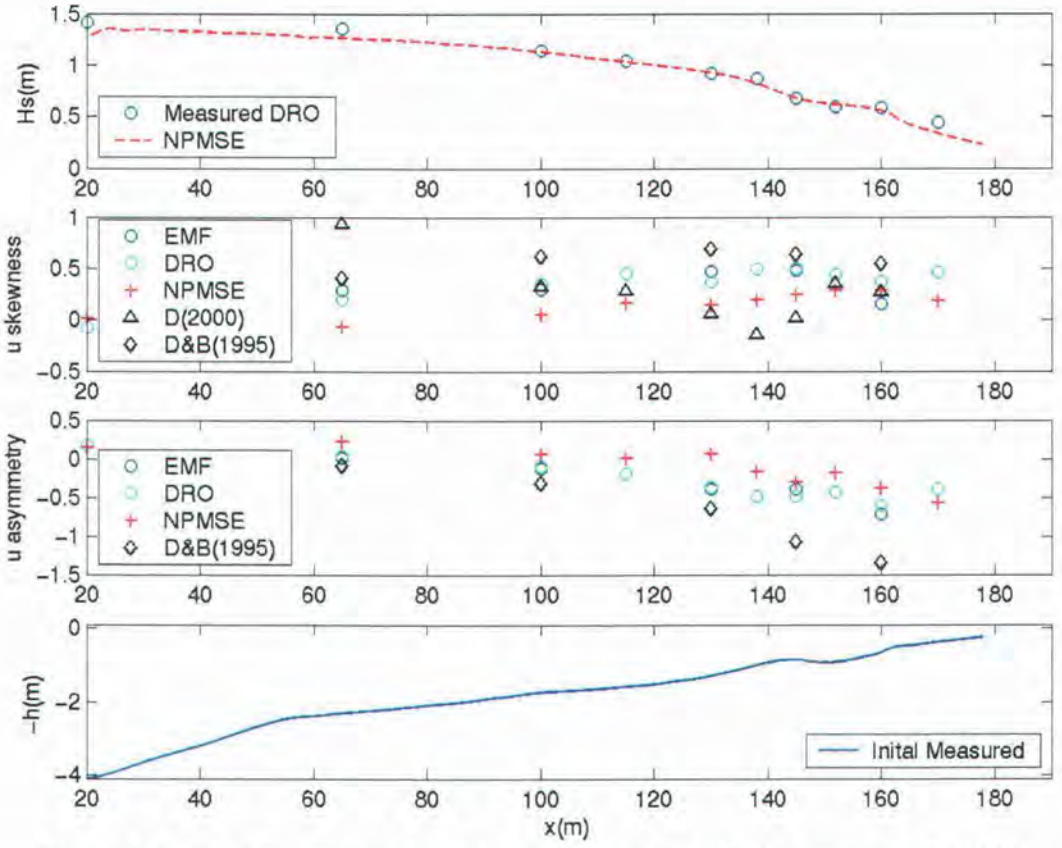

Figure 2.9. Wave parameter comparisons between NPMSE (red crosses), DB1995 (black diamonds), D2000 (black triangles), pressure-derived wave velocities (cyan circles), and the current meter measurements (blue circles); Comparisons of H_s (upper panel), wave velocity skewness (upper central panel), and wave velocity asymmetry (lower central panel). The cross-shore profile is shown in the lower panel.

The wave velocity skewness computed from the pressure-derived measurements does not compare well with the current-meter computed skewness, particularly near the two most significant breaking locations (near the sand bar crest and shoreward of the trough). There

are cross-shore locations where the skewness compares very well, but they are isolated, hence the poor skill (r^2-value) of 0.24. These differences are likely due to errors associated with the use of linear wave theory to convert from pressure to velocity for highly nonlinear, energetic waves. Also, relevant differences may be in the vertical locations of the measurements. The current meters are located 1/3 of the total water depth off the bed, but the pressure-derived velocities are corrected for a vertical location at the bed (and not taking into consideration bottom boundary layer effects). The NPMSE is not comparing well to the observations, hence a very poor skill value of 0.04 (Table 2.3). The model is not properly quantifying the observed velocity skewness, nor is it simulating the observed oscillations in the cross-shore trend. The NPMSE predicts a smooth and steady evolution of velocity skewness shoreward. The empirical models also appear to exhibit no skill when predicting the velocity skewness for this particular test hour. It is important to note that this particular test hour has predictions of velocity skewness by NPMSE which are significantly worse than the other test hours. This test hour was chosen to illustrate the predictions made by the empirical models. For the 4th test hour DB1995 shows significant skill (r^2-value of 0.91) and the NPMSE wave model and D2000 show some skill (r^2-values of 0.75 and 0.64, respectively) when predicting velocity skewness. Over all, NPMSE, DB1995, and D2000 show some skill for other test hours, while the pressure-derived velocities exhibited very little skill, with the exception of the 7th test hour comparisons.

The velocity asymmetry predictions were markedly improved compared with the skewness predictions. The NPMSE predictions tended to follow a similar cross-shore trend compared to the observations of wave velocity asymmetry (Figure 2.9, lower central panel). There are a few offshore locations where the wave model is predicting little asymmetry and two locations where the sign of the asymmetry is predicted incorrectly, which implies the model is pitching the waves in the opposite direction of the observations. This error does not appear to affect the model-to-data comparisons significantly, likely due to the very small values of predicted skewness at these locations (Table 2.4). The pressure-derived velocity asymmetry consistently compares very well with the observations by the current meter, with an average r^2-value of 0.82 and a standard deviation of 0.14. DB1995 predictions of wave velocity asymmetry are also consistently quite good, which is interesting since the empirical model typically over predicted the magnitude of the asymmetry in the surf zone.

The predictions of the nonlinear velocity quantities are rather variable by all models, as well as by the pressure-derived velocities. This variability simply illustrates the difficulty

of consistently making accurate predictions of wave velocity skewness and asymmetry.

Table 2.3. LIP11D 1B0304: Skill (r^2-values) of velocity skewness predictions by the NPMSE wave model, the pressure-derived velocities, DB1995, and D2000.

Test Hour	NPMSE	DRO	DB1995	D2000
1B0213	0.70	0.46	0.62	0.37
1B0304	0.04	0.24	0.12	0.01
1B0405	0.75	0.35	0.91	0.64
1B0707	0.58	0.71	0.10	0.61
1B0808	0.62	0.52	0.17	0.59
1B1010	0.54	0.23	0.05	0.31
Mean	**0.54**	**0.41**	**0.33**	**0.42**
Std. Dev.	**0.26**	**0.19**	**0.35**	**0.25**

Table 2.4. LIP11D 1B0304: Skill (r2-values) of velocity asymmetry predictions by the NPMSE wave model, the pressure-derived velocities, and DB1995.

Test Hour	NPMSE	DRO	DB1995
1B0213	0.99	0.98	0.96
1B0304	0.81	0.93	0.84
1B0405	0.82	0.94	0.90
1B0707	0.68	0.75	0.80
1B0808	0.48	0.69	0.78
1B1010	0.35	0.66	0.76
Mean	**0.69**	**0.82**	**0.84**
Std. Dev.	**0.24**	**0.14**	**0.08**

One-to-one comparisons of velocity skewness and asymmetry are shown in Figure 2.10. The velocity skewness (left panel) comparisons are made between the measured velocities and the pressure-derived velocities, NPMSE predictions, DB1995 predictions, and D2000 predictions. The same comparisons of velocity skewness are made of velocity asymmetry (right panel), except for D2000. These two panels magnify the quality of the pressure-derived velocity time series. As stated above, the asymmetry of the pressure-derived velocities compares very well, while the skewness oscillate around current meter observations. The NPMSE predictions of velocity skewness and asymmetry are

underpredicted, which is the opposite trend exhibited by the DB1995 predictions. Overall, these two comparisons illustrate the trends displayed by each model predictions of velocity skewness and asymmetry, as well as the pressure-derived velocity skewness and asymmetry.

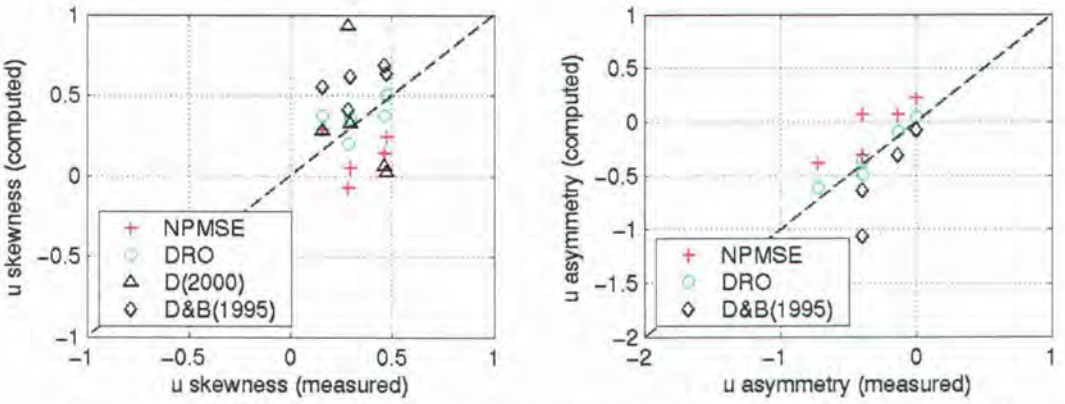

Figure 2.10. LIP11D 1B0304: One-to-one comparisons of predicted wave velocity skewness (left panel) and asymmetry (right panel). The measurements were from the measured velocity. The predictions were computed from the pressure-derived velocities (cyan circles), the velocity time series predicted by the NPMSE (red crosses), and from the empirical formulations of DB1995 (black diamonds) and D2000 (black triangles).

2.5 LIP11D: Test Case 1C

LIP11D Test Case 1C was designed to simulate mildly energetic, low-wave hydrodynamic conditions which were representative of calm conditions during which shoreward sand bar migration events have been observed (Kraus *et al.*, 1991). Waves with an offshore significant wave height of 0.6m and a peak period of 8 seconds were generated for all test hours in Test Case 1C which had the required measurements for the hydrodynamic comparison available. The generated waves typically shoaled to the sand bar location (x~140m) and then broke. The waves would re-shoal slightly and then break again near x~160m.

NPMSE and FUNWAVE were used to simulate the observed hydrodynamics of Test Case 1C for the 1st through the 5th, 8th, and 11th test hours. Other test hours were excluded from this study because all the necessary measurements required by the models and for the comparisons were not available. Both models were driven with the measured offshore water surface elevation time series and both produce predictions of water surface elevation time

series. Two empirical formulations were also used in this study to predict higher order quantities describing the nonlinearity of the hydrodynamics. These two formulations are DB1995 and D2000. Skewness and asymmetry predictions were compared with the observations and r^2-values were computed to describe the skill of each prediction tool.

The NPMSE model was driven with the measured water surface elevation from the wave gauge located at the wavemaker (x~20m). The NPMSE modeling domain was approximately 165m in length. The bathymetry began at the wavemaker and extended to the still water shoreline. The spatial step was approximately 5cm. The input time series was 819.2s long, with a temporal step of 0.1s. The wave model maintained 500 frequency components, giving it a modeled frequency range from 0.001Hz to 0.6Hz. The wave shape parameters B and γ were set to 1.0 and 0.7 respectively.

FUNWAVE utilized an input measurement time series 3,900.3s in length, with a time step of 0.1s. Nine 409.6s realizations were made from the measured times series and interpolated to time series 20,480 points in length with a new time step of 0.02s. The first 2,000s of the predicted water surface elevation were output from the model and used for the comparisons in this study, because they were representative of the entire simulation, and by using fewer points in time, the computational time was reduced. The spatial step for the 355m cross-shore domain was 0.25m. The source region was located 165m shoreward of the offshore boundary. The offshore sponge layer was 87.5m long, which was slightly longer than two offshore wavelengths. The onshore sponge layer was 27.5m long and extended shoreward from the still water shoreline. The slots, used to simulate run-up, were 179.5m long and extended seaward from the still water shoreline.

The wave parameter results of NPMSE and FUNWAVE, and the observations are shown in Figures 2.11 and 2.12. The fully dispersive wave model exhibited skill when predicting the cross-shore evolution of the H_s with an associated r^2-value of 0.86 (yellow-highlighted line in Table 2.5). More specifically, NPMSE performed well when predicting the shoaling wave height, however, it did not perform as well through the breaking region over the sand bar. Shoreward of the second breaking location, the model again appeared to perform well. Within FUNWAVE, the offshore wave height was over predicted and subsequently threw off the first three locations of the predicted time series output. The model appeared to 'recover' near the seaward edge of the slots and then produced better results to the most shoreward breaking location, beyond which the model predicts an increase of the wave height. Excluding the most seaward and shoreward predictions by FUNWAVE, the

model mostly predicts the shoaling and breaking events of the waves, with results similar to NPMSE. The FUNWAVE skills for predicting cross-shore wave height were computed using only the gauge locations shoreward of x=35m. Therefore, the most offshore predictions, at the source location, were excluded because of the increased variance. The FUNWAVE skill values for the predictions of skewness and asymmetry for waves and velocities were computed using all the available cross-shore gauge locations, hence, the source region predictions were included because the skill values were not sensitive to inclusion of the water surface elevation predictions near the wave paddle.

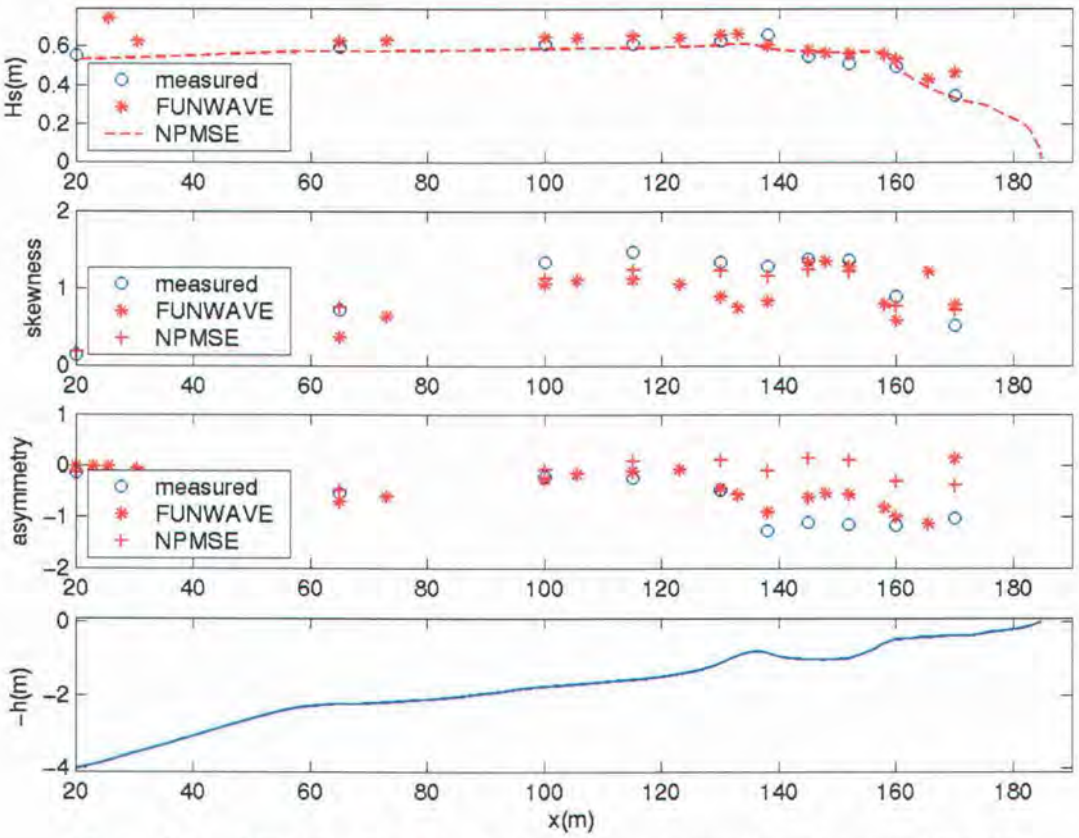

Figure 2.11. LIP11D 1C0405: Wave parameter comparisons between NPMSE (red crosses), FUNWAVE (red asterisks), and the wave gauge measurements (blue circles); Comparisons of H_s (upper panel), water surface elevation skewness (upper central panel), and water surface elevation asymmetry (lower central panel). The cross-shore profile is shown in the lower panel.

The skewness predictions by the NPMSE wave model exhibited significant skill (r^2-

value of 0.95), however the model exhibits no skill when predicting the wave asymmetry (r^2-value of 0.00). For all the test hours in Test Case 1C, the model consistently predicted the observed sign (+) of skewness. NPMSE predictions of skewness followed the cross-shore trend of the observations, with an increase of skewness in the shoaling region and a significant decline in wave skewness between the 8th and 9th wall-fixed instrument locations. FUNWAVE predictions of skewness oscillate throughout the cross-shore, and are mostly smaller than the observations. The wave asymmetry is predicted well by FUNWAVE, with the exception of the most onshore gauge location (which decreases the skill value of the model). The forward-pitching of the wave before and during breaking is simulated by FUNWAVE, but not by NPMSE. The fully dispersive wave model once again predicts pitching of the wave in the opposite direction of the observations immediately before and after the offshore breaking location. Overall, NPMSE performed well when predicting wave skewness. In contrast, it poorly predicted wave asymmetry (Table 2.5, 6th column). FUNWAVE did not predict the wave skewness as well as NPMSE, with an average skill value of 0.77 and a standard deviation of 0.11 (Table 2.5, 3rd column). This model performed well when predicting wave asymmetry, with the exception of the most onshore gauge location which was severely underpredicted, therefore, decreasing the skill values.

Table 2.5. LIP11D 1C: Skill (r2-values) of FUNWAVE and NPMSE when predicting the water surface elevation. Model-to-data comparisons between wave height (H_{rms}), wave skewness, and wave asymmetry.

Test Hour	FUNWAVE Hrms	NPMSE Hrms	FUNWAVE skewness	NPMSE skewness	FUNWAVE asymmetry	NPMSE asymmetry
1C0102	0.87	0.84	0.74	0.94	0.35	0.00
1C0204	0.53	0.77	0.69	0.89	0.14	0.14
1C0313	0.86	0.87	0.70	0.94	0.37	0.00
1C0405	0.85	0.86	0.77	0.95	0.33	0.00
1C0514	0.78	0.88	0.96	0.91	0.26	0.00
1C0807	NA	0.79	NA	0.94	NA	0.02
1C1110	NA	0.77	NA	0.73	NA	NA
Mean	**0.78**	**0.83**	**0.77**	**0.90**	**0.29**	**0.03**
Std. Dev.	**0.14**	**0.05**	**0.11**	**0.08**	**0.09**	**0.06**

The respective model skill (r^2) values for skewness are listed in Table 2.6, when comparing observations from the pressure sensors and model predictions with the current

meter observations (which are taken to be true). The asymmetry comparisons are also made between the EMF and DRO measurements, but only for the model predictions by NPMSE and DB1995. The wave velocity asymmetry skill values are listed in Table 2.7. The version of FUNWAVE used in this study does not predict wave velocities, therefore, wave velocity time series was computed from the predicted water surface elevation time series, using linear wave theory.

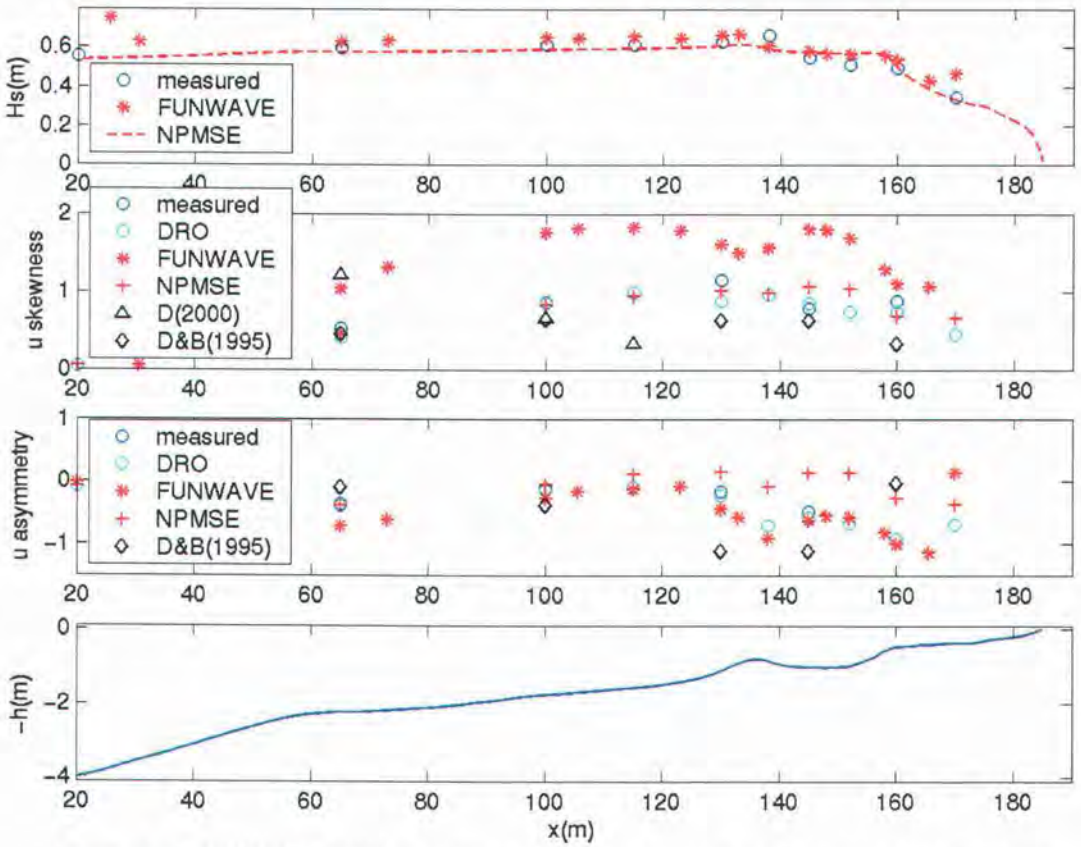

Figure 2.12. LIP11D 1C0405: Wave parameter comparisons between NPMSE (red crosses), FUNWAVE (red asterisks), DB1995 (black diamonds), D2000 (black triangles), the pressure-derived velocities (cyan circles), and the current meter measurements (blue circles); Comparisons of H_s (upper panel), wave velocity skewness (upper central panel), and wave velocity asymmetry (lower central panel). The cross-shore profile is shown in the lower panel.

FUNWAVE compares quite poorly with the current meter measurements of wave velocity skewness (Figure 2.12, upper middle panel) for test hour 0405. The Boussinesq model severely overpredicted the velocity skewness, even though it slightly underpredicted the wave skewness. The wave velocity skewness predictions by FUNWAVE show little skill,

hence they are quite poor for all the modeled test hours in Test Case 1C (which are shown in Table 2.6). The wave velocity skewness predicted by NPMSE appears to compare well with the pressure-derived velocity skewness, but has a cross-shore profile which differs from the current meter measurements, hence the skill value of 0.50 (Table 2.3). The NPMSE skill-values varies significantly between all the test hours simulated, which is indicated by the equivalent mean and standard deviation of the skill values. The empirical models also appear to exhibit almost no skill when predicting the velocity skewness for this particular test hour. D2000 shows some skill for most test hours, as opposed to DB1995 which shows no skill for the majority of test hours.

The velocity asymmetry predictions by FUNWAVE for all test hours were markedly superior to the skewness predictions. FUNWAVE appears to truly simulate the pitching of the wave due to wave shoaling and breaking, resulting in an average skill value of 0.76 and a standard deviation of 0.04 (Table 2.7). The NPMSE predictions were overall quite poor for all test hours. Similar cross-shore trends were exhibited by the model predictions of velocity asymmetry, as shown for test hour 0405 in the lower central panel of Figure 2.12. NPMSE appears to predict the offshore asymmetry evolution decently, but an offset exists between the predictions and measurements in the surf zone. DB1995 predictions of wave velocity asymmetry are mostly poor, with the exception of test hour 1110. The empirical model predictions of velocity asymmetry have a jumpy cross-shore profile, contributing to the poor model skill values listed in Table 2.8.

Table 2.6. LIP11D 1C: Skill (r2-values) of velocity skewness predictions by the FUNWAVE, NPMSE, D2000, and DB1995.

Test Hour	FUNWAVE	NPMSE	D2000	DB1995
1C0102	0.25	0.43	0.11	0.17
1C0204	0.22	0.19	0.47	0.29
1C0313	0.02	0.01	0.47	0.32
1C0405	0.22	0.50	0.37	0.10
1C0514	0.17	0.25	0.48	0.50
1C0807	NA	0.04	0.58	0.04
1C1110	NA	0.01	0.42	0.15
Mean	**0.18**	**0.20**	**0.42**	**0.22**
Std. Dev.	**0.09**	**0.20**	**0.15**	**0.16**

Table 2.7. LIP11D 1C: Skill (r2-values) of velocity asymmetry predictions by FUNWAVE, NPMSE, and DB1995.

Test Hour	FUNWAVE	NPMSE	DB1995
1C0102	0.69	0.21	0.27
1C0204	0.75	0.13	0.06
1C0313	0.80	0.08	0.10
1C0405	0.76	0.19	0.26
1C0514	0.79	0.08	0.04
1C0807	NA	0.35	0.10
1C1110	NA	1.17	0.77
Mean	**0.76**	**0.31**	**0.23**
Std. Dev.	**0.04**	**0.39**	**0.26**

2.6 DUCK94: September 1st –September 5th

This initial observed seaward bar movement period was highly energetic, with an offshore wave climate that was characterized by a mean H_{rms} of 1.7m and an average peak period of 6.3s. The short wave period is not uncommon on the East Coast of the US, and during large storm events a peak period of 4s has been commonly observed. Figure 2.13 shows the hydrodynamic predictions by NPMSE, compared with the measurements, for September 3rd during the 22nd hour. Due to the large offshore wave height in combination with the shallow water depths, FUNWAVE's offshore boundary conditions were violated, therefore, no comparisons were made with FUNWAVE for this 5-day time period.

The upper panel of Figure 2.13 compares the cross-shore predictions of H_{rms} by NPMSE (red-dash), with the pressure-derived measurements (blue-circles). The wave model performed well seaward of the offshore breaking location. The model did not quite dissipate enough energy during this initial breaking period, but appears to qualitatively predict the cross-shore wave evolution shoreward of the bar (r^2~0.7, Table 2.8). NPMSE showed skill when predicting the cross-shore evolution of the wave height for most test periods in this 5-day simulation, with an average r^2~0.72 and a standard deviation of 0.21 (Table 2.8).

The predictions of the nonlinear characteristics of the water surface elevation varied significantly during this simulation. Skewness predictions compared well with the pressure-derived observations (r^2~0.83) for this particular test hour (shown in Figure 2.13, upper

central panel). The two cross-shore locations that compare the least well with the observations are co-located with the location of the poorest predictions of H_{rms}. The most shoreward predictions of skewness, as well as at the instrument locations over the sand bar, compare very well with the observations.

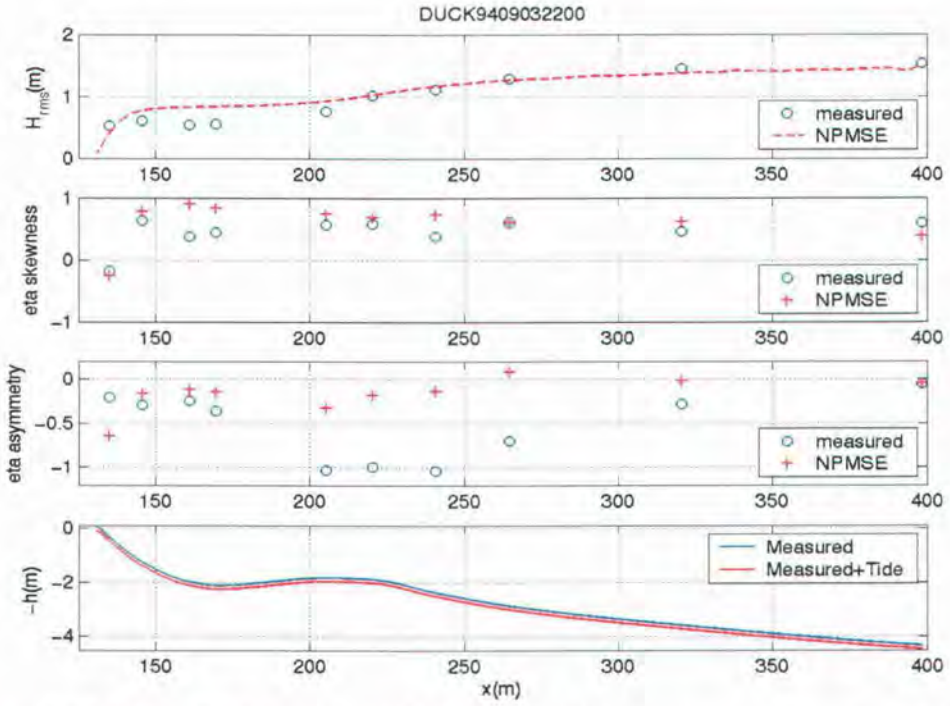

Figure 2.13. DUCK94 September 3rd, 22nd hour: Wave parameter comparisons between NPMSE (red crosses) and the pressure-derived water surface elevation (blue circles); Comparisons of H_{rms} (upper panel), water surface elevation skewness (upper central panel), and water surface elevation asymmetry (lower central panel). The cross-shore profile is shown in the lower panel.

The water surface elevation asymmetry predictions by NPMSE are compared to the pressure-derived observations in the lower middle panel of Figure 2.13. The asymmetry predictions compare very poorly with the observations throughout the central section of the cross-shore domain, and appear to somewhat improve near the sand bar. This test period of asymmetry predictions compared more poorly with the observations than most of the other test hours in this simulation (Table 2.8). The lower panel displays the bathymetry interpolated from measurements at the sonar altimeter locations with (red) and without (blue) the addition of the tide. The tidal influence on the total water depth was minimal for this test

period, but has a noticeable effect on the wave evolution, especially during energetic wave conditions, when the tide is typically greater than 0.5m. In this manuscript, results are only being shown when the tide was included, but preliminary simulations were performed with out the tidal influence, providing insight into the contributions to the hydrodynamics by the presence of the tide.

Table 2.8. DUCK94 September 3rd, 22nd hour: Skill (r^2-values) of NPMSE wave model when predicting the water surface elevation. Model-to-data comparisons between wave height (H_{rms}), wave skewness, and wave asymmetry.

Test Period	NPMSE H_{rms}	NPMSE skewness	NPMSE asymmetry
9032200	0.70	0.83	0.02
Mean	0.72	0.44	0.21
Std. Dev.	0.21	0.27	0.25

Figure 2.14 shows the nonlinear wave velocity quantities predicted by the models and empirical formulations compared to the observations from the pressure sensors and current meters. The upper central panel compares the cross-shore profiles of the velocity skewness. NPMSE again is performing quite well when predicting the skewness profile (r^2~0.83, Table 2.9), especially over the bar crest and near the shoreline. This is important because the shoreline and the bar crest are typically very active regions of sediment transport. These excellent comparisons of velocity skewness imply that the model could potentially perform well in combination with an energetics transport model when predicting bathymetric profile evolution during energetic wave conditions. The empirical formulations do not be compare well with the observations for this particular test period, but have similar averages (r^2~0.4) and standard deviations (r^2~0.3) of skill to the NPMSE and pressure-senor derived velocity skewness, for all test periods in this 5-day simulation.

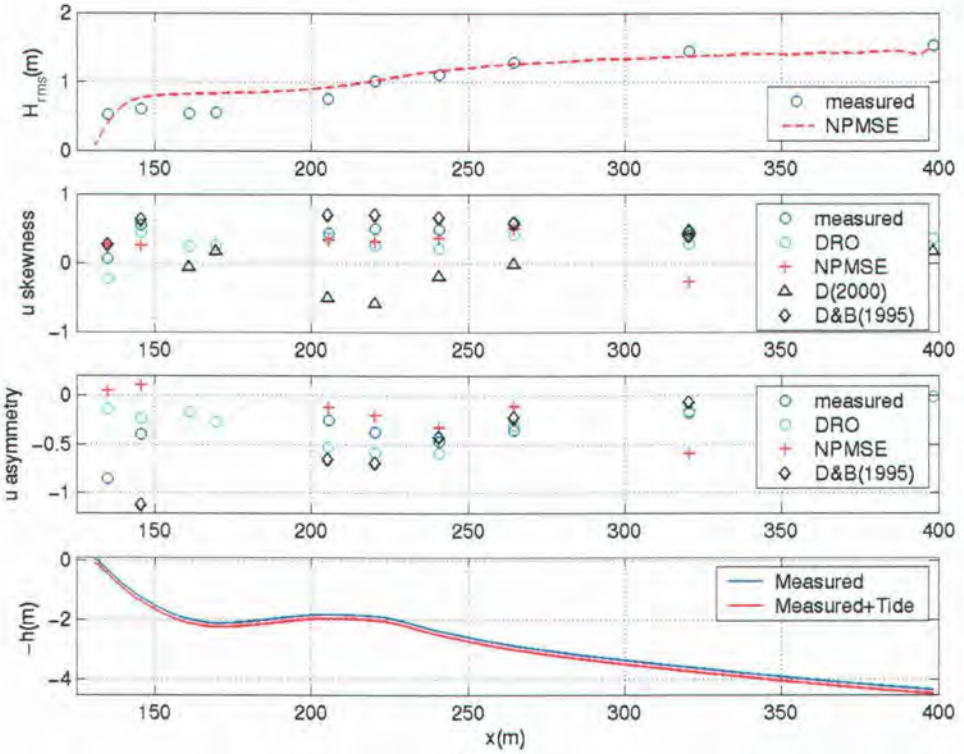

Figure 2.14. DUCK94 September 3rd, 22nd hour: Wave parameter comparisons between the current meter measurements (blue circles), pressure-derived velocities (cyan circles), NPMSE (red crosses), DB1995 (black diamonds), and D2000 (black triangles); Comparisons of H_{rms} (upper panel), wave velocity skewness (upper central panel), and wave velocity asymmetry (lower central panel). The cross-shore profile is shown in the lower panel.

The predictions of velocity asymmetry by NPMSE compare better with the velocity observations than the water surface elevation asymmetry predictions, but are still flawed. The predictions near the shoreline are especially poor compared to the current meter observations. The pressure-derived velocity asymmetry also compares poorly to the current meter observations, resulting in a test period skill value of 0.45 (Table 2.10). DB1995 is doing moderately well at predicting the velocity asymmetry for 22nd hour of September 3rd (r^2~0.59), but over all the predictions for asymmetry are quite varied, resulting in an r^2 standard deviation of approximately 0.59 and a mean of only 0.29. This test case is not the best representation of the mean skill predictions of velocity asymmetry, but served as a good visual representation of the common issues the models have near the shoreline and over the bar crest when predicting velocity asymmetry, for all test periods between September 1st and 5th, 1994.

Table 2.9. DUCK94 September 3rd, 22nd hour: Skill (r^2-values) of velocity skewness predictions by the NPMSE wave model, the pressure-derived velocities (DRO), DB1995, and D2000.

Test Period	NPMSE	DRO	DB1995	D2000
9032200	0.83	0.89	0.55	0.44
Mean	0.45	0.42	0.47	0.44
Std. Dev.	0.28	0.26	0.29	0.30

Table 2.10. DUCK94 September 3rd, 22nd hour: Skill (r^2-values) of velocity asymmetry predictions by the NPMSE wave model, the pressure-derived velocities (DRO), and DB1995.

Test Period	NPMSE	DRO	DB1995
9032200	0.42	0.45	0.59
Mean	0.29	0.24	0.29
Std. Dev.	0.24	0.29	0.59

The one-to-one comparisons of velocity asymmetry (right panel) and skewness (left panel) are shown in Figure 2.15. The NPMSE skewness predictions appear to compare very well with the DRO-derived skewness values, which both slightly underpredicted the velocity skewness compared with the current meter measurements (which are taken as true). DB1995 prediction were consistently minimally over-predicted, but on a whole compare significantly better than the D2000 predictions, which are mostly not shown in the figure because they are too offset from the measurements. The velocity asymmetry predictions were quite varied by the three models, hence their large distribution. This figure depicts that the best quantitative predictions of asymmetry were made by DB1995, but DB1995 was unable to make consistent skilled predictions of asymmetry throughout the cross-shore, let alone for all test periods.

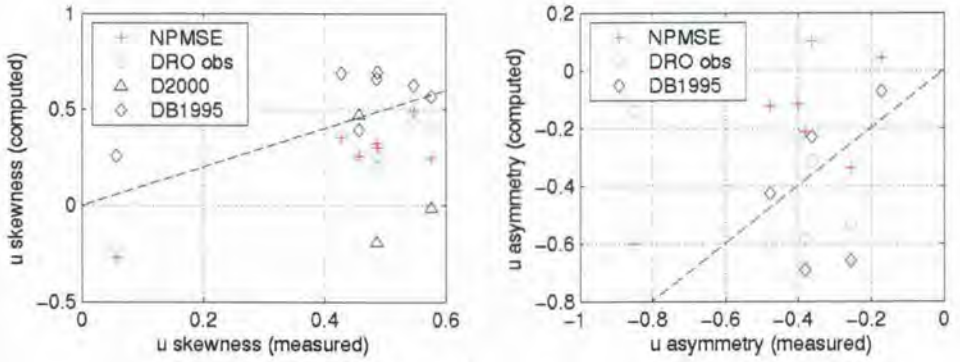

Figure 2.15. DUCK94 September 3rd, 22nd hour: One-to-one comparisons of wave velocity skewness (left panel) and asymmetry (right panel). The measurements were from the measured velocity. The comparisons were computed from the pressure-derived velocities (cyan circles) and the predicted by the NPMSE (red crosses), and from the empirical formulations of DB1995 (black diamonds) and D2000 (black triangles).

2.7 DUCK94: September 22nd – September 27th

September 22nd through the 27th is the period when onshore bar migration was observed at Duck Beach, NC, during DUCK94. The 5-day period was characterized by mildly energetic waves, with offshore H_{rms} ranging from about 0.5m to 1m (starting in the afternoon of the 22nd). The average peak period during this time period was approximately 8s, which is routinely measured during milder wave climates in this coastal region.

The wave height cross-shore profile is shown in the upper panel of Figure 2.16. The offshore wave height prediction by FUNWAVE is admittedly large, but it is a consequence of the method used by FUNWAVE to balance the effects generating propagating waves shoreward and seaward of the source region. This was discussed above in the LIP11D Test Case 1C hydrodynamic study in section 2.5. Ignoring the most offshore FUNWAVE prediction of wave height, the remainder of the profile compares relatively well to the pressure-derived observations seaward of the breaking location. The predicted cross-shore evolution of the wave height by both nonlinear wave models is strikingly similar, especially where they deviate from the measurements. The predicted wave heights at the two gauge locations surrounding the breaking location (x~145m) are larger than the observations, hence, the mediocre skill values of 0.45 for FUNWAVE and 0.35 for NPMSE.

The water surface elevation skewness predictions by the two nonlinear wave models

do not compare well with the observations onshore of x~220m, which approximately corresponds with offshore edge of the trough between the sand bar and the shoreline. In the trough, the wave skewness is significantly over predicted by both the models. Shoreward of the breaking location, FUNWAVE severely underpredicted the wave skewness, while NPMSE still overpredicted skewness compared to the observations. Offshore of this point, the comparisons are decent between the predictions and the measurements. The water surface elevation related skill values for this particular test period, as well as the mean and standard deviation of the skill values for all test periods in the 5-day simulation, are listed in Table 2.11.

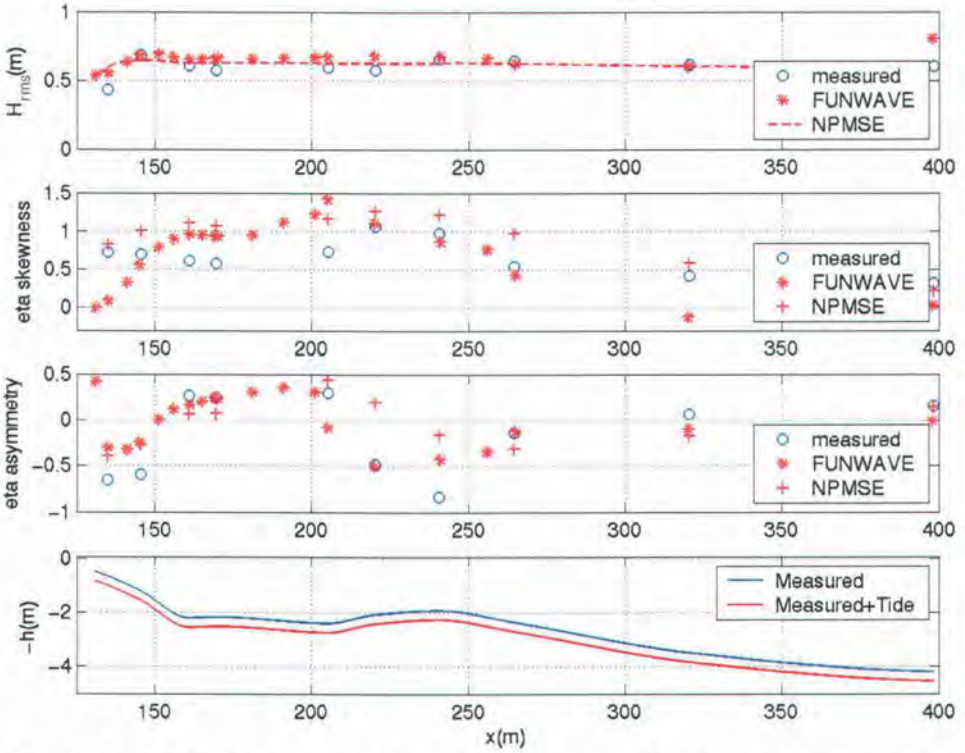

Figure 2.16. DUCK94 September 24th, 13th hour: Wave parameter comparisons between NPMSE (red crosses) and the pressure-derived water surface elevation (blue circles); Comparisons of H_{rms} (upper panel), water surface elevation skewness (upper central panel), and water surface elevation asymmetry (lower central panel). The cross-shore profile is shown in the lower panel.

The wave asymmetry predictions by FUNWAVE were markedly better than the skewness predictions. The cross-shore measured asymmetry evolution is qualitatively predicted well by both models, though FUNWAVE does a better job quantitatively, which is

reflected in its skill value of 0.73, compared with the skill exhibited by NPMSE (r^2~0.36). Impressively, both models predict the observed pitching of the wave forwards and backwards. NPMSE predicted the switching of the sign of the asymmetry more offshore than the observations, therefore,leading to the poor skill value. (This was likely due to predicted minimal forward-pitching of the waves (- asymmetry) over the bar, therefore, when they entered back into deeper water (over the trough) the NPMSE predicted the backward pitching of the wave (+ asymmetry) earlier than the observations.)

Table 2.11. DUCK94 September 24th, 13th hour: Skill (r^2-values) of NPMSE wave model when predicting the water surface elevation. Model-to-data comparisons between wave height (H_{rms}), wave skewness, and wave asymmetry.

Test Period	FUNWAVE H_{rms}	NPMSE H_{rms}	FUNWAVE skewness	NPMSE skewness	FUNWAVE asymmetry	NPMSE asymmetry
9241300	0.45	0.35	0.40	0.65	0.73	0.36
Mean	0.33	0.24	0.51	0.35	0.68	0.22
Std. Dev.	0.21	0.20	0.10	0.29	0.10	0.13

The cross-shore evolution of the observed velocity skewness is qualitatively predicted well by all the models (Figure 2.17). FUNWAVE is mostly over predicting the skewness, but exhibits the same general profile displayed by the observations. Once again, NPMSE is performing well over the bar and near the shoreline, but is noticeably different from the observations offshore of x=300m, leading to a skill value of 0.68. DB1995 and D2000 are both performing well by reproducing some of the quantitative observations. DB1995 predictions of velocity skewness oscillate slightly around the observations through out the cross-shore, which is better scene in Figure 2.24 (left panel), and leads to the model skill of 0.55 for this test period (Table 2.12). From the visual comparison, it appears that the skill should have been better, but the r^2-values are sensitive to the oscillations around the observations, such as exhibited by DB1995. D2000 exhibits more skill for this particular test period, but overall has a similar mean skill value and with larger variation within the population of predictions of velocity skewness for the test case. The large variations significantly decrease it value as a useful predictor of velocity skewness, as well as making other implications about the model application which will be discussed in the conclusions (Chapter 4).

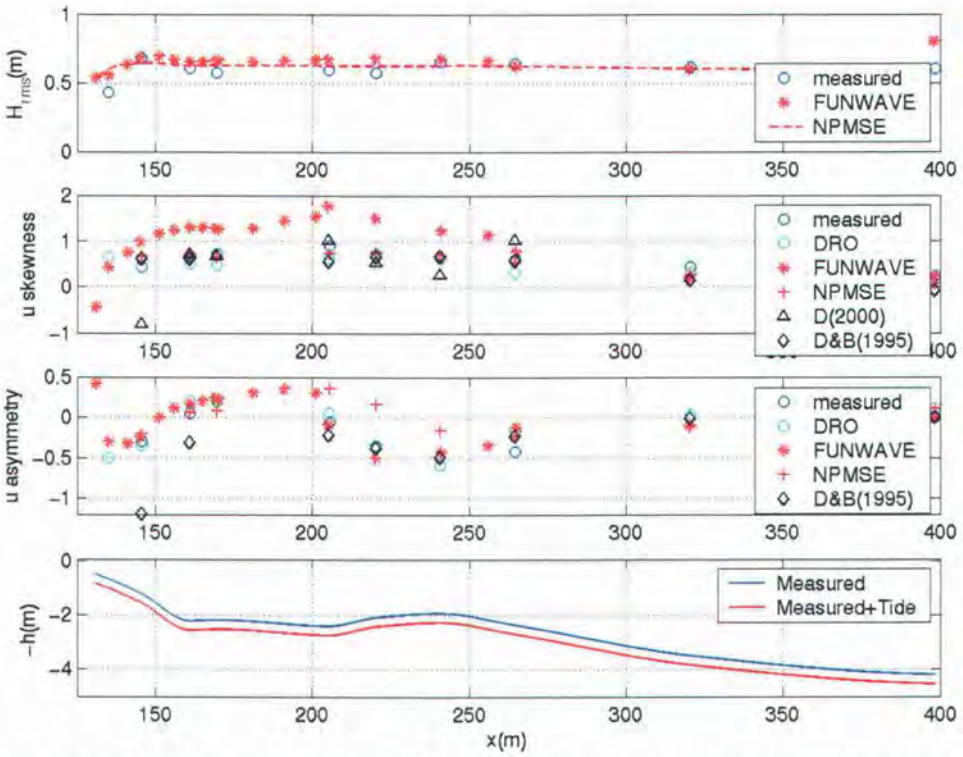

Figure 2.17. DUCK94 September 24th, 13th hour: Wave parameter comparisons between the current meter measurements (blue circles), pressure-derived velocities (cyan circles), NPMSE (red crosses), DB1995 (black diamonds), and D2000 (black triangles); Comparisons of H_{rms} (upper panel), wave velocity skewness (upper central panel), and wave velocity asymmetry (lower central panel). The cross-shore profile is shown in the lower panel.

For September 24th, 13th hour simulations, FUNWAVE is performing quite well when predicting the current-meter-observed velocity asymmetry by quantitatively reproducing many of the observations (r^2-values of 0.72, listed in Table 2.13). In contrast, NPMSE is performing quite poorly when predicting the velocity asymmetry observed during this test period (skill of 0.24). Again, one of the most significant problems with the predictions by NPMSE is the incorrect prediction of the sign of velocity asymmetry, which has been found to be sensitive to the frequency-weighted dissipation scheme utilized by the wave model. The sensitive asymmetry results explain the large standard deviation of the NPMSE skill for this 5-day test case, which are listed in Table 2.13. The pressure-derived velocity asymmetry quantities compare very well with the current-meter observations, hence the significant skill of 0.86 for this test period and a mean of 0.72 (with a standard deviation of 0.21). DB1995 performed poorly when predicting velocity asymmetry for this entire low wave simulation, typically due to one to three gauge location predictions that were extreme, consequently

ruining the model skill. The most onshore gauge location prediction by DB1995 tended to be quite poor and is subsequently not seen in many of the plots due to the extreme value lying outside the figure boundaries.

Table 2.12. DUCK94 September 24th, 13th hour: Skill (r^2-values) of velocity skewness predictions by FUNWAVE, NPMSE, the pressure-derived velocities, DB1995, and D2000.

Test Period	FUNWAVE	NPMSE	DRO	DB1995	D2000
9241300	0.80	0.68	0.59	0.55	0.82
Mean	0.50	0.38	0.41	0.33	0.34
Std. Dev.	0.38	0.37	0.32	0.31	0.40

Table 2.13. DUCK94 September 24th, 13th hour: Skill (r^2-values) of velocity asymmetry predictions by FUNWAVE, NPMSE, the pressure-derived velocities, and DB1995.

Test Period	FUNWAVE	NPMSE	DRO	DB1995
9241300	0.71	0.24	0.86	0.21
Mean	0.56	0.20	0.72	0.14
Std. Dev.	0.29	0.21	0.21	0.14

2.8 DUCK94: October 2nd – October 4th

This first observed seaward bar movement period in October 1994 was less energetic than the September migration. The offshore wave climate was characterized by a mean H_{rms} of 1.1m. Figure 2.18 shows the hydrodynamic predictions by NPMSE, compared with the measurements, for October 4th during the 1st hour. Due to the large offshore wave height in combination with the shallow water depths, FUNWAVE was unable to remain stable for these simulations, therefore, no comparisons were made with FUNWAVE for this 3-day time period.

The cross-shore evolution of the H_{rms} was predicted well by NPMSE compared to the pressure-derived measurements (Figure 2.18). NPMSE showed some skill when predicting the cross-shore evolution of the wave height for most test periods in this 5-day simulation, with an average r^2~0.63 and a standard deviation of 0.32 (Table 2.14). The wave model exhibited more skill over all for the previous offshore bar movement case, discussed in

section 2.6.

The predictions of the nonlinear characteristics of the water surface elevation varied significantly during this simulation. Skewness predictions compared well with the pressure-derived observations (r^2~0.73) for this particular test hour (shown in Figure 2.18), but not nearly this well for all the test periods, resulting in an average skill of 0.45 (Table 2.14). The cross-shore location that compares the least well with the observations is the gauge located around x=169m, which is the measurement location that consistently compares poorly with the predictions. The pressure sensors and current meters located around x=135m, 145m, and 160m were out of service during this particular test hour, and for the majority of this test case. There is a possibility that the model skill values, primarily associated with the water surface elevation predictions, are affectedly adversely by the lack of data from these instruments for comparison. Note that in the previous field case comparisons predicted and measured H_{rms} and eta skewness compared well at the two most shoreward instrument locations, resulting in better model skill.

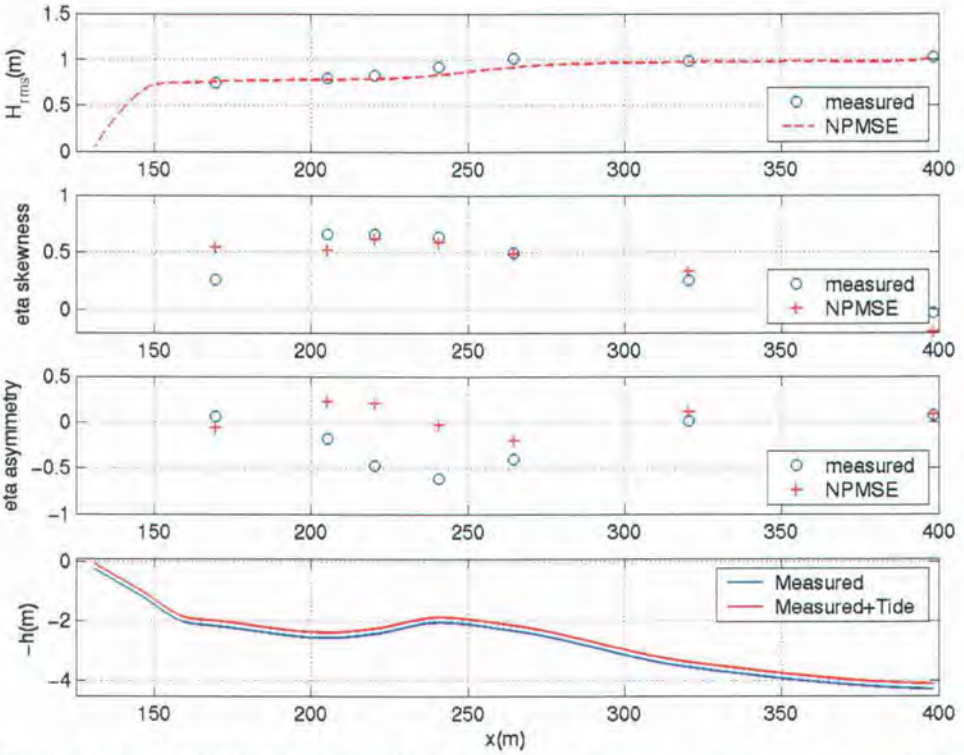

Figure 2.18. DUCK94 October 4th, 1st hour: Wave parameter comparisons between NPMSE (red crosses) and the pressure-derived water surface elevation (blue circles); Comparisons of H_{rms} (upper panel), water surface elevation skewness (upper central panel), and water surface elevation asymmetry (lower central panel). The cross-shore profile is shown in the lower panel.

The cross-shore measured asymmetry evolution is predicted well by NPMSE seaward of the bar crest, but through the trough the predictions are rather poor, leading to the poor model skill of 0.02 for this particular test period (Table 2.14). The fully dispersive wave model did not predict the forward pitching of the wave as significantly as was observed over the bar, therefore,resulting in the severe under prediction of the wave asymmetry in the trough. NPMSE also predicted the switching of the sign of the asymmetry more offshore than the observations. This was probably because the model did not pitch the waves forward enough over the bar therefore, when entering back into deeper water (over the trough) the NPMSE predicted the backward pitching of the wave earlier than the observations. This is similar to the predictions by NPMSE in the first offshore bar movement field case (section 2.6).

Table 2.14. DUCK94 October 4th, 1st hour: Skill (r^2-values) of NPMSE wave model when predicting the water surface elevation. Model-to-data comparisons between wave height (H_{rms}), wave skewness, and wave asymmetry.

Test Period	NPMSE H_{rms}	NPMSE skewness	NPMSE asymmetry
10040100	0.86	0.73	0.02
Mean	0.63	0.45	0.20
Std. Dev.	0.32	0.24	0.27

Figure 2.19 shows the nonlinear wave velocity quantities predicted by NPMSE and the empirical formulations compared to the observations from the pressure sensors and current meters. The wave model consistently under predicts both the skewness and asymmetry. NPMSE and DB1995 are producing similar qualitative skewness results (Table 2.15), especially over the bar crest, except that the empirical model is consistently over predicting both of the nonlinear quantities. The D2000 skewness predictions do not compare well with the observations for this particular test period (r^2~0.00), but comparatively have a better average skill (r^2~0.47) for this 5-day simulation.

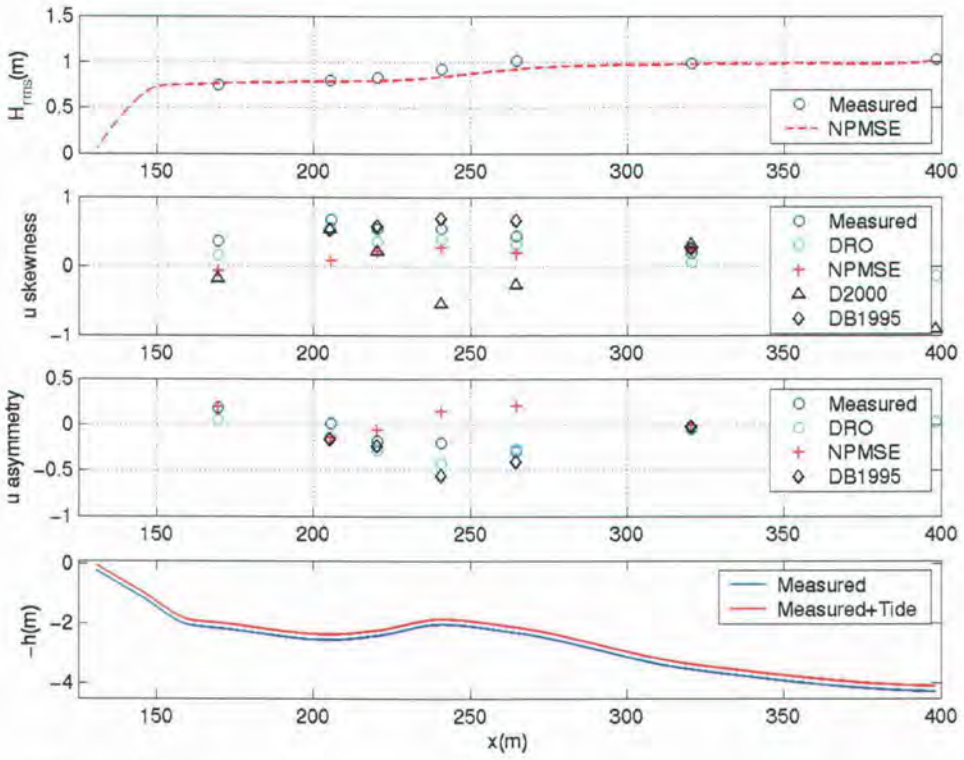

Figure 2.19. DUCK94, October 4th, 1st hour: Wave parameter comparisons between the current meter measurements (blue circles), pressure-derived velocities (cyan circles), NPMSE (red crosses), DB1995 (black diamonds), and D2000 (black triangles); Comparisons of H_{rms} (upper panel), wave velocity skewness (upper central panel), and wave velocity asymmetry (lower central panel). The cross-shore profile is shown in the lower panel.

The predictions of velocity asymmetry by NPMSE compared poorly with the observations for this test period, hence the poor skill of 0.14 (Table 2.16). The wave model performed rather poorly when predicting wave asymmetry for the entire test case, hence the average skill of 0.25 with a standard deviation of 0.31. The pressure-derived velocity asymmetry does not compare well with the current meter observations (especially compared to the skewness predictions) resulting in a test period skill value of 0.51 (Table 2.16). DB1995 is doing moderately well at predicting the velocity asymmetry for 1st hour of October 4th (r^2~0.55), which is only slightly better than its average model skill value for the 3-day test period.

Table 2.15. DUCK94 October 4th, 1st hour: Skill (r^2-values) of velocity skewness predictions by the NPMSE wave model, the pressure-derived velocities, DB1995, and D2000.

Test Period	NPMSE	DRO	DB1995	D2000
10040100	0.47	0.97	0.47	0.00
Mean	0.53	0.63	0.51	0.47
Std. Dev.	0.29	0.26	0.30	0.30

Table 2.16. DUCK94 October 4th, 1st hour: Skill (r^2-values) of velocity asymmetry predictions by the NPMSE wave model, the pressure-derived velocities, and DB1995.

Test Period	NPMSE	DRO	DB1995
10040100	0.14	0.51	0.55
Mean	0.25	0.65	0.50
Std. Dev.	0.31	0.25	0.23

2.9 DUCK94: October 10th – October 20th

This second observed seaward bar movement period in October 1994 ranged from very energetic to mild wave conditions over the course of the 10-day migration. The offshore wave climate was characterized by a H_{rms} ranging from 0.5m to 2+m. Figure 2.20 shows the hydrodynamic predictions by NPMSE, compared with the measurements, for October 18th during the 7th hour. Once again, due to the large offshore wave height in combination with the shallow water depths no comparisons were made using predictions by FUNWAVE.

For this particular test period, the cross-shore evolution of the H_{rms} was predicted well by NPMSE compared to the pressure-derived measurements, primarily over the sand bar and shoreward of the large trough (Figure 2.20, upper panel). The model consistently under predicted the mild de-shoaling of the wave over the large trough region, during high tide. Overall, the model performed well predicting the cross-shore evolution of the wave height, resulting in decent model skill values, with an average r^2~0.69 and a standard deviation of 0.18 (Table 2.17).

The predictions of the nonlinear characteristics of the water surface elevation by the fully dispersive wave model were mostly not significant for this test case. Skewness

predictions did not compare well quantitatively with the pressure-derived observations (r^2~0.13) (shown in Figure 2.20, upper central panel) for this test period, nor very well over all for the test case (r^2~0.32).

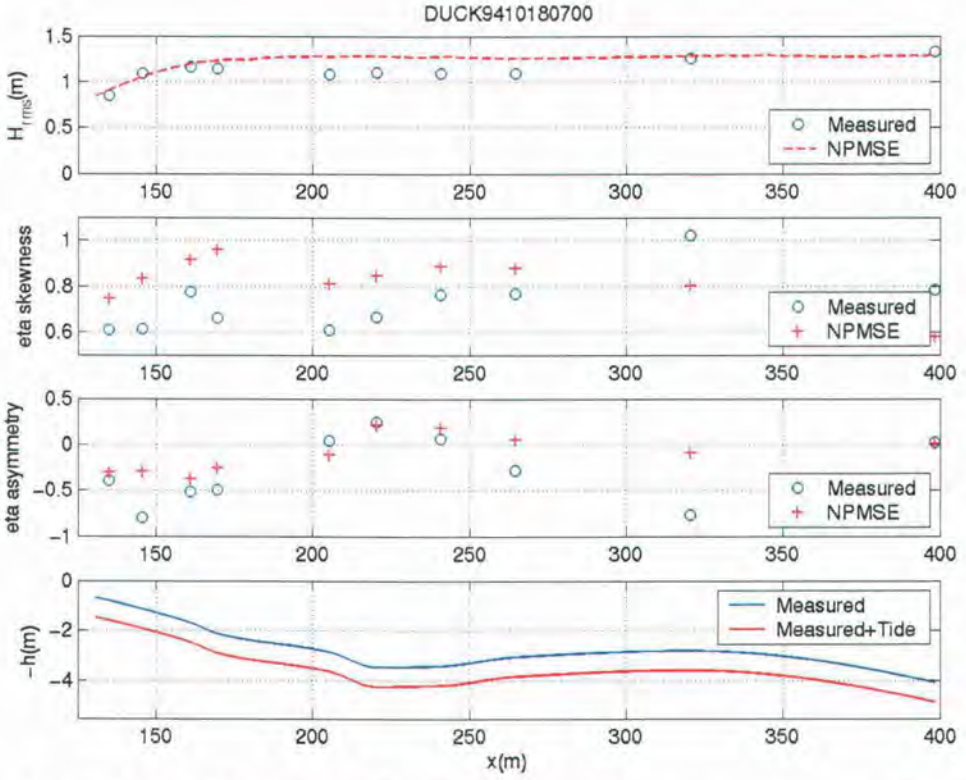

Figure 2.20. DUCK94 October 18th, 7th hour: Wave parameter comparisons between NPMSE (red crosses) and the pressure-derived water surface elevation (blue circles); Comparisons of H_{rms} (upper panel), water surface elevation skewness (upper central panel), and water surface elevation asymmetry (lower central panel). The cross-shore profile is shown in the lower panel.

Similar to the wave skewness predictions, the cross-shore measured asymmetry evolution is not predicted well by NPMSE. The fully dispersive wave model was able to predict the qualitative pitching of the wave as due to shoaling and de-shoaling around the bar crest and trough. NPMSE again was minimally pitching the waves forward (small negative asymmetry value) over the bar crest (x~325m). The waves were observed to pitch significantly more forward than the predictions, as indicated by the large negative asymmetry value. Therefore, upon entering back into deeper water (over the trough) the NPMSE predicted the backward pitching of the wave (x~260m) earlier than the observations

(x~245m). This is similar to the predictions made by NPMSE in the previous offshore bar movement sections (section 2.6 and 2.8). In the lower panel, one can see the tide was rather high and altered the total water depth significantly over the bar crest and near the shoreline. It should be noted that the tide plays a significant role in the hydrodynamics for many of the test periods in this test case, by largely altering the breaking location of the waves and the subsequent re-shoaling region of the waves over the trough.

Table 2.17. DUCK94 October 18th, 7th hour: Skill (r^2-values) of NPMSE wave model when predicting the water surface elevation. Model-to-data comparisons between wave height (H_{rms}), wave skewness, and wave asymmetry.

Test Period	NPMSE H_{rms}	NPMSE skewness	NPMSE asymmetry
10180700	0.90	0.13	0.33
Mean	0.69	0.32	0.24
Std. Dev.	0.18	0.25	0.22

Figure 2.21 shows the nonlinear wave velocity quantities predicted by NPMSE and the empirical formulations compared to the observations from the pressure sensors and current meters. The upper central panel compares the cross-shore profiles of the velocity skewness. The wave model is largely under predicting the velocity skewness, but tended to perform better for other test periods. D2000 and DB1995 are producing similar qualitative skewness results through the trough, but then deviate from each other in the surf zone. The D2000 skewness predictions do not compare well with the observations for this particular test period shoreward of the offshore breaker line.

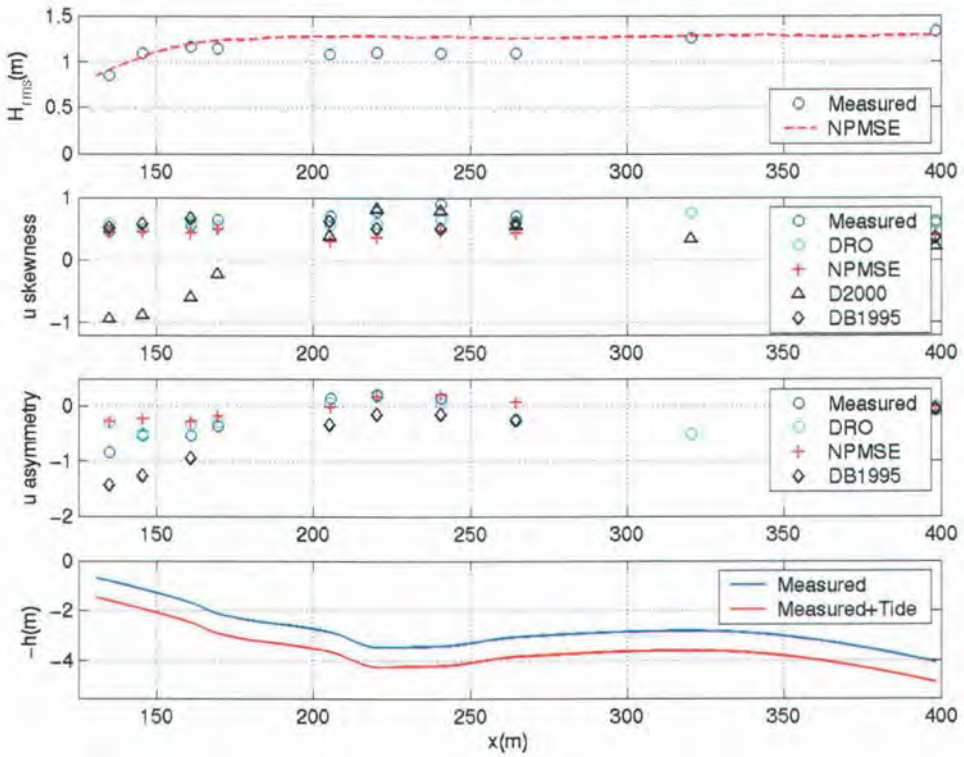

Figure 2.21. DUCK94, October 18th, 7th hour: Wave parameter comparisons between the current meter measurements (blue circles), pressure-derived velocities (cyan circles), NPMSE (red crosses), DB1995 (black diamonds), and D2000 (black triangles); Comparisons of H_{rms} (upper panel), wave velocity skewness (upper central panel), and wave velocity asymmetry (lower central panel). The cross-shore profile is shown in the lower panel.

The predictions of velocity asymmetry by NPMSE were mediocre for the hydrodynamic simulations of October 18th, during the 7th hour, hence the average skill value of 0.38 and standard deviation of 0.27 (Table 2.19). The pressure-derived velocity asymmetry compared very well with the current meter observations, resulting in a test period skill value of 0.90 and an average test case skill of 0.70 (Table 2.19). DB1995 was doing decently well at predicting the velocity asymmetry for the test period (r^2~0.66), which is better than the average test case skill, as well as the NPMSE test case skill.

Table 2.18. DUCK94 October 18th, 7th hour: Skill (r^2-values) of velocity skewness predictions by the NPMSE wave model, the pressure-derived velocities, DB1995, and D2000.

Test Period	NPMSE	DRO	DB1995	D2000
10180700	0.02	0.39	0.65	0.15
Mean	0.40	0.38	0.40	0.29
Std. Dev.	0.26	0.25	0.27	0.23

Table 2.19. DUCK94 October 18th, 7th hour: Skill (r^2-values) of velocity asymmetry predictions by the NPMSE wave model, the pressure-derived velocities, and DB1995.

Test Period	NPMSE	DRO	DB1995
10180700	0.47	0.90	0.66
Mean	0.38	0.70	0.50
Std. Dev.	0.27	0.18	0.26

2.10 Summary of Results

The NPMSE predictions of skewness and asymmetry ranged significantly in their quality. The velocity skewness predictions were found to be consistently better than the velocity asymmetry predictions for the field studies, the opposite was found to be true for the lab cases. The nonlinear quantity results were found to be rather sensitive to the frequency weighting parameter, F, which was kept constant at 0.5 for all studies. As a reminder, F=0 dictates that only f^2_n-weighted dissipation will occur in the model, where as F=1 dictates that only frequency-independent dissipation is modeled. The predictions of the asymmetry for the Mase-Kirby case were found to improve significantly when a smaller F was used, though the skewness comparisons were found to degrade. Similar results were found when testing F in the lab simulations of LIP11D. The sensitivity of the asymmetry predictions to the breaking model parameters suggests improvements need to be made to the dissipation scheme or a new breaking model needs to be employed.

One explanation for the quality prediction of nonlinearity by FUNWAVE is that it is fully nonlinear, where as NPMSE is a frequency-domain model and only correct to the 2nd-order in nonlinearity.

The Mase-Kirby comparisons were also significantly improved when multiple realizations were modeled and ensemble averaged prior to computing the nonlinear

quantities. Improvements to the comparisons of wave skewness and asymmetry using the ensemble averaging approach can be seen in Kaihatu (2001). NPMSE results were also improved by optimizing the number of modeled frequency components, which was done for this hydrodynamic study.

A proposed method of modeling the nonlinear quantities of velocities is by using empirical models, which are more computationally efficient than most nonlinear wave models. Two proposed empirical formulations are DB1995 and D2000, which are both functions of the Ursell parameter. D2000 was found to show more skill when predicting velocity skewness, and had a small standard deviation of the model skill for all the lab test runs. DB1995 was found to overall exhibit more skill when predicting the velocity skewness for the field simulations. The skill of DB1995 was better than the D2000 model skill for the first two offshore bar movement cases of DUCK94, and its standard deviation was slightly better for these test cases. However, D2000 performed better than DB1995 for the 10-day offshore bar simulation at the end of October, when the wave conditions varied significantly. The skill exhibited by both models was basically equivalent for the shoreward bar movement simulation, but the DB1995 had a slightly smaller standard deviation of the test period model skill values.

The comparisons of the model skill for each of the applicable simulations revealed that overall the nonlinear wave models performed better at predicting the velocity skewness than the empirical formulations. However, D2000 did show more skill than the other models for the onshore bar movement simulation in LIP11D Test Case 1C and exhibited about the same skill at NPMSE for the 10-day offshore bar movement simulations, though NPMSE had a smaller standard deviation of the test period skill values. For the remaining offshore bar movement lab and field studies, NPMSE showed more skill than the empirical formulations, though the model skill values for the test periods during the initial offshore bar movement (early September) were quite close for all the utilized models. FUNWAVE exhibited the most model skill when predicting the velocity skewness for the shoreward bar movement during DUCK94, in late September. NPMSE showed better model skill values than the empirical formulations, for the onshore bar movement simulations as well. From these test case results, it can be concluded that the nonlinear wave models overall performed better when predicting velocity skewness for the field studies and the energetic lab case. When D2000 was performing well compared to the other empirical formulation, it also was performing on par, if not better, than the

nonlinear wave models.

Chapter 3

BATHYMETRIC EVOLUTION MODELING: LAB AND FIELD STUDY

In this study we attempted to simulate the nearshore environment using wave, circulation, and sediment transport models to predict the bathymetric evolution using a feedback system. Our approach was to model a cross-shore profile of the processes in this dynamic region using a fine computation grid (dx~5cm). This is different than the majority of the previous studies in which the morphological evolution was computed only at the instrument locations, which were typically sparse in the model domain [Gallagher *et al*, 1998; Hoefel and Elgar, 2003; Long and Kirby, 2003].

In the current study bathymetric predictions were made for two lab cases and four bar movement events observed in the field. The skill of the model series were gauged using Least Squares Regressions (r^2-values) of the measured versus the predicted volumetric transport and bathymetry.

3.1 Model Series Implemented in Lab Study

In this study the waves, currents, and evolution of the bathymetry were all modeled, and implemented in a feedback system within which they were allowed to interact. The wave parameters were determined by the Kaihatu (2001) nonlinear fully dispersive wave model (NPMSE). From the wave module, the predicted water surface elevation, near-bed oscillatory wave velocity, and wave speed were used to drive the undertow model of Garcez Faria *et al.* (2000). The predicted near-bottom undertow, in addition to the predicted wave velocities, were subsequently used to determine the velocity moments required to drive a sediment transport model based on Bailard (1981). The evolution of the bathymetry was updated hourly, corresponding to the end of each LIP11D test hour. The predicted hourly bathymetry was then run through a smoothing routine, in which a bathymetry vector was constructed from 21-point averages of the predicted bathymetry, resulting in a smoothing window of approximately 1m. The new bathymetric vector was then re-interpolated onto the wave model grid and utilized as the input bathymetry for the following test hour. The small scale smoothing routine was implemented to smooth over any small scale features predicted by the model (<1m wide) as well as remove any small scale oscillations which could have

potentially resulted in instability of the wave model.

3.2 Circulation and Sediment Transport Models

The Garcez Faria *et al.* (2000) undertow model predicts the vertical profile of the undertow as a function of cross-shore location. The model also consists of components which solve for the onshore directed mass transport and wave induced set-up. The cross-shore sediment transport was predicted using an energetics-type model given by Bailard (1981). The predicted cross-shore directed total velocities were used to drive the sediment model, which predicted the change in the bathymetry as a function of time and space.

3.2.1 Undertow Model

The Garcez Faria *et al.* (2000) circulation model determines the vertical profile of the undertow. A turbulent eddy viscosity closure was implemented to parameterize the effects of turbulence. The undertow model includes breaking effects via a wave roller model (Reussink *et al.*, 2001) and the convective acceleration of the current. The circulation model solves for the surface mass flux, setup, and the vertical structure of the undertow at each cross-shore step. Garcez Faria *et al.* (2000) assumed stationary wave conditions, straight and parallel depth contours, and random waves that were narrow banded in frequency and direction.

The surface mass flux is initially using the depth-integrated and phase-averaged conservation of mass equation for straight and parallel contours with a no-flow boundary at the shoreline (Equation 3.1)

$$\overline{\int_h^\eta \rho[U(z)+\tilde{u}(z)+u'(z)]dz = 0} \tag{3.1}$$

The over bar indicates time averaging, η is the water surface elevation, h is the local water depth, and ρ is the water density. The velocity has been broken into the mean, wave, and turbulent components. Assuming irrotational flow below the trough level and from an Eulerian point of view, there is a net onshore mass transport by waves (q_w), limited to the trough-to-crest region (Equation 3.2).

$$q_w = \overline{\int_{\eta_t}^{\eta_c} \rho\tilde{u}(z)dz} \tag{3.2}$$

where the subscripts c and t refer to the crest and trough, respectively.

There is also an onshore mass transport contribution from the turbulent wave roller (q_r), which occurs above the wave trough. The turbulent wave roller model used by Reussink *et al.* (2001) was utilized to determine the wave roller contribution to the mass transport. The model solves the roller energy balance (Stive and DeVriend, 1994)

$$\frac{d}{dx}(2E_r C\cos\bar{\theta}) = -D_r + D_{br} \tag{3.3}$$

where E_r is the roller energy, D_r is the roller dissipation, D_{br} is the wave dissipation due to breaking (determined by the wave model), C is the wave celerity, and θ is the wave angle. According to Duncan (1981), the roller dissipation is defined as

$$D_r = \frac{2gE_r \sin\beta}{C} \tag{3.4}$$

where β is taken to be 0.1 (Walstra, 1996). The roller energy is assumed to be equal to zero at the offshore boundary, and the equations can then be solved using a forward stepping routine from the offshore boundary towards the shore. The surface mass flux contribution from the roller is defined as

$$q_r = E_r \frac{\cos\theta}{C} \tag{3.5}$$

The total onshore mass transport in the trough to crest region of the wave is the linear addition of the wave and roller mass transport contributions. The depth-averaged offshore-directed return flow, U_r, can then be determined from the total onshore mass transport, the water depth below the trough (h_t) and the water density (Equation 3.6).

$$U_r = \frac{q_w + q_r}{-\rho h_t} \tag{3.6}$$

The set-up is the next major component necessary to determine the vertical profile of the undertow. The set-up is calculated by depth-integrating the time-averaged cross-shore momentum balance from the bottom to the mean water level (Equation 3.7) (Garcez Faria *et al.*, 2000).

$$\frac{\partial S_{xx}}{\partial x} + \frac{\partial M_r}{\partial x} + \frac{\partial \rho U_r^2(\bar{\eta}+h)}{\partial x} = -\rho g(\bar{\eta}+h)\frac{\partial \bar{\eta}}{\partial x} \tag{3.7}$$

S_{xx} is the cross-shore radiation stress, which has contributions from wave and roller energy. M_r is the momentum flux associated with the roller (M_r=Cq_r) and the last term on the left-hand side is the momentum flux of the depth-averaged undertow (U_r).

The vertically dependent undertow is derived from the time-averaged vertical momentum

equation (Equation 3.8), neglecting molecular viscous stresses.

$$\frac{\partial}{\partial x}(uw)+\frac{\partial}{\partial z}(w^2)=-\frac{1}{\rho}\frac{\partial P}{\partial z}-g+\frac{\partial}{\partial x}\left(\frac{\tau_{xz}}{\rho}\right)+\frac{\partial}{\partial z}\left(\frac{\tau_{zz}}{\rho}\right) \tag{3.8}$$

u and w are the total cross-shore and vertically directed velocities, respectively. P is the pressure, g is the acceleration due to gravity, and τ_{xz} and τ_{zz} are the viscous stresses. Stationary wave conditions, as well as straight and parallel contours are assumed. Garcez Faria *et al.* (2000) made the following assumptions to further reduce the momentum equation for the region between the top of the bottom boundary layer and the wave trough level: (1) wave and turbulent velocity components are independent of each other; (2) turbulence is near isotropic, therefore, higher order statistics of the cross-shore turbulent velocities will be approximately equal to the same higher order statistics of the vertical turbulent velocities (Stive and Wind, 1982); (3) the wave shear stress can be approximated by (Rivero and Arcilla, 1995)

$$\frac{\partial\rho\widetilde{u}\widetilde{w}}{\partial z}=-\frac{1}{2}\frac{\partial}{\partial x}\rho[\overline{\widetilde{u}^2}-\overline{\widetilde{w}^2}] \tag{3.9}$$

and (4) a first-order eddy viscosity closure for the turbulent shear stress is given by

$$-\rho\overline{u'w'}=\rho\mu_z\frac{\partial U}{\partial z} \tag{3.10}$$

where μ_z is the time-invariant turbulent eddy viscosity. A more in-depth discussion of the validity of these assumptions can be found in Garcez Faria *et al.* (2000). A solution for the depth dependant undertow is found by depth-integrating equation 3.10 twice.

$$\frac{\partial}{\partial z}\left(\rho\mu_z\frac{\partial U}{\partial z}\right)=\frac{1}{2}\frac{\partial}{\partial x}[\rho(\overline{\widetilde{u}^2}-\overline{\widetilde{w}^2})]+\rho g\frac{\partial\overline{\eta}}{\partial x}+\frac{\partial\rho U_r^2}{\partial x}=F(x) \tag{3.11}$$

F(x) can be assumed independent of elevation based on empirical evidence from laboratory studies [Nakoda and Kondoh, 1982; Stive and Wind, 1982, 1986]. Equation 3.11 is the expression for the vertically varying undertow

$$U(z)=U_r+\frac{1}{\rho\mu}F(x)[\frac{1}{2}z^2+hz+\frac{3h^2-h_t^2}{6}z^2]+\frac{\widetilde{\tau}_{bx}}{\rho\mu}\left[z+h-\frac{h_t}{2}\right] \tag{3.12}$$

where the depth-independent turbulent eddy viscosity, μ, shall be used instead of μ_z and τ_{bx} is the bed shear stress in the x-direction. In the present study, the turbulent eddy viscosity is determined following Sancho *et al.* (1995). Garcez Faria *et al.* (2000) define the bottom shear stress as

$$\tilde{\tau}_{bx} = \rho C_f \overline{|\tilde{u}_b|} U_b \tag{3.13}$$

where the subscript b denotes near-bed quantities and C_f is the friction coefficient, which was set to 0.01.

For the remainder of the thesis, the Garcez Faria *et al.* (2000) undertow model will be referred to as GF2000.

3.2.2 Bailard's Sediment Transport Model

Bailard (1981) and Bailard and Inman (1981) extended the Bagnold (1966) transport formulation to include effects from oscillatory velocities, in addition to the mean velocity (Equation 3.18). This equation also considers multi-directional flow, therefore, accounts for the cross-shore and longshore velocity effects in the cross-shore evolution of the bathymetry.

$$\begin{aligned}\left\langle \vec{i}_t \right\rangle = {} & \rho c_f \frac{\varepsilon_b}{\tan\phi}\left[\left\langle |\vec{u}_t|^2 \vec{u}_t \right\rangle - \frac{\tan\beta}{\tan\phi}\left\langle |\vec{u}_t|^3 \right\rangle \hat{i}\right] \\ & + \rho c_f \frac{\varepsilon_s}{w}\left[\left\langle |\vec{u}_t|^3 \vec{u}_t \right\rangle - \frac{\varepsilon_s \tan\beta}{w}\left\langle |\vec{u}_t|^5 \right\rangle \hat{i}\right]\end{aligned} \tag{3.14}$$

Consistent with Bagnold (1966), c_f is the friction coefficient due to the bed material, ρ is the fluid density, and w is the sediment fall velocity. $\vec{u}_t$ is the total velocity, which is composed of the oscillatory (ũ) and mean (ū) velocity contributions. The addition of the oscillatory velocity contribution accounts for the wave-generated flow field. $< >$ indicates time averaging and $\hat{i}$ is the cross-shore directed vector, which implies that longshore uniformity is assumed.

The nonlinear combinations of the total velocity are referred to as the velocity moments. These moments comprise the energy available to the system, some of which is assumed to be utilized to transport sediment in the form of bed load and suspended load. $|\vec{u}_t|^3$ and $|\vec{u}_t|^5$ have been previously referred to as the even velocity moments, while $|\vec{u}_t|^2 \vec{u}_t$ and $|\vec{u}_t|^3 \vec{u}_t$ can be described as the odd velocity moments (Guza and Thornton, 1985; Roelvink and Stive, 1989). These velocity moments are functions of skewness, only.

The volumetric transport rate can be computed by simply dividing the immersed weight transport rate by $(\rho_s-\rho)g$, where ρ_s is the sediment density and g is the gravitational acceleration. Assuming mass conservation in the cross-shore directions, no longshore

gradient of the sediment flux and that the porosity of the bed remains constant, the local rate of change in the bathymetry can be quantified as

$$\frac{dQ_x}{dx} = \mu \frac{dh}{dt} \tag{3.15}$$

where μ is the packing factor (μ=1- p, where p is the porosity of the bed) and Q_x is the rate of volumetric sediment transport in the cross-shore direction, per unit width of beach (Gallagher *et al.*, 1998). In this study, for all sediment transport simulations we used a constant μ=0.7 (Thornton *et al.*, 1996).

3.3 Model Validation Using LIP11D Data Set: Test Cases 1B and 1C

Test Cases 1B and 1C were used for model validation in the lab sediment transport study. Data from the fixed wave gauges, pressure sensors, and velocity meters, as well as the sonic profiler were used for this study. The sonic profile measurements provided a dense vector of approximately 39,000 bathymetric measurement points every 0.01m in the cross-shore. The model series initial input bathymetry was generated from the sonic profile data.

In Test Case 1B, the erosion simulation, the sand bar developed around 145m from the paddle and proceeded to move offshore about 10m (Figure 3.1). The wave climate was intended to simulate hydrodynamic conditions immediately prior to- and during storm events, hence bar formation and offshore directed bar movement were expected. Large ripples were also formed in the trough of the bar. The ripples were not smoothed over to generate the initial input bathymetry for Test Case 1C. During Test Case 1C, the bar moved onshore less than 5m. Onshore bar movement is understood to be quite slow, therefore, less than 5m of onshore bar movement over the course of 13hrs is reasonable.

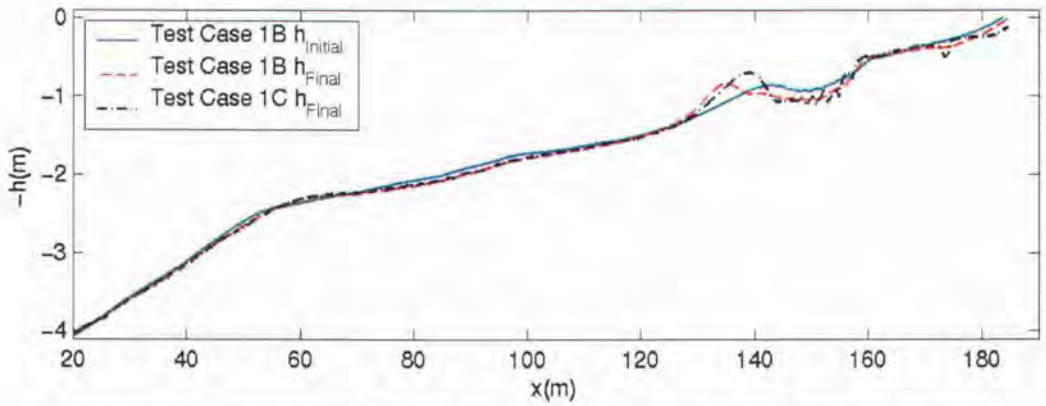

Figure 3.1 Measured profile at the beginning of Test Case 1B (blue -), final of Test Case 1B (which is also the initial profile for Test Case 1C) (red --), and the final profile of Test Case 1C (black -.).

The offshore boundary of the bathymetry was fixed for all test cases. This was done by setting the cross-shore gradient of the predicted volumetric transport equal to zero. After each test hour simulation, the predicted bathymetry would be smoothed to remove any discontinuities. A new bathymetric vector would be generated containing 21-point (~1m) averages of the predicted profile. This new vector would then be interpolated onto the original 5cm cross-shore grid and utilized by the following test hour simulations. Test Case 1C model series did not implement any other smoothing routines while predicting the bathymetric evolution. Due to issues with the predicted bathymetry of the first 8m into the domain (measured from the offshore boundary), a routine was used while post-processing, to force the predicted vertical elevation from that 8m location to the offshore boundary in a linear fashion, which could potentially alter the total amount of sediment within the computational domain, which implies that the total amount of sediment may not have been conserved in this domain. This post-processing routine was found to not significantly alter the predicted bathymetry. Once again, the vertical elevation of the offshore boundary is kept fixed at the offshore elevation of the measured input bathymetry for the Test Case simulation (Test Case 1B, test hour 0213 initial measured bathymetry).

3.3.1 LIP11D: Test Case 1B - Offshore Bar Movement

Waves, currents, and the subsequent change in the bathymetry were simulated for the

2nd through the 12th hour of Test Case 1B. The NPMSE wave model was driven with the measured water surface elevation at the wavemaker. The wave parameters γ and B in the dissipation scheme were set to 0.7 and 1, respectively. According to Thornton and Guza (1983), these wave parameter values fell within a reasonable range for lab cases. The modeled water surface elevation and wave velocity time series were around seven minutes in length, with a 0.1s time step, for each simulated test hour. These predicted time series were taken to be representative of the hydrodynamics for the test hour, which was found to be reasonable through comparison of hydrodynamic statistics. The model took a spatial step of approximately 5cm in the shoreward direction. An example of the predicted significant wave height (red dashed-line) for test hour 0304 is shown in the upper panel of Figure 3.2. The observed significant wave height at the instrument locations is shown by the blue circles. The measured pressure sensor time series at each of the gauge locations was converted to water surface elevation using linear wave theory, from which the significant wave height was computed for these comparisons. The predictions compare quite well with the observations, even throughout the two most intense breaking locations. The difference in the predicted and observed offshore significant wave height can be ascribed to differences in wave height estimates from the offshore wave gauge and pressure sensor, since the model is being driven with the wave gauge measurement yet the cross-shore comparisons are being made with the converted pressure sensor data.

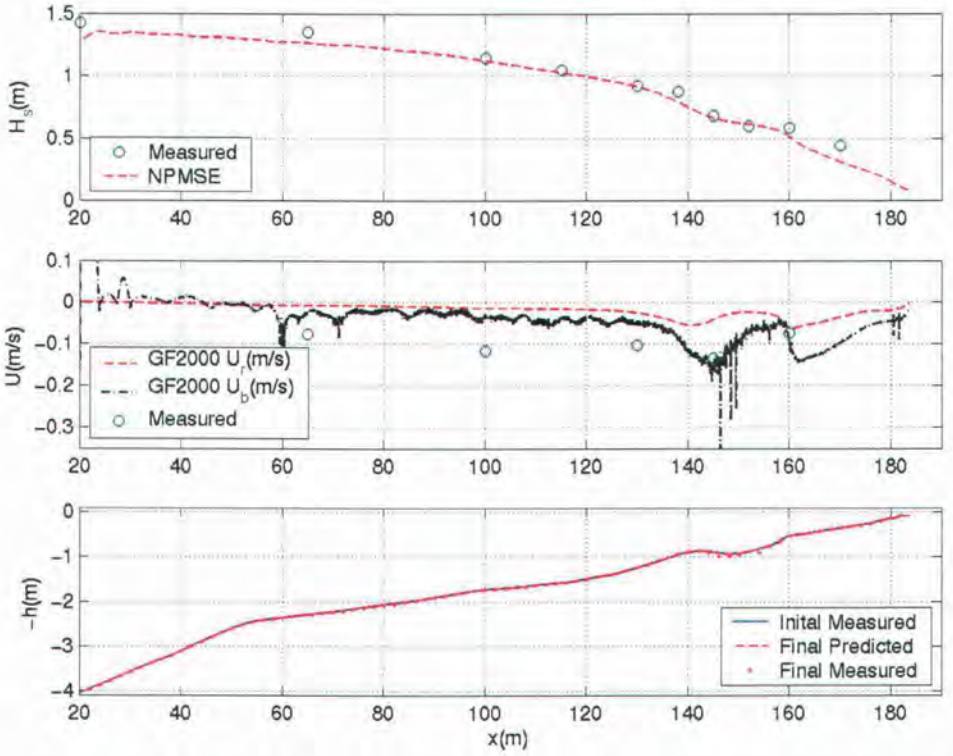

d

Figure 3.2. LIP11D Test Case 1B0304: Upper panel -Predicted significant wave height by NPMSE (red --) compared to measurements from the pressure sensor data (DRO). Center panel – Predicted depth-averaged return flow (red --) and near-bottom velocity (black -.) by GF2000. Lower panel - Initial predicted bathymetry from the start of the 2nd hour (blue -), predicted bathymetry at the end of the 3rd hour (red --), and measured bathymetry at the end of the 3rd hour (red ...).

The circulation model, GF2000, utilizes the computed wave energy, dissipation, wavenumber, water surface elevation, and wave velocity at each cross-shore step. Both the depth-averaged return flow and the near-bed mean velocity are underpredicted offshore of the surfzone, compared with measurements by the current-meters. The maximum observed current during this test hour was well predicted by the near-bed mean velocity, but the predictions are very noisy in this region, presenting stability issues with the modeling scheme. The most shoreward current meter measurement is well predicted by both the near-bed and depth-averaged mean velocities. The predictions of the vertically dependent undertow and the near-bed time-average velocity were noisy, therefore, we assumed that the depth-averaged return flow, U_r, was a good approximation for the near-bottom velocity and utilized it to generate the total velocity time series. Reniers *et al.* (2003) used this approach successfully when simulating the morphological evolution of a beach embayment. A comparison of the

cross-shore profiles of the predicted depth-averaged return flow (U_r) and the predicted near-bed mean velocity (U_b) for test hour 0304 are shown in the center panel of Figure 3.2. For this particular test hour, the magnitude of the depth-averaged return flow was approximately half that of the near-bed mean velocity around the breaking locations. From the visual comparison, it appears that substituting the depth-averaged return flow for the near-bed velocity is not ideal. However, through the simulations of Test Case 1B, we found that the use of the depth-averaged return flow predicted the observed changes in the bathymetry. The bathymetry predictions when using the near-bed velocity were extremely noisy therefore, obscuring the true cross-shore shape of the resulting profile. Due to noise in the predicted bathymetry, the model series became unstable unless multiple smoothing routines were applied to the predicted near-bed velocities and resulting profile, which resulting in smoothing over of the dominant features of interest (such as the sand bar profile).

The two strongest offshore directed currents correspond to the breaking locations due to limited water depth over the sand bar and at the shoreline. Overall, the prediction of the offshore directed flow throughout the cross-shore drove the observed offshore bar migration.

The predictions of the offshore directed, time-averaged velocities were not compared to measurements of the 5 wall-fixed current meters (which were located at 1/3 of the total local water depth off the bed), because the observations were mostly made of local free-stream velocity. Therefore, the current meter observations were not representative of the depth-averaged return flow or the near-bed mean velocity.

The Bailard-based sediment transport model was driven with the computed velocity time series that was assembled by adding the temporally constant undertow velocities to the predicted wave velocity time series from the wave model. The bed load and suspended load efficiency factors were kept constant for this simulation at 0.135 and 0.25, respectively. These values were chosen based on the work of Bailard (1981) and Thornton *et al.* (1996). Following the work of Church and Thornton (1993) a friction coefficient of 0.003 and an internal friction angle of 0.63 were kept constant for all test hours. According to Dean and Dalrymple (2002) a quartz-sand grain diameter of 0.22mm has an associated fall velocity of 0.028m/s, which was also kept constant for duration of the simulation.

The direction and quantity of transport is a direct function of the accuracy of the predicted velocity moments. The velocity moments due to only the measured and predicted wave velocity were compared (Fig. 3.3). The upper two panels depict the even velocity moments and the lower two panels depict the odd velocity moments. The magnitude and

direction of the predicted (wave-only) velocity moments appear to compare well with the current meter and pressure sensor generated (wave-only) velocity moments. The predicted moments near the shoreward breaking location were under predicting the observed pressure-derived moments, but compare quite well with the observed current-derived moments. This discrepancy between the two instruments at this location can be attributed to the error associated with the linear conversion of the pressure time series to water surface elevation time series and potentially issues with the current meter measurements, which will be discussed further when discussing Figure 3.4. The most shoreward comparisons between the predictions and the pressure-derived moments are rather poor. After the shoreward breaking location, the model predicts a consistent decrease in the velocity moments towards the shoreline, which could be expected due to the complete dissipation of the wave energy prior to the still water shoreline. The measured pressure-derived wave velocity moments indicate that a significant amount of transport should occur near the shoreline, especially due to the influence of the even moments. We are not including swash transport, therefore, we cannot predict bathymetric evolution in the swash zone. No significant bathymetric change was observed near the shoreline during either Test Case 1B or 1C (Fig. 3.1). Most of the observed bathymetric change occurred around the sand bar region, while the terrace-like shape of the bathymetry near the shoreline was preserved throughout the experiment.

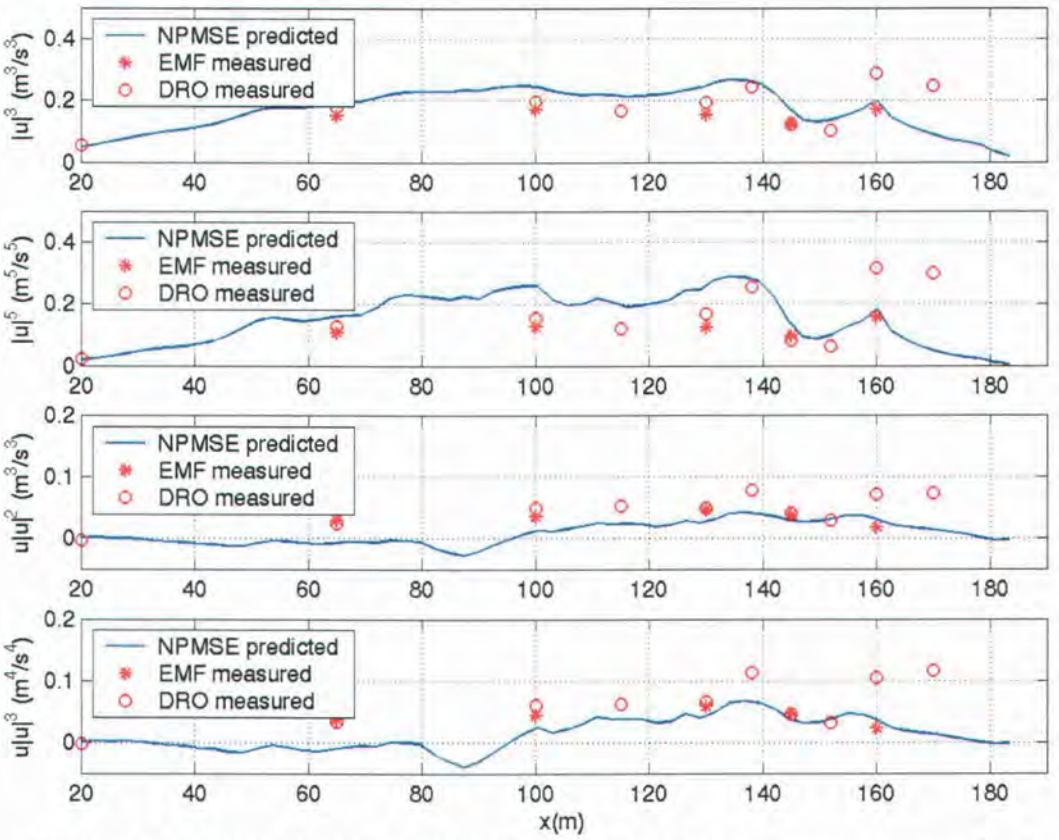

Figure 3.3. LIP11D Test Case 1B0304: Bailard velocity moments composed from the predicted oscillatory velocity time series at each modeled cross-shore location (blue -), compared to the moments produced from the current meter measurements (EMF)(red *), and from the pressure sensor measurements (DRO)(red o).

The volumetric sediment transport rate was predicted as a function of cross-shore location by the Bailard-based energetics-type model. Figure 3.4 shows a comparison between the cross-shore profiles of the predicted and "measured" sediment transport rates ($Q(m^3/s)$). The volume of sediment transport, as a function of both bed load and suspended load, was not measured directly during the experiment. Only volumes of suspended sediment were measured, in the water column, during the test hours. We estimated a measured transport rate using the measured velocity time series from the current meters to drive the sediment transport model, as was done by Thornton *et al.* (1996) and Gallagher *et al.* (1998).

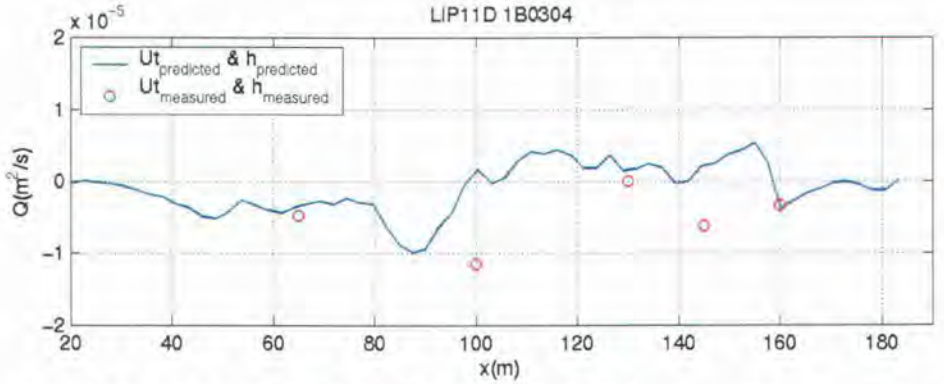

Figure 3.4. LIP11D Test Case 1B0304: Bailard-based predicted cross-shore volumetric transport (Q) profile using the predicted near-bed wave velocity (NPMSE) and predicted depth-averaged undertow (GF2000) (blue -). The predicted transport is being compared to the 'measured' transport, which is computed with Bailard's formulation using measured velocity time series from the current meters (EMF). The red stars are the computed transport as a function of the predicted bathymetry.

The cross-shore profile and magnitudes of the predicted and observed transport rates compare well. The discrepancy around x=100m corresponds to a location where the even velocity moments are being consistently overpredicted, while the odd velocity moments are being slightly underpredicted. The error associated with localized comparisons appears to oscillate through out the simulation (Table 3.1). As seen in the velocity moment comparisons (when using the current meter measurements), the predicted transport at the shoreward breaking location compares very well with the observed transport.

The spatial derivative of the volumetric transport is what dictates the predicted change in the bathymetry by the Bailard (1981) sediment transport model. We are primarily concerned with quantitatively predicting the change in Q with changes in space. From the above figure, it can be seen that we are comparing well with the derivative of Q with respect to x. As a note, when proceeding in the onshore direction (from the offshore boundary), a negative gradient followed by a positive gradient is indicative of offshore bar movement, where as the opposite is true for onshore bar movement.

Volumetric transport skill values, for all applicable hours in Test Care 1B, vary widely. They have a mean of 0.19 and a standard deviation of 0.16 (Table 3.1, grey highlighted section). These skill values have a large standard deviation, relative to the mean value, due to the incredibly small values of volumetric transport and overprediction by the model series in two primary locations. It is also important to take into consideration that only

5 cross-shore locations are being compared, therefore, when two locations compare poorly, this will significantly weaken the skill-values. Though the overall transport predictions show little skill, the predictions of the bathymetric evolution show significant skill (Table 3.1). The average bathymetric prediction skill is 1.0, with a standard deviation of 0.00. The skill predictions remain quite good when the barred region is isolated and compared to the local measured bathymetry. In the barred region, the model series has an average r^2-value of 0.95 and a standard deviation of 0.05. To test the sensitivity of the r^2-values, we computed the skill using the final measured bathymetry as the true component versus the initial measured bathymetry as the predicted component, which resulted in a skill value of 1.0. This indicates our gauge of skill is not very sensitive to small bathymetric changes, and we found it to be more indicative of the existence of similar trends between the truth and test components.

Table 3.1. LIP11D 1B0304: Summary of skill (r^2-values) associated with the volumetric transport and bathymetric evolution predictions. The predicted transport is compared to the computed transport using measured total velocity with the measured bathymetry ($\mathbf{Q_{hm}}$). The bar profile ($\mathbf{h_{bar}}$) comparisons are made between x=125m to x=166m.

Test Hour	Q_{hm}	h_{prof}	h_{bar}
1B0213	0.46	1.00	0.98
1B0304	0.04	1.00	0.98
1B0405	0.20	NA	NA
1B0707	0.01	1.00	0.95
1B0808	0.27	NA	NA
1B1010	0.17	NA	NA
1B1213	NA	1.00	0.88
Mean	**0.19**	**1.00**	**0.95**
Std. Dev.	**0.16**	**0.00**	**0.05**

The sonic profiler produced a vector of measured bathymetry which is more resolved than the model series. To compare the measured and predicted bathymetries, the measured bathymetry is interpolated onto a grid with the same resolution and sample locations as the prediction grid. The program utilized to generate these measured bathymetries is a standard Matlab routine, 'pchip', which is the same program used to generate the initial measured input bathymetry for the model series. Therefore, the interpolation program and sample locations are consistent throughout the test hours and corresponding comparisons.

The Test Case 1B profile comparisons between the measured and predicted bathymetries for the 2nd, 3rd, 4th, 6th, 7th, 8th, 9th, 10th, and 12th hours are shown in Figure 3.5 (top to bottom). The hours with only predicted bathymetries (no crosses) lacked corresponding sonic profiler measurements, therefore, no profile data was available for comparison. As mentioned in section 2.2.2, measurements were not taken during all test hours and some of the measured data was riddled with error and consequently excluded from the current study. In Test Case 1B, the 6th, 9th, and 11th hours did not have measured water surface elevation and/or measured bathymetry at the beginning of the test hour. For the duration of Test Case 1B the same offshore wave climate was produced for all test hours. Therefore, for the 6th, 9th, and 11th hours the measured offshore water surface elevation for the respective previous test hours were used to drive the wave model.

The model series was able to qualitatively predict the offshore bar movement event. During Test Case 1B, the offshore bar moved approximately 10m seaward, while maintaining its shape and the onshore terrace did not appear to adjust in shape or cross-shore location. The predicted sand bar profile was slightly smoothed causing the predicted bar crest vertical location to be underpredicted, while the predicted cross-shore location of the bar crest corresponded with the observations. The terrace was predicted to also move slightly offshore, while maintaining its shape, which is contrary to the observations. This slight under prediction and smoothing of the offshore bar by the model and seaward movement of the terrace is potentially due to incorrect values for the efficiency factors and/or error in the predicted cross-shore current structure and vertical location of the predictions. These potential sources of error will be further discussed in the Summary of Results, in section 3.6. The model series performed very well exhibiting significant overall skill. For all test hours included in this study, the r^2-value was 1.0 when comparing the entire profile, and 0.98 when comparing the sand bar region between the 125thm and 166thm of the profiles.

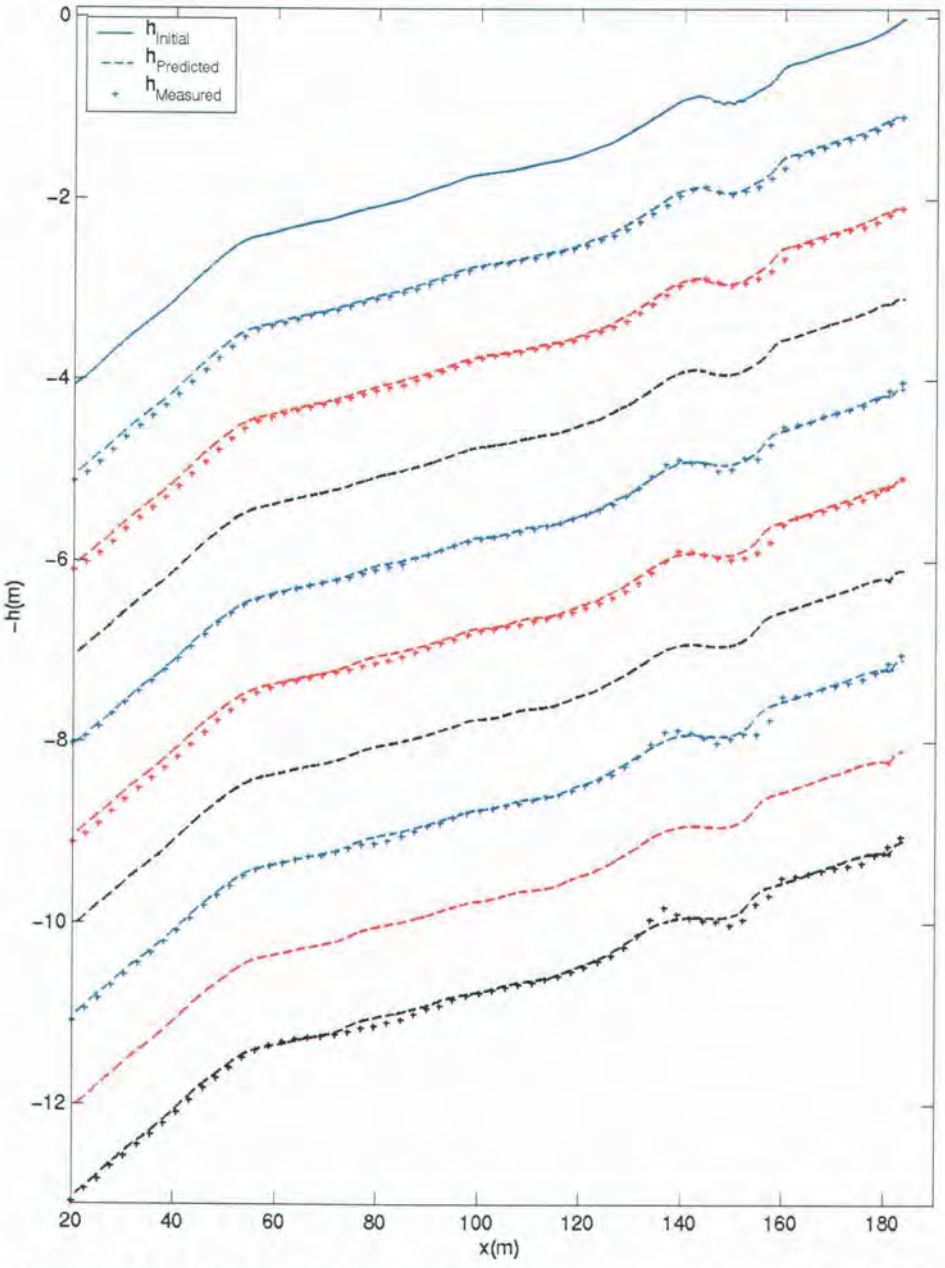

Figure 3.5. LIP11D Test Case 1B0304: Comparisons of measured (+) and predicted (- -) final bathymetries for the 2nd, 3rd, 4th, 6th, 7th, 8th, 9th, 10th and 12th hours. The solid line is the initial input measured bathymetry for the 11 hour simulation.

3.3.2 LIP11D: Test Case 1C - Onshore Bar Movement

The hydrodynamics and morphodynamics were simulated for the 1st through the 5th, 7th, 11th, and 13th hours of Test Case 1C. Once again, the NPMSE wave model was driven with measured water surface elevation, which was recorded by the wave gauge located at the wavemaker. Consistent with Test Case 1B, the wave parameters γ and B in the dissipation scheme were set to 0.7 and 1, respectively. The modeled water surface elevation and wave velocity time series were around 13.5min in length (which is approximately double the length of the Test Case 1B prediction time series) with a 0.1s time step. The 13.5min-modeled water surface elevation time series were found to be representative of each hour-long simulation, though minor differences were found in some of the higher order nonlinear velocity statistics at the most onshore gauge locations. The model took a spatial step of approximately 5cm in the shoreward direction. An example of the predicted significant wave height (red dashed-line) for test hour 0405 is shown in the upper panel of Figure 3.6. The observed significant wave height at the instrument locations was represented by the blue circles. The measured pressure sensor time series at each of the gauge locations was converted using linear theory to water surface elevation, from which the significant wave height was computed. The model predictions of significant wave height compared well quantitatively to the observations offshore of the breaking location. The modeling breaking commenced prior to the observed breaking, which was potentially due to the defined dissipation parameters, γ and B. Due to the early wave breaking, the model did not dissipate enough energy prior to re-shoaling, hence the over predicted significant wave height in the bar trough region. Shoreward of the onshore breaking location, the comparisons of wave height were again quite good. As a reminder, the difference in the predicted and observed offshore significant wave height was because we used the wave gauge measurements to drive the model, yet we make the cross-shore comparisons with the converted pressure sensor data.

The predictions of undertow, for test hour 0405, by the circulation model, GF2000, are shown in the central panel of Figure 3.6. To be consistent with Test Case 1B, the depth-averaged return flow, U_r, was used to generate the total velocity time series, in addition to the predicted cross-shore directed wave velocities. A cross-shore profile of the predicted depth-averaged return flow and the near-bed mean velocity (U_b) for test hour 0405 are shown in the center panel of Figure 3.6. The cross-shore locations of the strongest predicted return flow

corresponded to the shoreward breaking location over the terrace. Two smaller offshore directed flows were predicted; one at the shoreline and the other over the sand bar. Offshore of the sand bar an insignificant depth-averaged return flow and near-bed velocity were predicted. The overall predicted weak return flow was hydrodynamically consistent with observed and predicted onshore bar migration and was of similar magnitude and direction as the measured current. The predicted spike in the undertow, co-located with the terrace, generated an offshore migration of the terrace in the model results, which was not consistent with the 0405 test hour observations.

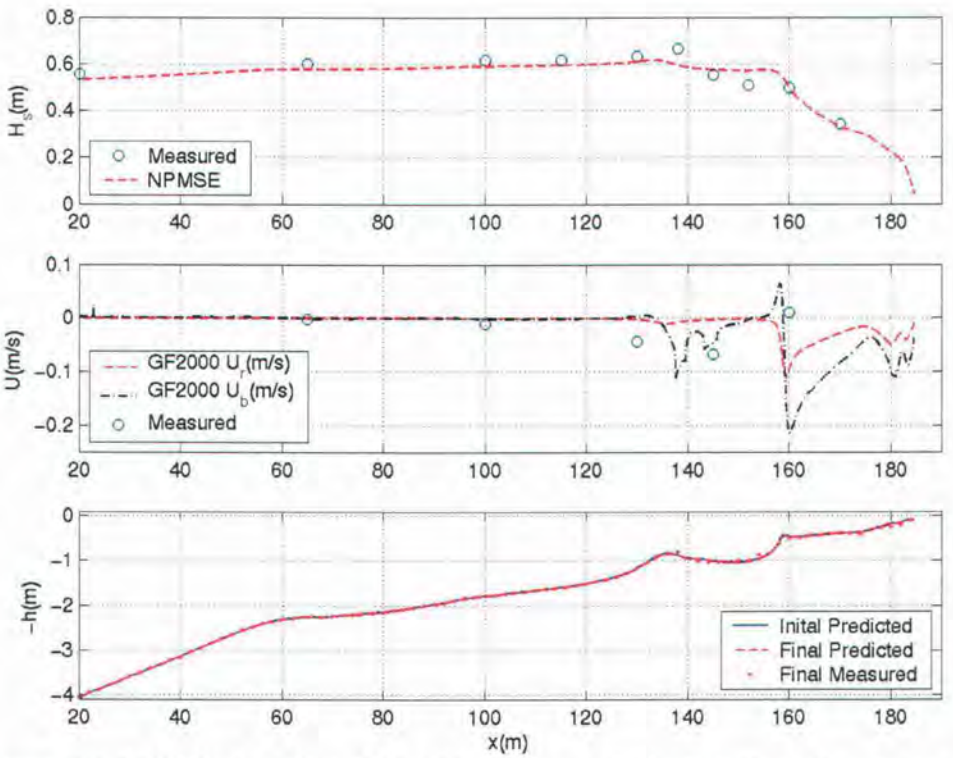

Figure 3.6. LIP11D Test Case 1C0405: Upper panel -Predicted significant wave height by NPMSE (red - -) compared to measurements from the pressure sensor data (DRO). Center panel – Predicted undertow (red - -) by GF2000. Lower panel - Predicted bathymetry from the start of the 4th hour (blue -), predicted bathymetry at the end of the 4th hour (red - -), and measured bathymetry at the end of the 4th hour (red -.).

The Bailard-derived sediment transport model was driven by the predicted total velocity time series. Similarly to Test Case 1B, the bed load and suspended load efficiency factors, which were kept constant for the duration of the test case simulation, were 0.135 and 0.25, respectively. The friction coefficient of 0.003 and an internal friction angle of 0.63

were kept constant for all test hours. A fall velocity of 0.028m/s was also kept constant for the duration of the simulation. The predicted bathymetry for test hour 0405 is shown as the red dashed-line in the lower panel of Figure 3.6. The measured final bathymetry is plotted on a coarser grid than the sonic profiler measurements and the model grid.

The predicted and measured velocity moments, as a function of only the wave velocity, are compared in Figure 3.7. The red asterisks are the moments computed from the current measurements (EMF). The red circles are the moments generated from the measured pressure time series (DRO). As a reminder, the upper two panels are the even velocity moments and the lower two panels are the odd velocity moments. The predictions appear to compare well with the current-meter and pressure-sensor derived velocity moments offshore of the sand bar trough. The moments in the trough were over predicted compared with both sets of observations. The predicted moments at shoreward breaking location were over predicted compared to the observed current-derived moments, but appear to compare well with the pressure-derived moments. The pressure-derived moments slightly shoreward of the onshore breaking location compare well with the predictions from the NPMSE wave model. It is important to note that the instruments located at x=160m appear to be slightly onshore of the location of the peak wave velocity moments. The discrepancy between the current meters and pressure sensors at x=160m could be once again attributed error associated with the linear conversion of the pressure time series to water surface elevation time series in a location with highly nonlinear wave characteristics or potentially due to issues with the current meter measurements. The cross-shore variability of the DRO measurements appear more intuitive with larger magnitude moments observed near the wave breaking locations. It is also intuitive that large signals would be exhibited by the oscillatory velocities for this particular onshore bar movement study, when the current is expected to be weak. This was the same location in Test Case 1B where the current meter and pressure sensor generated moments significantly disagreed. The most shoreward comparisons between the predicted and the pressure-derived moments were rather good.

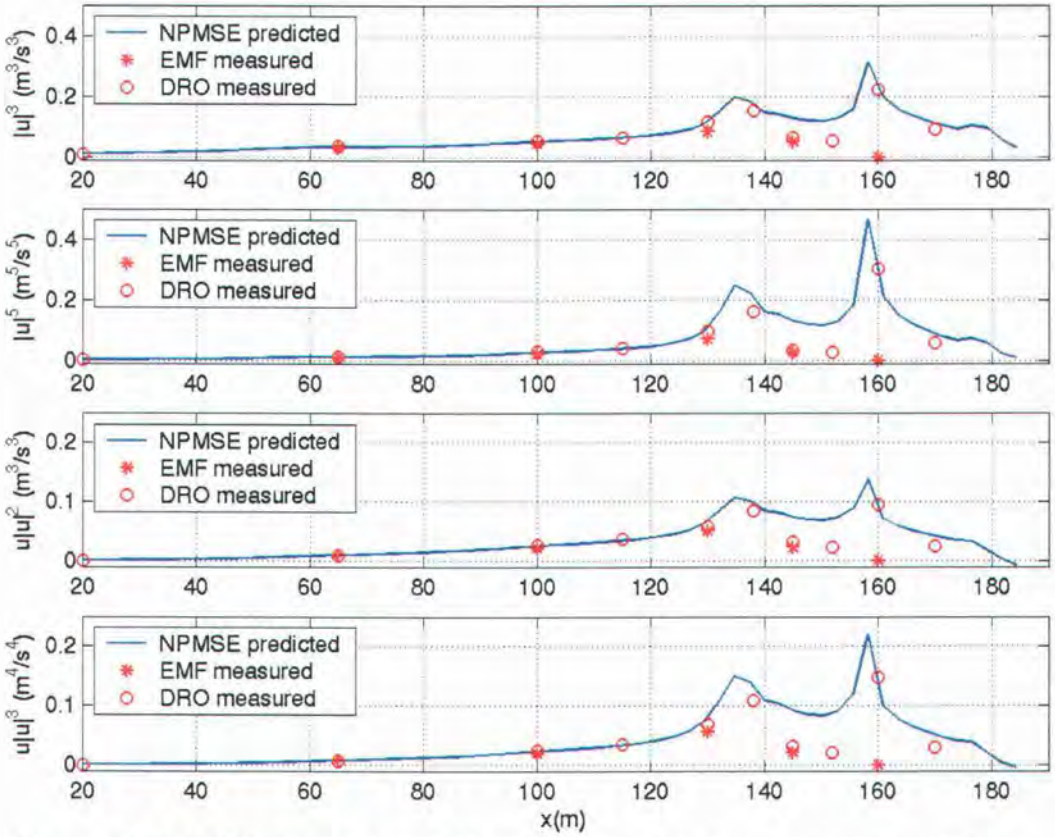

Figure 3.7. LIP11D Test Case 1C0405: Bailard velocity moments composed from the predicted oscillatory velocity time series at each modeled cross-shore location (blue -), compared to the moments produced from the current meter measurements (EMF)(red *), and from the pressure sensor measurements (DRO)(red o).

The volumetric sediment transport rate was predicted for each test hour in Test Case 1C using a Bailard's formulated energetics-type model. Figure 3.8 shows a comparison between the cross-shore profiles of the predicted and "measured" sediment transport rates ($Q(m^3/s)$). As a reminder, we computed the "measured" transport rate using the sediment transport model with the measured bathymetry and the measured velocity time series from the current meters.

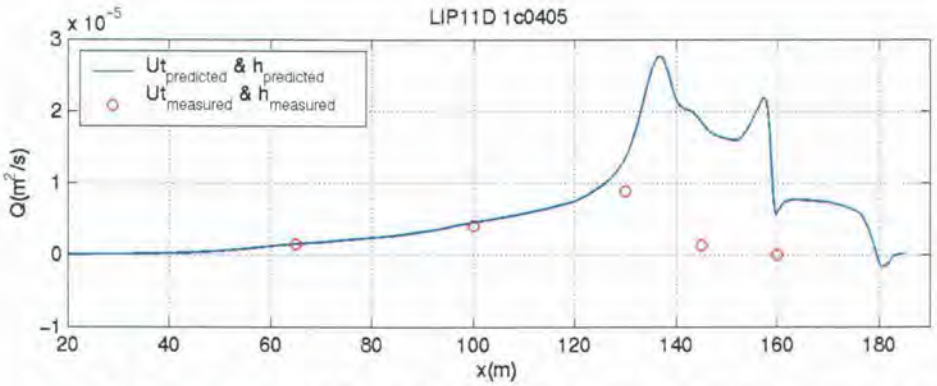

Figure 3.8. LIP11D Test Case 1C0405: Bailard-based predicted cross-shore volumetric transport (Q) profile (blue -) as a function of the predicted near bed wave velocity (NPMSE) and predicted depth-averaged undertow (GF2000). The predicted transport is being compared to the 'measured' transport (red o), which is computed with Bailard's formulation, using measured velocity time series from the current meters (EMF) and measured bathymetry.

Offshore of the sand bar, the predicted and observed volumetric transport rates compare quantitatively well. Around x=130m the wave model is predicting the initiation of breaking where as the observed breaking begins around x=140m, hence the skill of the model series at sediment transport predictions for test hour 0405 is rather poor (r^2~0.08) (Table 3.2). Due to this discrepancy, the volumetric transport is predicted to increase significantly starting around x=130m. The observations show that there is an increase in the volume of transported sediment due to the initiation of wave breaking. In the trough, shoreward of the bar, and at the most shoreward current meter location, a decreasing amount of sediment is being transported by the measured velocities. In Figure 3.7 it appeared that the instruments located at x=160m were shoreward of the maximum of the wave-only velocity moments. This could explain the over prediction of the volumetric transport, compared with the current meter observations, at this location. The significant difference between the measured and predicted transport at x=145m can be mostly attributed to the consistent overprediction of the local wave-velocity moments by the NPMSE model, when compared to the current meter observations. Similar to the velocity moment comparisons, the cross-shore profile of the predicted Q is more intuitive than the current meter observations. The increased transport predicted near the breaking locations near the sand bar is expected because bar migration was observed. Also, the cross-shore trend of the velocity moments is similar to the trend exhibited by the predicted volumetric transport, because the current is expectantly weak, because onshore bar migration is a function of increased wave skewness, which typically dominates

the mean velocities, as shown here by the model predictions. The predicted depth-averaged return flow is locally insignificant, therefore, no significant contribution is made by the local current (x=145m) to the predicted transport.

Volumetric transport skill values, for all simulated hours in Test Care 1C, are shown is Table 3.2. The average r^2-value for the transport comparisons is 0.08, with a standard deviation of 0.05 (grey-highlighted section). Even though the over all transport predictions show little skill, the predictions of the bathymetric evolution show significant skill (Table 3.2). The average bathymetric prediction skill is 1.0, with a standard deviation of 0.00. The skill predictions remain quite good when the predicted barred region is isolated and compared to the local measured bathymetry. In the sand bar region, from x=125m to x=166m, the model series has an average r^2-value of 0.98 and a standard deviation of 0.04.

Table 3.2. LIP11D Test Case 1C0405: Summary of skill (r^2-values) associated with the volumetric transport and bathymetric evolution predictions. The predicted transport is compared with the computed transport using measured total velocity and bathymetry ($\mathbf{Q_{hm}}$). The bar profile ($\mathbf{h_{bar}}$) comparisons are made between x=125m to x=166m.

Test Hour	Q_{hm}	h_{prof}	h_{bar}
1C0102	0.02	1.00	1.00
1C0204	0.07	1.00	1.00
1C0313	0.05	1.00	0.99
1C0405	0.08	1.00	0.99
1C0514	0.15	NA	NA
1C0807	0.03	NA	NA
1C1110	0.13	NA	NA
1C1300	NA	1.00	0.91
Mean	**0.08**	**1.00**	**0.98**
Std. Dev.	**0.05**	**0.00**	**0.04**

As a reminder, the measured bathymetry is interpolated onto a grid with the same resolution and sample locations as the prediction grid in order to compute the skill of the model at making the bathymetric evolution predictions for each test hour.

The Test Case 1C profile comparisons between the measured and predicted bathymetries for the 1st through the 5th, 7th, 11th, and 13th hours are shown in Figure 3.9 (top to bottom). The figure set-up follows that of the LIP11D, Test Case 1B figure set-up.

Once again, the hours with only predicted bathymetries (no crosses) lacked

corresponding measurements of the bathymetry. As mentioned in section 2.2.2, measurements were not taken during all test hours and some of the measured data was riddled with error and consequently excluded from the current study. In Test Case 1C, the 6^{th}, 7^{th}, 9^{th}, 10^{th}, 12^{th}, and 13^{th} hours did not have measured water surface elevation and/or measured bathymetry at the beginning of the test hour. Similarly to Test Case 1B, the same offshore wave climate was produced for all test hours in Test Case 1C. Therefore, for the 6^{th}, 7^{th}, 9^{th}, 10^{th}, 12^{th}, and 13^{th} hours the measured offshore water surface elevation for the respective previous test hours were used to drive the wave model.

During Test Case 1C, it appeared that the sand bar moved almost 5m shoreward, and more significantly, the cross-shore shape was altered. The bar profile thinned and became more peaked, with an extremely steepened shoreward slope. The seaward slope of the sand bar steepened slightly and the feature grew to about one-and-a-half times its original size height. Interestingly, a small trough-like shape formed around 10m seaward of the still water shoreline. A slight vertical growth of the seaward edge of the terrace was also observed during Test Case 1C.

The model series was able to qualitatively predict the onshore bar movement event, which is contradictory to Bailard (1981) model simulations by Gallagher *et al.* (1998) of the DUCK94 onshore bar movement event. Two significant differences between the Gallagher *et al.* (1998) study and ours is we use a finer resolution model grid, therefore, enabling us to make more detail cross-shore predictions, and we predict the flow field in a feedback system, allowing for influence by the morphology.

The predicted bar migration was onshore directed, but the cross-shore shape of the bar is admittedly broad compared with the observations. The model did not predict any vertical growth of the bar. In fact, a slight flattening of the bar profile was predicted, similar to the Test Case 1B sand bar predictions. The direct cause of the predicted retention of the initial bar shape and unpredicted vertical growth of the bar is not well understood. As a reminder, the quantities of predicted bed load or suspended load transport are directly related to the defined efficiency factors. The two modes of transport are obviously different and it can be assumed the associated patterns of deposition would also be different for each transport mechanism. For this particular test case simulation, no superfluous smoothing routines were utilized, therefore, the evolved bathymetry is likely not a result of post-processing the model predictions at the close of each test hour.

The profile of the trough and offshore bathymetry were predicted well by the model series.

The profile offshore of the bar accounts for 2/3 of the total cross-shore bathymetry somewhat owing to the model skill value of 1.0 which was quantified for the bathymetric predictions of the final test hour. The development of a small secondary trough-like feature was qualitatively predicted by the model. However, the magnitude of the observed hourly growth of the trough-like feature was not predicted by the model series.

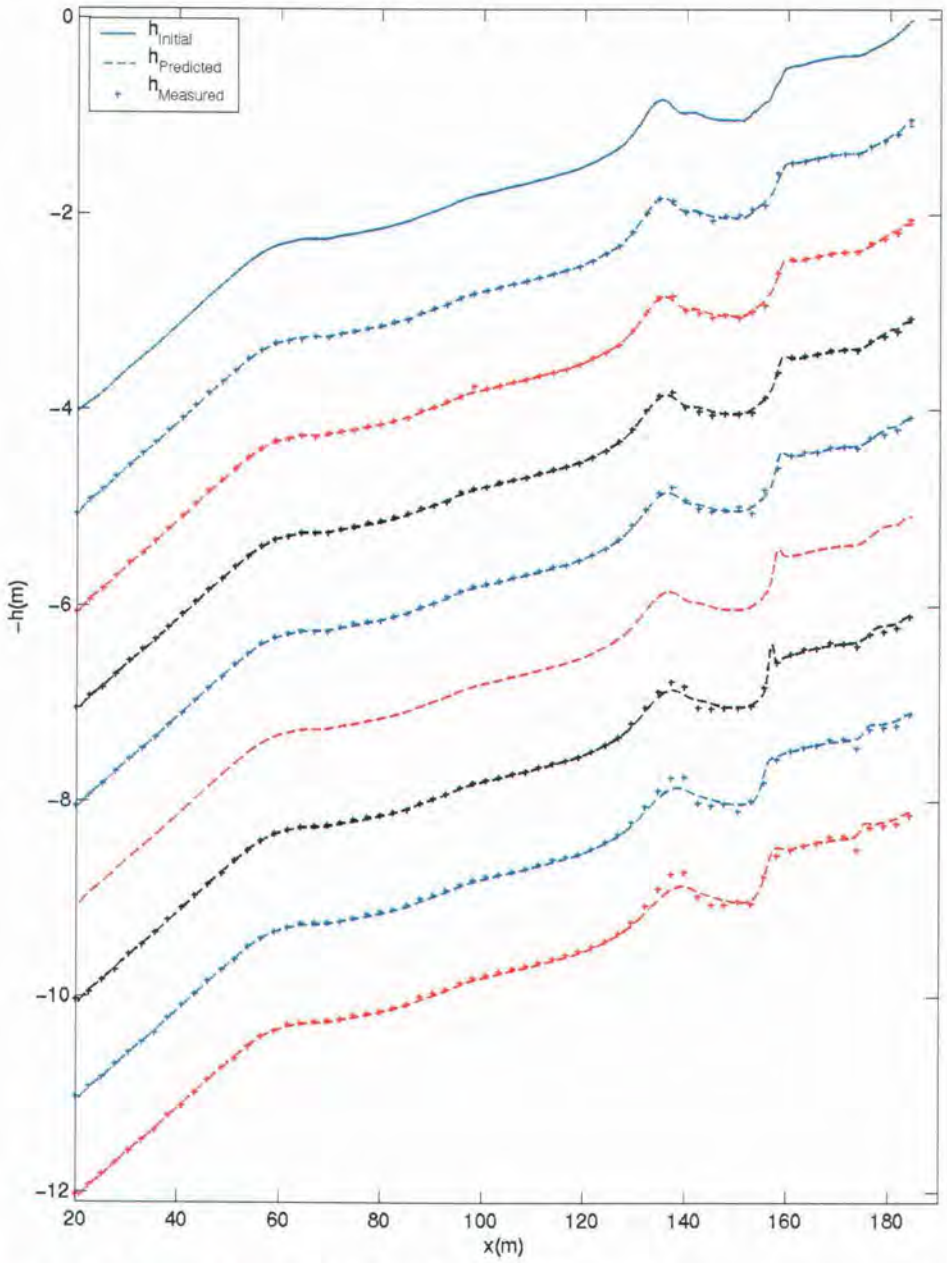

Figure 3.9. LIP11D Test Case 1C0405: Comparisons of measured (+) and predicted (- -) bathymetries for the 1st through the 5th hours and the 7th, 11th and 13th hours. The solid line is the initial input measured bathymetry for the 13 hour simulation.

3.4 Model Series Implemented in Field Study

In this study the waves and bathymetric evolution were modeled assuming shore-normal wave propagation. Measurements were used for the required cross-shore and longshore mean velocities. Attempts were made to model the cross-shore mean velocity, using GF2000, but the predictions consistently compared poorly with the observations, hence we decided to utilize measured mean velocities. We could still test the efficacy of using a wave model, therefore, the wave parameters were determined by the Kaihatu (2001) nonlinear fully dispersive wave model (NPMSE).

The predicted water surface elevation and near-bed oscillatory wave velocities are utilized from the wave module. The measured free-stream undertow and longshore current, and the predicted cross-shore wave velocities were used to determine the velocity moments required to drive a sediment transport model based on Bailard (1981) (therefore, the longshore oscillatory velocities were neglected by our model series). The evolution of the bathymetry was updated every 3 hours, corresponding to the end of each DUCK94 test period. The predicted hourly bathymetry was then run through a smoothing routine, in which a bathymetry vector was constructed from 21-point averages of the predicted bathymetry. The new bathymetric vector was then re-interpolated onto the wave model grid, using 'pchip' in Matlab, and then utilized as the input bathymetry for the following test hour. The small scale smoothing routine was implemented to smooth over any small scale features predicted by the model (<1m wide) which could have potentially resulted in instability of the wave model.

3.5 Model Validation Using DUCK94 Data Set

The data collected by the SPUV instruments discussed above in section 2.2.3 were also utilized in the sediment transport study. The water surface elevation time series derived from the pressure sensor time series was once again used to drive the wave model from the offshore boundary of x ~ 398m. Our focus is on the bar movement periods, starting on the 1st of September, 23rd of September, 2nd of October, and the 10th of October, and will also be used to make comparisons of multi-day bathymetric evolution predictions in the present sediment

transport study. The measured profiles for the 1st of September and then the ending profiles for each of the mentioned bar movement periods are shown in Figure 3.10.

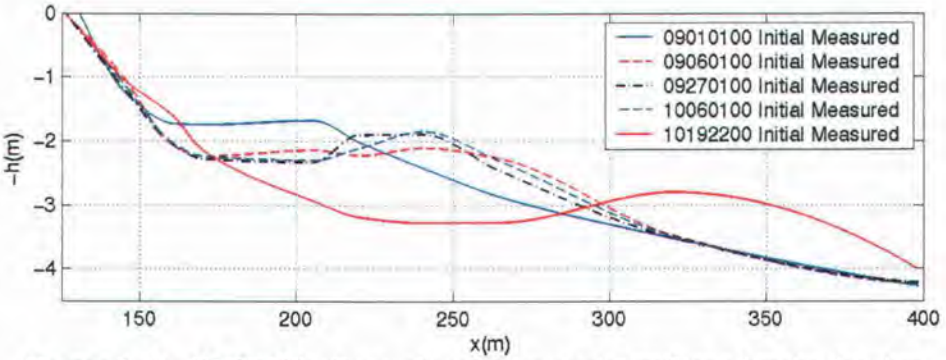

Figure 3.10. DUCK94: Cross-shore bathymetric profiles after the four bar movement events modeled in this study. In chronological order the profiles are the 1st hour of September 1st, September 6th, September 27th, and October 6th, and the 22nd hour of October 19th.

In this study, we used the measured longshore and cross-shore currents. We assumed that the simulations would be more valuable if known sources of large error associated with the undertow modeling were initially removed. The mean current was determined by initially breaking the velocity time series into 17-minute realizations. The realizations were then ensemble averaged to generate one 17-minute realization, which was then time-averaged to obtain the mean current at that instrument location for the test period [following Gallagher *et al.* (1998)]. The measurements were then interpolated to the grid spacing of the wave model using 'pchip' in MATLAB. We artificially forced the current measurements to zero at the modeling domain boundaries.

Volumetric transport comparisons are made between the predictions and measurements for test periods within each of the four simulations. The predictions were made using the Bailard sediment transport formulation, which was driven with the predictions of cross-shore oscillatory velocities, predicted bathymetry, and measured cross-shore and longshore currents. The measurements were computed from Bailard predicted sediment transport using measured total cross-shore and longshore velocities, as well as measured bathymetry. Following Gallagher *et al.* (1998), a cross-shore variable fall velocity was implemented. The profiles shown in all the figures are with respect to NGVD. The measured tide was added linearly to all the profiles (predicted and measured) during the model simulations of the test periods so that the models accounted for the total water depth (tide +

NGVD water depth).

3.5.1 DUCK94: Offshore Bar Movement Periods

The offshore sand bar migration events were typically characterized by storm events in which the offshore waves consistently exceeded 1m with peak periods less than 7s. The onshore bar movement event occurred during periods when the wave climate was less energetic. The wave heights typically ranged between 0.5m to 1m during this milder wave climate, with a peak period over 6s.

3.5.1.1 DUCK94: September 1st – September 5th

The initial observed seaward bar migration occurred between September 1st and the 5th, with the majority of the migration occurring in the latter half of the 5-day period. The sand bar migrated approximately 40m offshore, as shown in Figure 3.11. The profile of the bar became elongated, while the shoreline slope and shape was mostly preserved. Mega ripples were observed migrating through the broadened trough (Gallagher *et al.*, 1998).

For this particular test case, three approached were taken to model the bathymetric evolution during this tests period: 1. Our model series which was described in section 3.4; 2. Again, following Gallagher *et al.* (1998), by utilizing measured longshore and cross-shore velocity time series to drive the Bailard (1981) sediment transport model, and then interpolating the predicted Q at the instrument locations onto the same grid used by our model series to take the spatial derivative; and 3. Following the approach of Gallagher *et al.* (1998), who utilized measured longshore and cross-shore velocity time series to drive the Bailard (1981) sediment transport model. Gallagher *et al.* (1998) used a specialized differencing scheme, because of the varying distances between the instrument locations, which is thoroughly discussed in their paper, as well as in Plant *et al.* (2004). The specialized differencing routine utilized by Gallagher *et al.* (1998) reduces to our finite differencing scheme when using an evenly spaced grid. These three approaches to modeling the bathymetric evolution at Duck Beach for the first 5 days of September proved to have significantly different results. One test hour of all three bathymetric predictions is compared below in Figure 3.12.

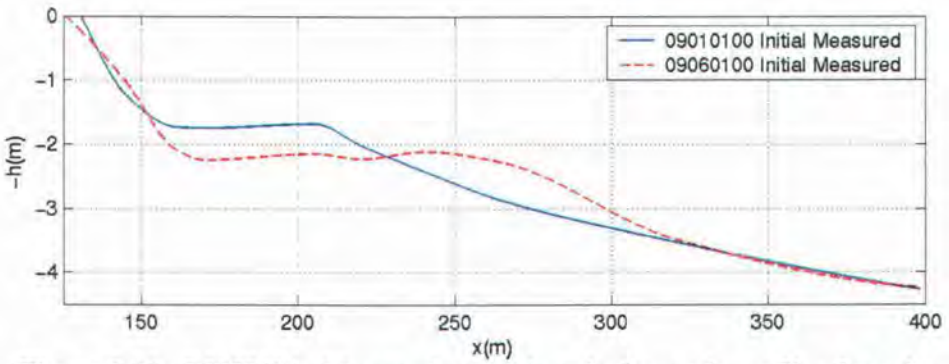

Figure 3.11. DUCK94: Measured cross-shore bathymetric profiles from the 1st hour of September 1st and September 6th. The bar-crest moved approximately 35m offshore.

Test period predictions from the 22nd hour on the 3rd of September are compared with the observations in Figure 3.12. The upper panel compares the cross-shore profile of the prediction wave height and the measured wave height, which was computed from the pressure-sensor measurements. The predicted wave heights offshore of the bar compare very well with the observations, but are over predicted shoreward of x~210m. The predicted waves likely stopped breaking due to the predicted trough in the bathymetry around x~200m, thereby resulting in the over predicted wave height.

The measured longshore and cross-shore currents are plotted in the central panel of Figure 3.12. The time averaged measurements by the current meter are marked by the asterisks. The strong longshore current contributed significantly during this time period to the predicted transport because it greatly contributed to the large volume of transported suspended sediment (Thornton *et al*, 1996). The current was observed to be moving mostly in the Southern direction throughout this 5-day offshore bar migration event. The measured cross-shore current was markedly strong during the 5-day test period, with observed maximums exceeding 1m/s. The maximum observed offshore-directed current was observed near the measured crest of the sand bar.

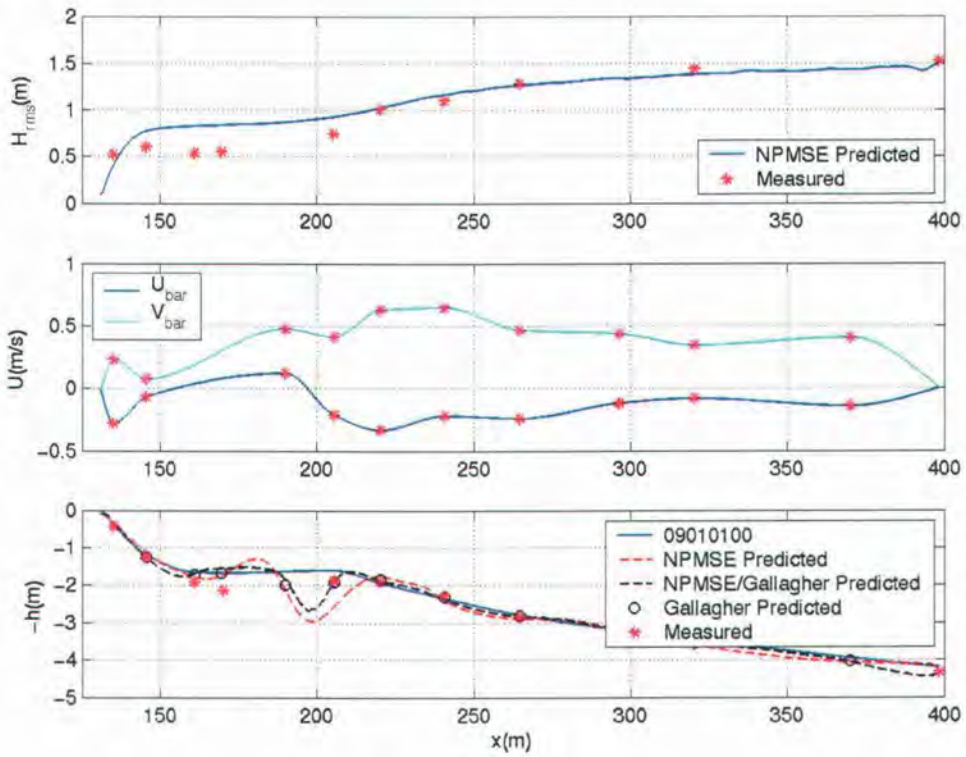

Figure 3.12. DUCK94 September 3rd, 22nd hour: Upper panel -Predicted H_{rms} by NPMSE (blue) compared to pressure-derived measurements (red asterisks). Center panel – Measured cross-shore (red asterisks) and longshore (purple asterisks) currents, with the interpolated current used by the model series (solid lines). Lower panel – Measured input bathymetry from the 1st hour of September 1st (blue line); predicted bathymetries at the end of the 22nd hour on the 3rd day by the model series (red dash), model series using the measured total cross-shore and longshore velocities (black dash) and using Gallagher *et al.* (1998) approach. Measured bathymetry at the end of the 22nd hour (red asterisks).

The initial measured bathymetry from the 1st hour on the 1st day of September is shown in the lower panel of Figure 3.12. In the same order as their descriptions, the resulting bathymetries by the three approaches are: 1. NPMSE Predicted; 2. NPMSE/Gallagher Predicted; and 3. Gallagher Predicted. The model skill was quite good for the profile evolution predictions at the instrument locations through the 22nd hour on the 3rd day of September (r^2=0.94), with the exceptions being near x~169m and 205m. The bathymetric evolution predictions following the 3rd approach compared well with the observations, but did not continue to compare better than the predictions by the 1st approach (r^2=0.94). Bathymetric evolution predictions have been found to be quite sensitive to the routine implemented to determine the spatial derivative of the volumetric transport (Plant *et al.*, 2004). It was found that the results produced using the same discretizing routine of Gallagher *et al.* (1998) (3rd

approach) were more stable and produced less error in the morphologic predictions, potentially because comparison were only made at the instrument locations. Our comparisons showed that indeed the results produced using the Gallagher *et al.* (1998) (3rd) approach were more stable, but potentially less accurate because they used only 11 points in their cross-shore bathymetry, where we were using over 5,000 points. The use of the total measured velocity time series improved the results using the same grid spacing as the model series (approach 2), as seen in Figure 3.12 when comparing the black and red dashed lines. A more in-depth discussion of the Gallagher *et al.* (1998) discretizing routine can be found in Plant *et al.* (2004). As a reminder, for an evenly spaced computation domain, the discritizing routine used in Gallagher *et al.* (1998) reduces to the finite differencing scheme we use for taking spatial first-derivatives in our transport calculations.

The volumetric transport predictions appear to qualitatively simulate the measurements shoreward of the bar crest, as shown in Figure 3.13 (r^2=0.62). The predictions seaward of the bar appear to be significantly larger than, and in the opposite direction of, the observations. However, the predicted spatial derivative of the volumetric transport is very similar to the observations.

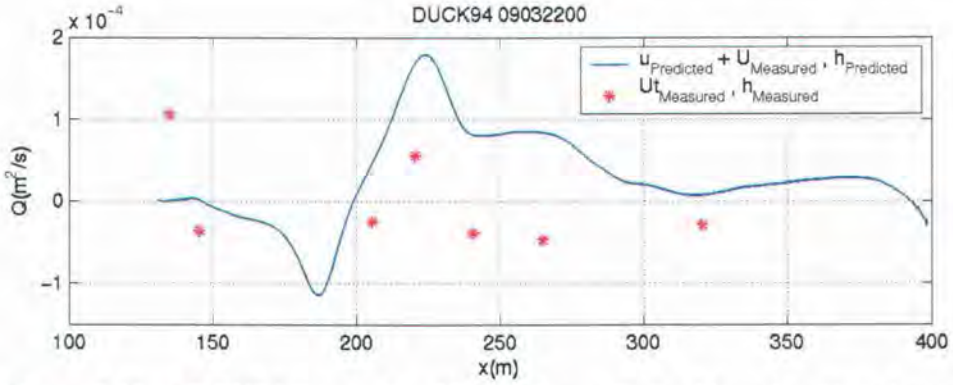

Figure 3.13. DUCK94 September 3rd, 22nd hour: Bailard-based predicted cross-shore volumetric transport (Q) profile (blue -) as a function of the predicted near bed wave velocity (NPMSE) and measured currents. The predicted transport is being compared to the 'measured' transport (red asterisks), which is computed with Bailard's formulation, using measured velocity time series from the current meters and measured bathymetry.

The model skill values for the predicted volumetric transport of the profiles shown in Figure 3.14 are listed in Table 3.3. The skill of the profiles predictions by the model series

(approach 1) (h_{prof}), using the predicted volumetric transport interpolated onto the model series grid (approach 2) (h_{ng}), and the predictions using the approach of Gallagher *et al.* (1998) (approach 3) (h_{gal}) are also listed in Table 3.3. The model series (1st approach), on average, did not exhibit significant skill when predicting the volumetric transport, but performed well at producing the observed local water depth at the instrument locations. The model skill when predicting the morphological evolution admittedly mostly declined with increasing time into the simulation, indicating that this model series goes unstable with increasing number of days (as opposed to longer time scales) when modeling consistently energetic wave conditions.

Table 3.3. DUCK94 September 1st-5th: Summary of skill (r^2-values) associated with the volumetric transport and bathymetric evolution ($\mathbf{h_{prof}}$, $\mathbf{h_{ng}}$, $\mathbf{h_{gal}}$) predictions for the profiles shown in Figure 3.14. The predicted transport is compared with the computed transport using measured total velocity and bathymetry ($\mathbf{Q_{hm}}$).

Test Period	Q_{hm}	h_{prof}	h_{ng}	h_{gal}
9010100	0.00	1.00	1.00	1.00
9011000	0.98	1.00	1.00	1.00
9020100	0.19	0.99	1.00	1.00
9021000	0.56	0.99	1.00	1.00
9030100	0.14	0.98	0.99	0.99
9031000	0.52	0.96	0.99	0.97
9040100	0.72	0.87	0.97	0.94
9041000	0.68	0.72	0.84	0.82
9050100	0.52	0.78	0.74	0.62
9051000	0.82	0.73	0.68	0.49
9052200	0.93	0.73	0.71	0.56
Mean	**0.55**	**0.89**	**0.90**	**0.85**
Std Dev.	**0.32**	**0.12**	**0.13**	**0.20**

The predicted profiles (using approach 1), compared to the observations, in Figure 3.14 display the decline in the model skill with increasing time. The predicted bathymetry became over-run with large-scale oscillations, which we think are mostly a result of the interpolating routine, 'pchip'. Due to the consistently energetic wave climate, the predicted bathymetry began to show instability in the model series about half-way through the simulation. The offshore bump in the bathmetry is due to the post-processing routine (which includes the interpolation of the new bathymetry using 'pchip').

The bar crest and trough region are predicted poorly by the model series near the end of the simulation. The shoreline shape and slope were preserved by the model series.

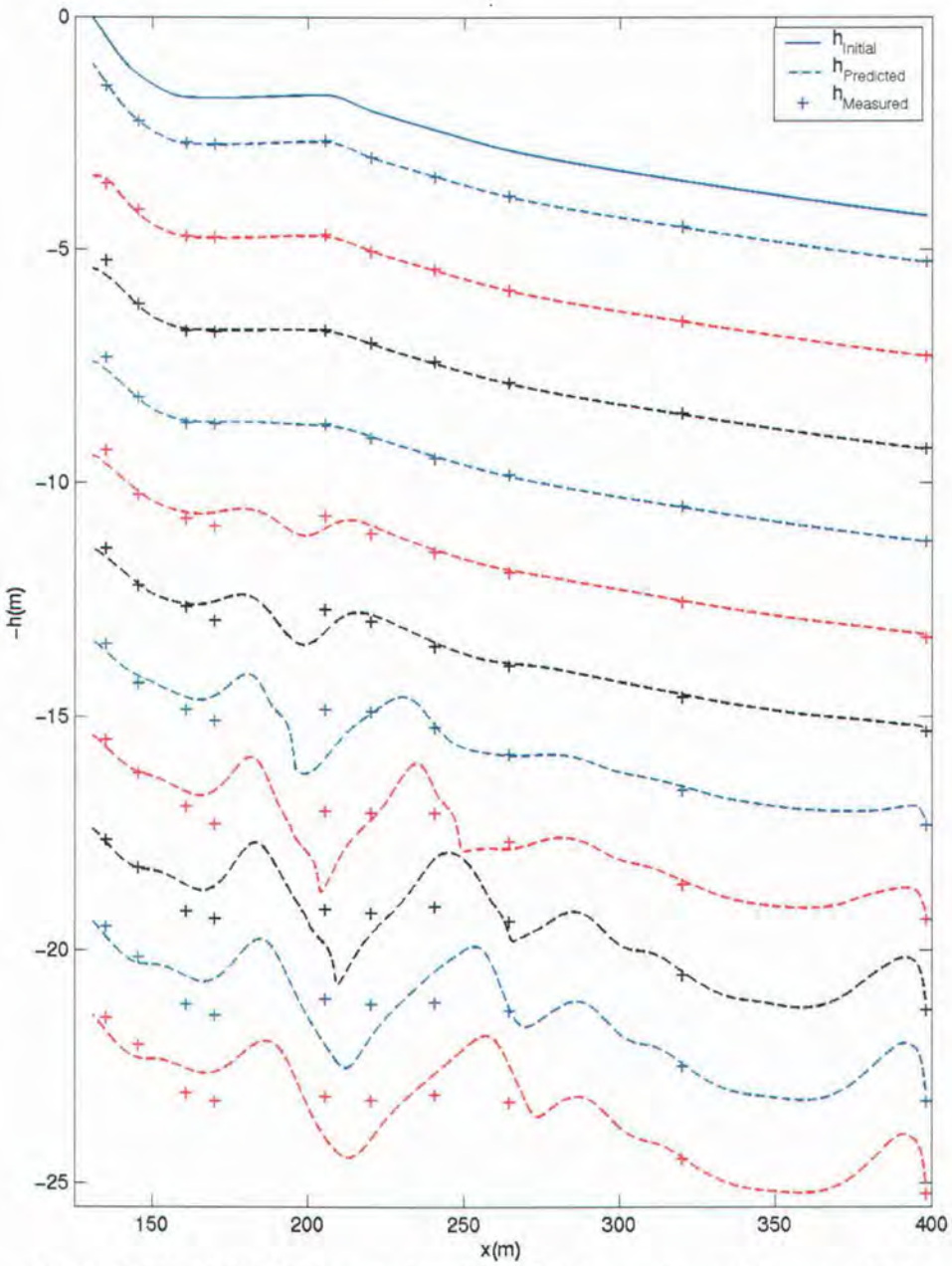

Figure 3.14. DUCK94 September 1st – 5th: Comparisons of measured (+) and predicted (--) bathymetries for the 1st through the 5th of September, at the end of the 1st-hour and 10th–hour test periods. The solid line is the initial input measured bathymetry from the 1st hour on the 1st day of September. The bottom compared bathymetries are for the 22nd hour on the 5th of September. The model skill for these compared profiles is 0.85.

3.5.1.2 DUCK94: October 2nd – October 4th

The observed offshore bar migration event in early October occurred between the 2nd and the 4th. The sand bar migrated approximately 25m offshore, as shown in Figure 3.15. The bar became sinusoidal in shape, with smoothed edges that peaked over a broad bar, while the shoreline slope and shape was once again preserved.

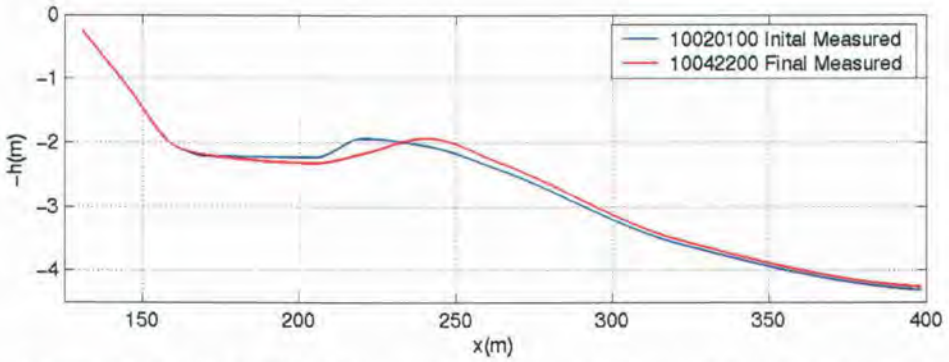

Figure 3.15. DUCK94: Measured cross-shore bathymetric profiles from the 1st hour of October 2nd and the 22nd hour of October 4th. The bar-crest moved approximately 15m offshore.

Test period predictions from the 3rd of October during the 13th hour are compared with the observations in Figure 3.16. The upper panel compares the cross-shore profile of the prediction wave height and the measured wave height, which was computed from the pressure-sensor measurements. The waves are predicted to break from the offshore gauge location, which is contrary to the measurements. The predictions begin to compare well after the initial strong breaking period over the bar, and into the shoreline. The predicted waves potentially broke offshore of the observed breaker line from the bump (x~275m) predicted in the bathymetry which was not instrumented, so no bathymetric data was available in this region from the SPUV instruments.

The measured longshore and cross-shore currents are plotted in the central panel of Figure 3.16. The measurements are represented by the asterisks. The longshore current contributed significantly during this time period to the observed transport, and was found to be necessary input into the model series to improve the bathymetric evolution predictions.

The cross-shore current increased in strength over this time period, but was not nearly as strong at the observed longshore current. The vertical instrument locations varied with respect to their closeness to the seabed, therefore, the vertical maximum of the cross-shore current may not be observed by the instruments. The longshore current has been observed to have a more uniform vertical profile, especially in the trough.

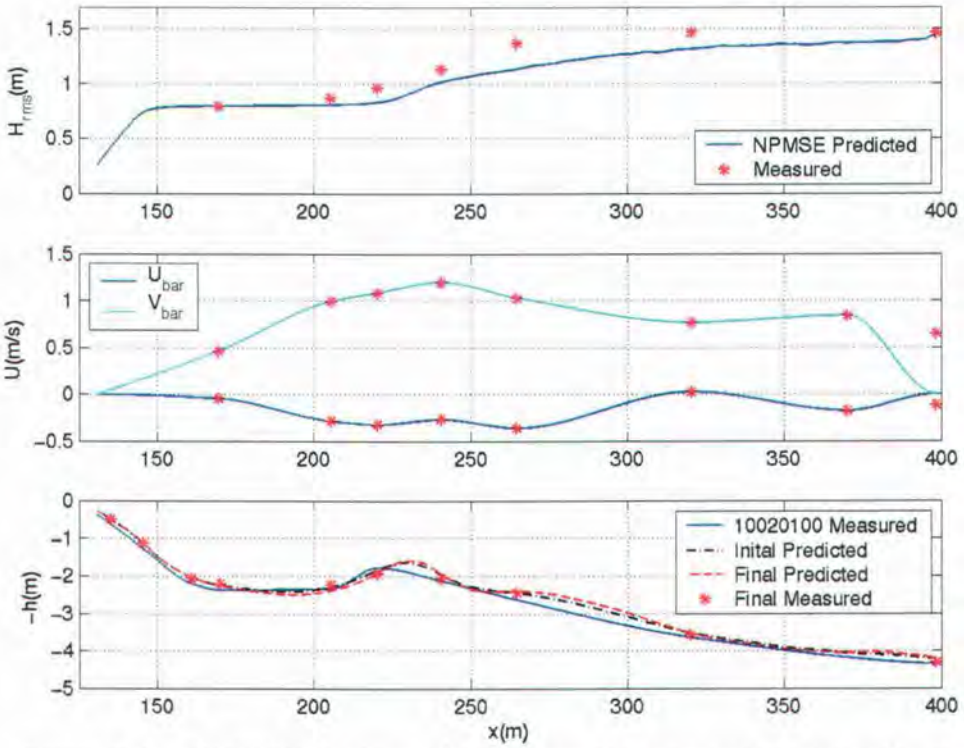

Figure 3.16. DUCK94 October 3rd, 13th hour: Upper panel -Predicted H_{rms} by NPMSE (blue) for the Initial Predicted bathymetry (black dash-dot) compared to pressure-derived measurements (red asterisks). Center panel – Measured cross-shore (red asterisks) and longshore (purple asterisks) currents, with the interpolated current used by the model series (solid lines). Lower panel – Measured input bathymetry from the 1st hour of October 2nd (blue line); initial (black dash) predicted, final (red dash) predicted, and measured bathymetry (red asterisks) at the end of the 13th hour on the 3rd day of October.

The initial measured input bathymetry from the 1st hour on October 2nd is shown in the bottom panel of Figure 3.16 by the blue line. The initial predicted input and final output profiles for this specific 3-hr test period are also shown in the lower panel. The measured final bathymetry is shown by the red asterisks corresponding to the gauge locations. From this comparison about half-way through the simulation, the model is performing quite well at

predicting the morphological evolution of the offshore bar movement, though oscillations between the measurement locations are already present.

The predicted and measured transport are compared in Figure 3.17. The maximum magnitude of the volumetric transport was not predicted by the model series, but the cross-shore trend was qualitatively predicted. The local minimum predicted by the models around x~245m is not present in the measurements, due to the sparse instrument array, there truly is not enough cross-shore data to know how correct the model truly is. The observed onshore directed transport (-) is qualitatively predicted by the model series, but it is an order of magnitude less than the observations.

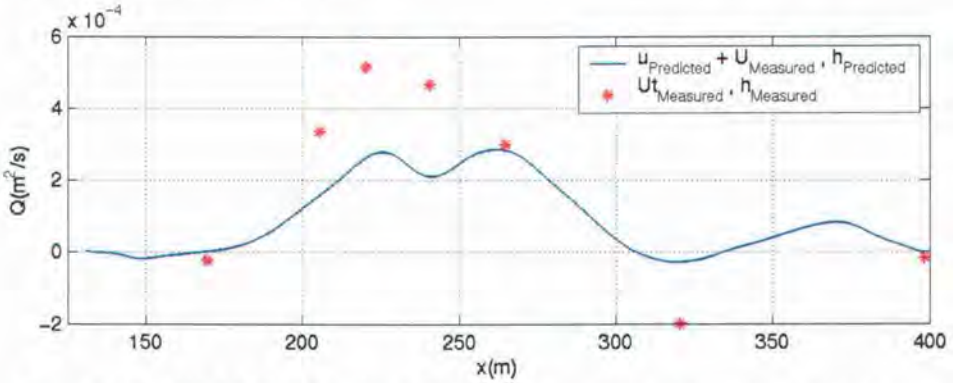

Figure 3.17. DUCK94 October 3rd, 13th hour: Bailard-based predicted cross-shore volumetric transport (Q) profile (blue -) as a function of the predicted near bed wave velocity (NPMSE) and measured currents. The predicted transport is being compared to the 'measured' transport (red asterisks), which is computed with Bailard's formulation, using measured velocity time series from the current meters and measured bathymetry.

Table 3.4 lists the model skill values for the 1st and 13th hours of each day being simulated, which correspond to the profiles compared in Figure 3.18. The statistical values are computed using the skill values from each test period in the 3-day test case, and are shown in the grey boxes. The model series showed significant skill when predicting the volumetric transport for this particular test period (r^2=0.84, yellow-highlighted), and overall had an average skill of 0.72 for the test case.

Table 3.4. DUCK94 October 2nd-4th: Summary of skill (r^2-values) associated with the volumetric transport and bathymetric evolution ($\mathbf{h}_{profile}$) predictions for the profiles shown in Figure 3.21. The predicted transport is compared with the computed transport using measured total velocity and bathymetry ($\mathbf{Q}_{hm}$).

	Q_{hm}	$h_{profile}$
10020100	0.59	1.00
10021300	0.98	1.00
10030100	0.81	1.00
10031300	0.84	1.00
10040100	0.74	0.98
10041300	0.86	0.98
10042200	0.95	0.99
Mean	0.72	0.99
Std. Dev.	0.25	0.01

Figure 3.18 shows profile comparisons between the predictions (dashed lines) and measurements for the 1st and 13th hour of October 2nd, 3rd, and 4th. The 22nd hour profile from the 4th is also compared to the measurements (crosses). The predictions compared well with the observations at the instrument locations, though the predicted bathymetry was forming oscillations which were likely not present in nature. We think they are a result of the interpolating routing, 'pchip', but no formal conclusions have been reached as of yet. A more in-depth discussion can be found in the conclusions.

Figure 3.19 displays comparison between bathymetric measurements and predictions in the format as the previous figure. The predicted bathymetries in the lower figure are generated using the bathymetric predictions at the instrument locations **only**, and simply interpolating these results to the model grid locations. The interpolation is performed using 'pchip' in Matlab, which is the same interpolation routine utilized to generate the initial input bathymetry for each of the four field test periods. We are offering this visual comparison because this is typical presentation format used in most papers on the topic of modeling morphological evolution. In most of the previous studies [Thornton *et al.*, 1996; Gallagher *et al*, 1998; Hoefel and Elgar, 2003; Henderson *et al.*, 2003; Long and Kirby, 2003] , bathymetric predictions are only made at the instrument locations, therefore, predictions are only shown at the instrument locations, which can be potentially misleading, as demonstrated by comparing Figures 3.18 and 3.19.

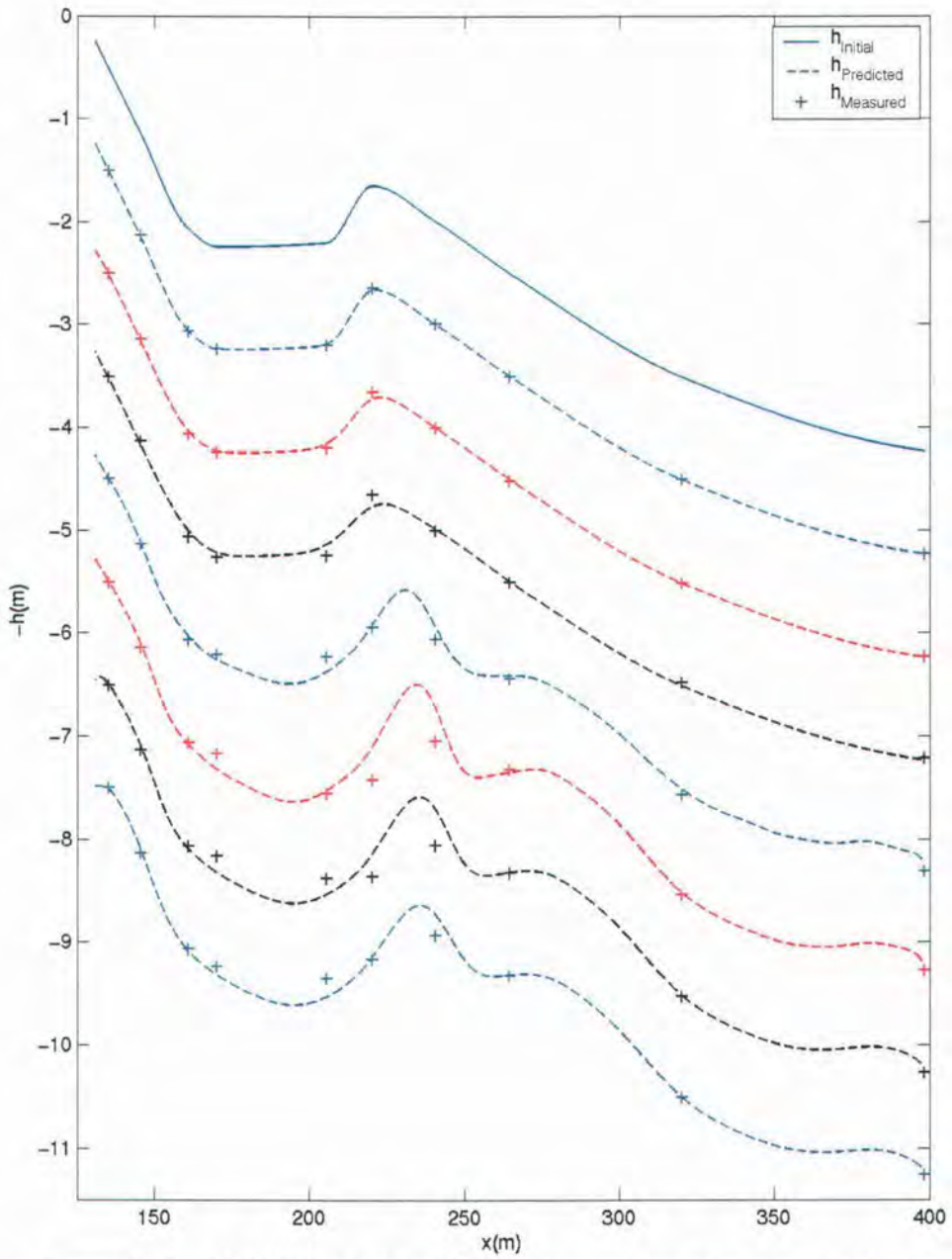

Figure 3.18. DUCK94 October 2nd-4th: Comparisons of measured (+) and predicted (--) bathymetries for the 1st and 13th hours of Oct. 2nd-4th (top to bottom). The final bathymetry comparison (on the bottom) is for the 22nd hour on the Oct. 4th. The solid line is the initial input measured bathymetry, from the 1st hour on Oct. 2nd, for the 3-day simulation. The total bathymetric predictive skill exhibited by the model series for these particular test hours was (r^2) 0.80.

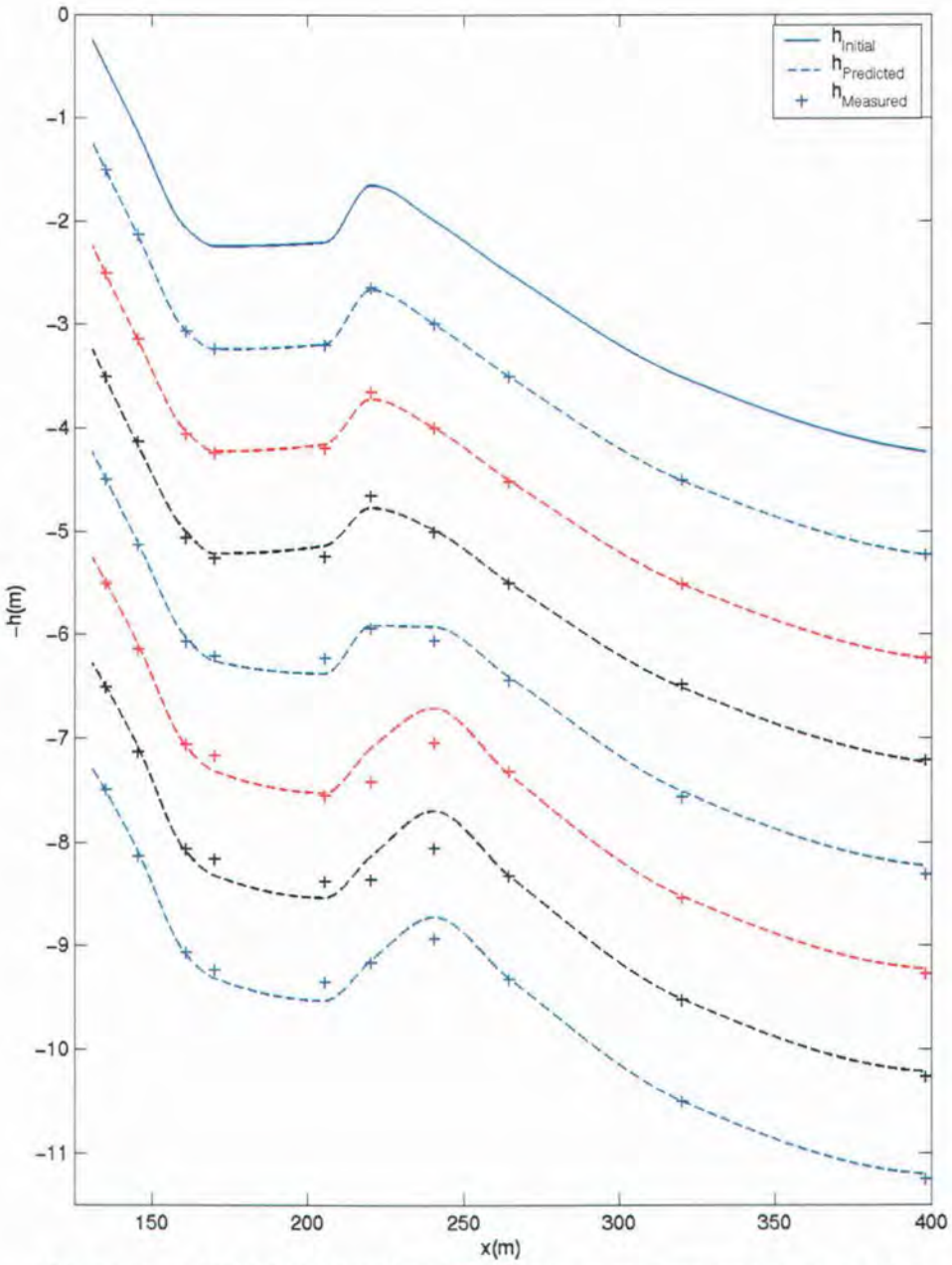

Figure 3.19. DUCK94 October 2nd-4th: Same as previous figure, but the predictions at the instrument locations only were utilized to generate a bathymetry using 'pchip', which is the same Matlab routine used to interpolate the initial input bathymetry from the measurements.

3.5.1.3 DUCK94: October 10th –October 20th

The largest observed seaward bar migration event in mid-October occurred between the 10th and the 20th. The sand bar migrated approximately a 100+m offshore, as shown in Figure 3.20. The sinusoidal shape of the bar became more exaggerated. The shoreline developed a small, steep terrace-shape and the slope became slightly milder.

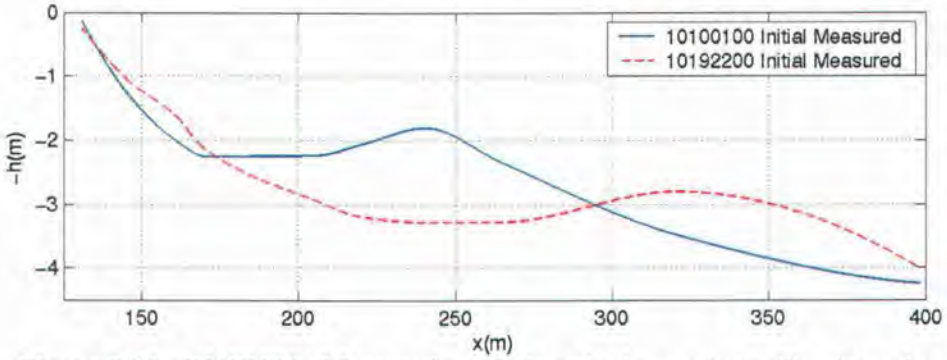

Figure 3.20. DUCK94: Measured cross-shore bathymetric profiles from the 1st hour of October 10th and the 22nd hour of October 19th. The bar-crest moved approximately 80m offshore.

Test period predictions from the 14th of October during the 1st hour are compared with the observations in Figure 3.21. Similar to the early October study in Section 3.5.1.2, the waves are predicted to break (x~315m) offshore of the observed breaker line (x~265m). Again, the predictions begin to compare well after the initial strong breaking period over the bar, and into the shoreline. The predicted waves did brake offshore of the observed breaker line because of the large bar predicted in the bathymetry. The predicted bar only had instrument locations on either end of it, so no bathymetric data was available in this region from the SPUV instruments, but CRAB surveys are available for days when the wave height did not exceed 2m.

The measured longshore and cross-shore currents are plotted in the central panel of Figure 3.21. The time averaged measurements by the current meter are marked by the asterisks. The longshore current again contributed significantly during this time period to the observed transport, and was found to be necessary input into the model series to improve the bathymetric evolution predictions. The dominant longshore current direction changed significantly during this 10-day test case. The longshore current profile show in Figure 3.21

displays a current moving in the Northern direction, where as in Figure 3.16 the current is moving in the Southern direction. The maximum observed offshore directed current is observed slightly shoreward of our predicted bar crest. This differs from observations by Trowbridge and Young (1989), who found that the maximum cross-shore current is typically located over the crest of the bar due to the decrease in water depth the fluid must increase in velocity to maintain the flow. This visual comparison could imply that we are predicting the bar crest to move offshore too rapidly, resulting in the unnaturally large bar profile around x=275m.

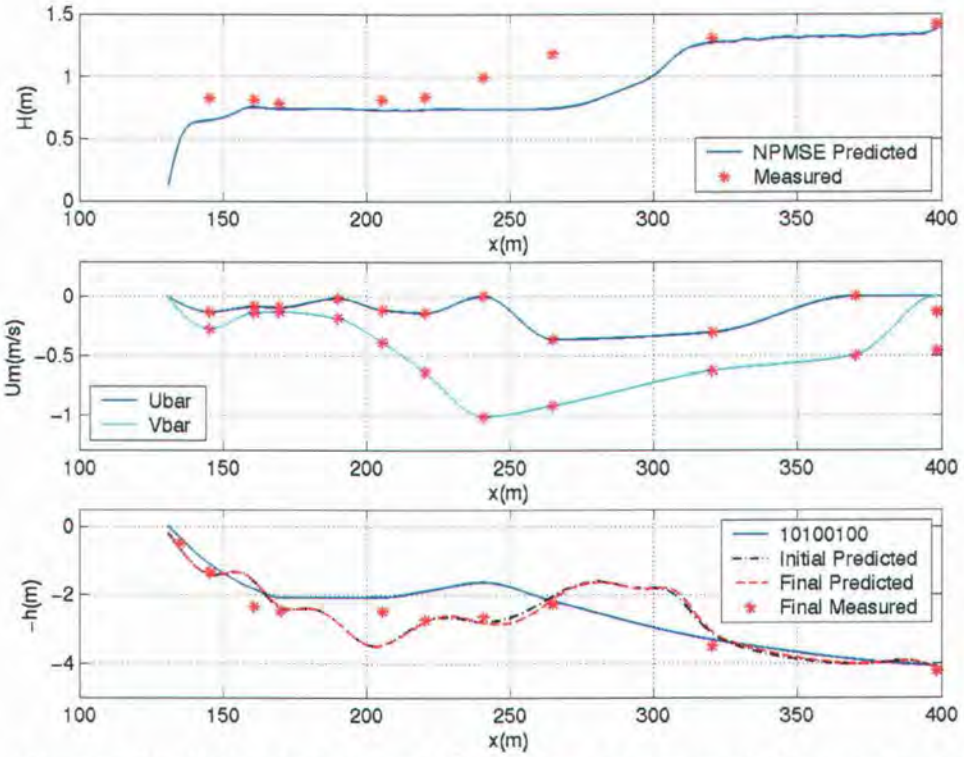

Figure 3.21. DUCK94 October 14th, 10th hour: Upper panel -Predicted H_{rms} by NPMSE (blue) compared to pressure-derived measurements (red asterisks). Center panel – Measured cross-shore (red asterisks) and longshore (purple asterisks) currents, with the interpolated current used by the model series (solid lines). Lower panel – Measured input bathymetry from the 1st hour of October 10th (blue line); initial (black dash) predicted, final (red dash) predicted, and final measured bathymetry (red asterisks) for the 10th hour on the 14th day of October.

The initial measured bathymetry from the 1st hour on the 10th day of October is shown (in blue) in the lower panel of Figure 3.21. The model skill was quite good for the profile evolution predictions at the instrument locations through the 10th hour on the 14th of October

(r^2=0.82), with the exception of the comparison near x~205m. The predicted bar profile is admittedly large, but no data was available in this region to assist in ascertaining the major source of error.

The bar shape is reflected in the volumetric transport profile predictions show in Figure 3.22. The predictions appear to qualitatively simulate the measurements (r^2=0.72). The broad profile of predicted significant volumetric transport is no supported by current findings in the literature. To obtain a bar profile shape which has been measured in the field, the transport profile would need to have steeper slopes, with a sharper peak near the transport maximum, which would produce a bar shape that is less broad.

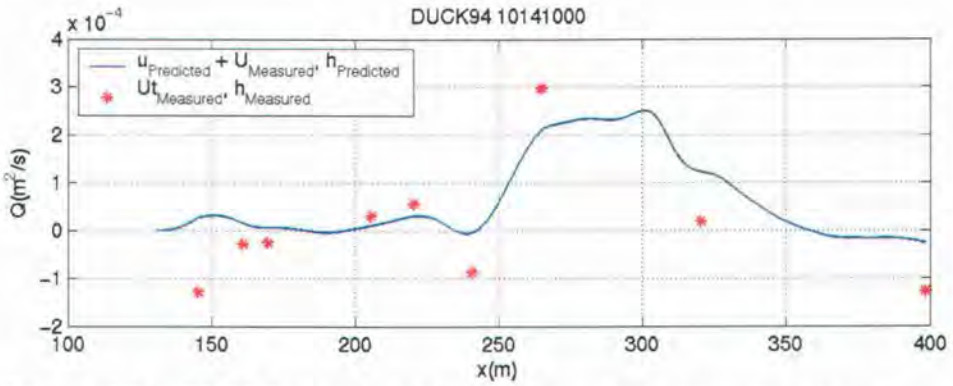

Figure 3.22. DUCK94 October 14th, 10th hour: Bailard-based predicted cross-shore volumetric transport (Q) profile (blue -) as a function of the predicted near bed wave velocity (NPMSE) and measured currents. The predicted transport is being compared to the 'measured' transport (red asterisks), which is computed with Bailard's formulation, using measured velocity time series from the current meters and measured bathymetry.

The model skill values for the predicted profiles (h_{prof}) shown in Figure 3.23 are listed in Table 3.5, along with the skill of the volumetric transport predictions (Q_{hm}). The model series, on average, did not exhibit significant skill when predicting the volumetric transport, but performed well at producing the observed local water depth at the instrument locations. The model skill when predicting the morphological evolution admittedly mostly declined with increasing time into the simulation, indicating that this model series is not ready to be utilized for long term predictions (O(months) or longer).

Table 3.5. DUCK94 October 10^{th}-20^{th}: Summary of skill (r^2-values) associated with the volumetric transport and bathymetric evolution ($\mathbf{h_{profile}}$) predictions for the profiles shown in Figure 3.26. The predicted transport is compared with the computed transport using measured total velocity and bathymetry ($\mathbf{Q_{hm}}$).

Test Period	Q_{hm}	h_{prof}
10100100	0.24	1.00
10110100	0.79	0.91
10120100	0.69	0.82
10130100	0.83	0.82
10140100	0.1	0.86
10150100	0.67	0.75
10160100	0.39	0.68
10170100	0.06	0.72
10180100	0.57	0.74
10190100	0.11	0.75
10192200	0.21	0.70
Mean	**0.43**	**0.79**
Std. Dev.	**0.30**	**0.10**

The profiles compared in Figure 3.23 display the decline in the model with increasing time. The predicted bathymetry became ridden with artificial oscillations, which we think are mostly a result of the interpolating routine, 'pchip'. Due to the changes in the wave climate, switching between energetic and calm waves, during this 10-day period, the bathymetry predictions did not become as unstable as seen in Figure 3.14 for the initial offshore bar movement period in September. The large scale oscillations predicted in that early September bar migration period were also predicted in this test case, but on a smaller, milder-sloping scale. The offshore enlargement of the bathymetry is due to the instability of the model series in combination with the processing routines (which include the interpolation using 'pchip') and using the measured currents. The measured currents will obviously not respond to the predicted changes in the bathymetry, therefore, generating a gap in the feedback routine where one segment of the model is unaffected by the previous predictions. This gap prevents the stabilizing influence of a strengthened undertow over the large bars in the model simulations.

The bar crest and trough region appear to be qualitatively predicted by the model series, though a second bar/trough feature is predicted near the shoreline where the terrace-

like formation was observed. These features near the shoreline may be an artifact of our practice to smoothly force the observed currents to zero near the shoreline, thereby generating sharp slopes in the current profiles, which translate into large transport spatial gradients in the sharply sloping regions. The large volumetric transport gradient produces significant bathymetric change when using an energetics-type transport model.

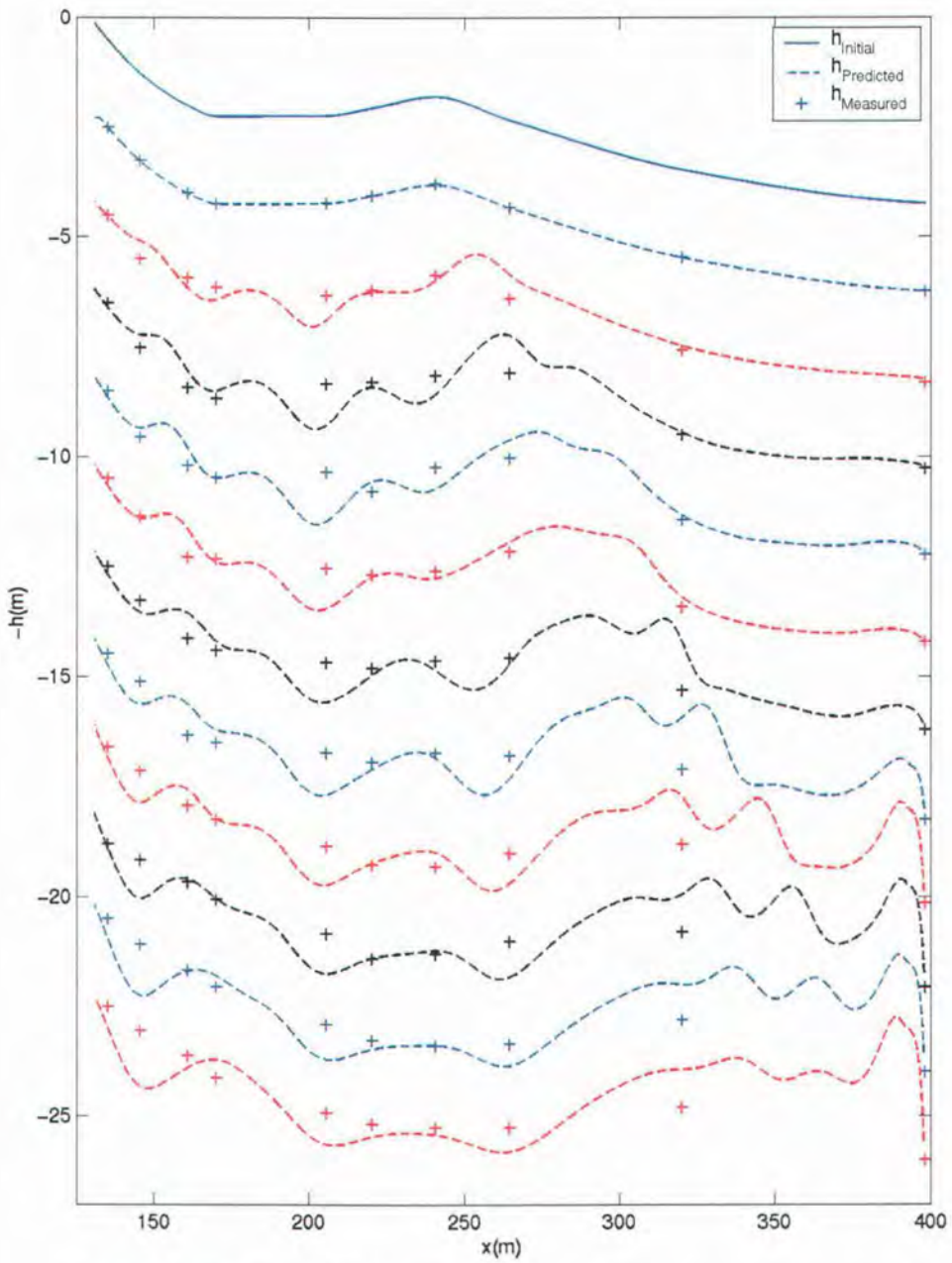

Figure 3.23. DUCK94 October 10th– 20th: Comparisons of measured (+) and predicted (--) bathymetries for the 1st hour of Oct. 10th-20th (top to bottom). The final bathymetry comparison (on the bottom) is of the 22nd hour on the Oct.20th. The solid line is the initial input measured bathymetry, from the 1st hour on Oct. 10th, for the 10-day simulation. The total bathymetric predictive skill exhibited by the model series for these particular test hours was (r^2) 0.4612.

3.5.2 DUCK94: Onshore Bar Movement Periods: September 23rd – September 27th

The offshore sand bar was observed to migrate approximately 20m shoreward between September 22nd and 27th. The offshore wave climate was characterized by mildly energetic waves which ranged in size from 0.5m to a little over 1m. The peak periods were appreciable longer than observed during the offshore bar movement events. The bar profile became elongated with the bar crest vertical elevation somewhat reduced by the shoreward sediment transport. The slope and shape of the shoreline was maintained during this 5-day period. Most of the transport occurred between the 23rd and 27th of September, which is the period modeled in this simulation.

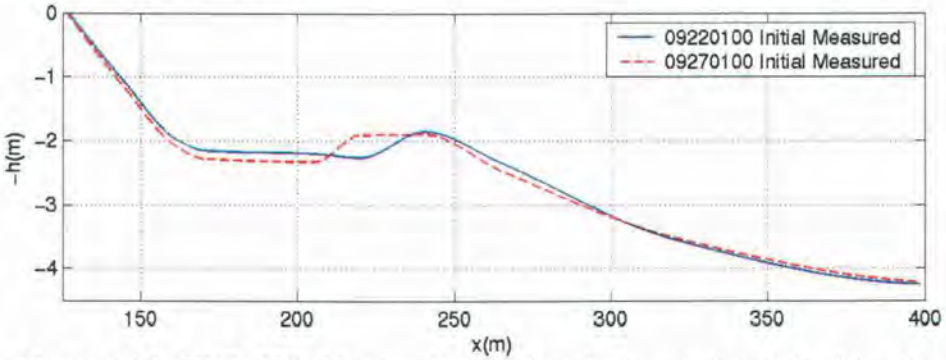

Figure 3.24. DUCK94: Measured cross-shore bathymetric profiles from the 1st hour of September 22nd and September 27th. The bar-crest moved approximately 15m onshore.

Test period predictions from the 24th of September during the 19th hour are compared with the observations in Figure 3.25. The cross-shore evolution of the wave height was predicted well by NPMSE using the predicted bathymetry. The maximum wave height observed near the shoreline was not predicted by the wave model, but it appears to not be a consequence of the predicted bathymetry in this region.

The measured longshore and cross-shore currents are plotted in the central panel of Figure 3.25. The longshore current is mostly on the same order of magnitude with the cross-shore current during this time period. The maximum cross-shore current is measured slightly shoreward of the bar crest and appears to be offshore directed, resulting in slight localized erosion which is deposited on the shoreward face of the bar.

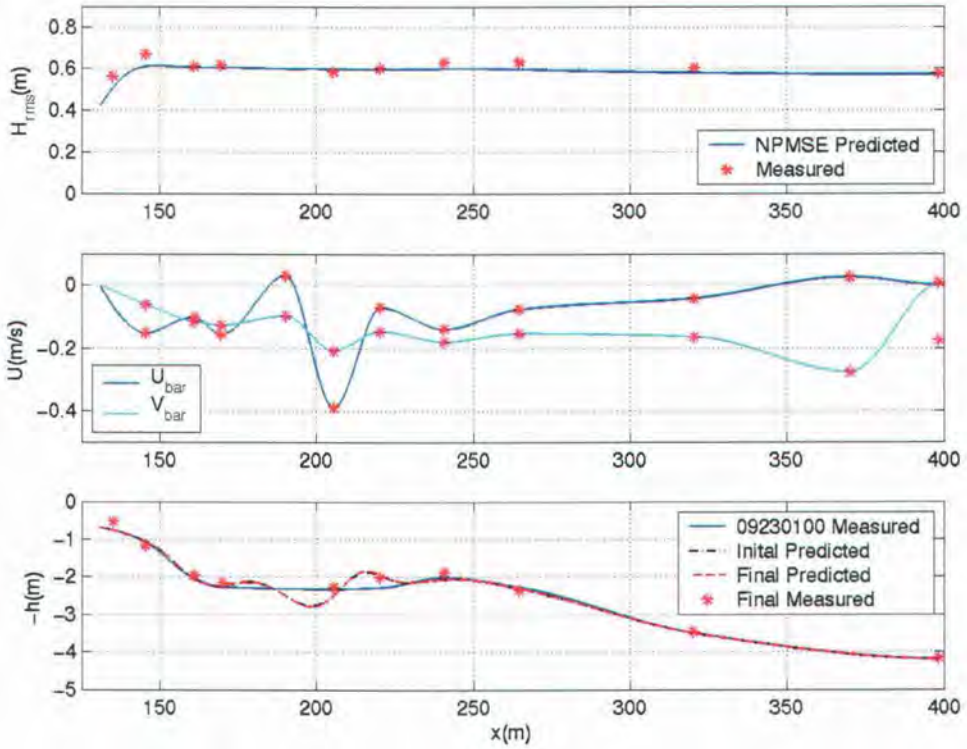

Figure 3.25. DUCK94 September 24th, 19th hour: Upper panel -Predicted H_{rms} by NPMSE (blue) compared to pressure-derived measurements (red asterisks). Center panel – Measured cross-shore (red asterisks) and longshore (purple asterisks) currents, with the interpolated current used by the model series (solid lines). Lower panel – Measured input bathymetry from the 1st hour of September 23rd (blue line); initial (black dash) predicted, final (red dash) predicted, and final measured bathymetry (red asterisks) for the 19th hour on the 24th day of September.

The profiles shown in the lower panel of Figure 3.25 are of the initial measured input bathymetry, initial predicted input bathymetry for the test period, final predicted bathymetry for the test period, and the final measured test period bathymetry. The measurements and predictions compare well at the instrument locations, resulting in model skill of 0.99 (Table 3.6, yellow highlighted row). The superfluous oscillation in the trough is likely a result of the interpolation routine used in the post-processing of each test period. The onshore bar migration is being predicted well qualitatively, as seen in Figure 3.27, which is contrary to the findings of Gallagher *et al.* (1998), who was unable to predict onshore bar migration.

The volumetric transport is also consistently predicted well by the model series for this onshore bar movement test case. The skill values for the model series predicting the volumetric transport for this field case are significantly better than for the onshore bar movement lab case, which implies the undertow model was potentially not performing well

for the lab case (LIP11D Test Case 1C).

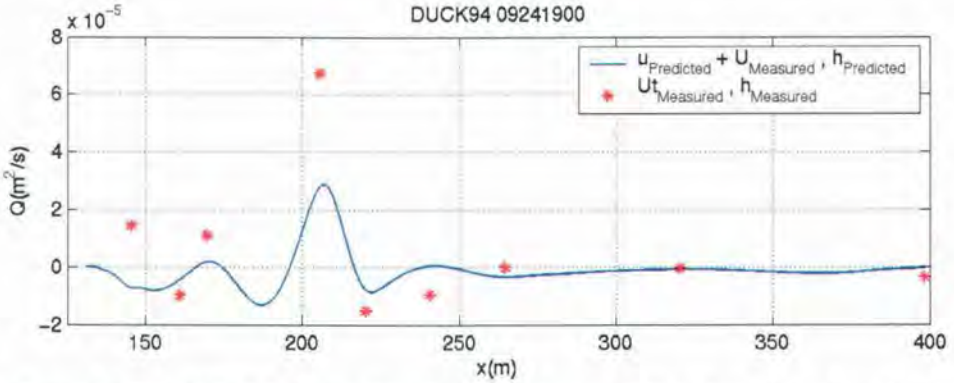

Figure 3.26. DUCK94 September 24th, 19th hour: Bailard-based predicted cross-shore volumetric transport (Q) profile (blue -) as a function of the predicted near bed wave velocity (NPMSE) and measured currents. The predicted transport is being compared to the 'measured' transport (red asterisks), which is computed with Bailard's formulation, using measured velocity time series from the current meters and measured bathymetry.

The model skill values for the predicted profiles (h_{prof}) shown in Figure 3.27 are listed in Table 3.6, along with the skill of the volumetric transport predictions (Q_{hm}). The model series, on average, did exhibit significant skill when predicting the volumetric transport and producing the observed local water depth at the instrument locations. The model skill again mostly declined when predicting the morphological evolution with increasing time into the simulation, but at a much slower rate than seen in the offshore bar movement simulations. This slower decline in the model skill is likely attributable to the milder wave climate, which resulted in slower bathymetric rate of changes, thereby making the simulations more stable.

Table 3.6. DUCK94 September 23rd–27th: Summary of skill (r^2-values) associated with the volumetric transport and bathymetric evolution ($\mathbf{h}_{profile}$) predictions for the profiles shown in Figure 3.27. The predicted transport is compared with the computed transport using measured total velocity and bathymetry ($\mathbf{Q}_{hm}$).

Test Period	Qhm	hprof
9230100	0.33	1.00
9231000	0.93	0.99
9231900	0.86	0.99
9240100	0.77	0.99
9241000	0.97	0.99
9241900	0.80	0.99
9250100	0.97	0.98
9251000	0.97	0.98
9251900	0.97	0.98
9260100	0.94	0.99
9261000	0.88	0.98
9261900	0.88	0.96
9262200	0.87	0.96
Mean	**0.83**	**0.98**
Std. Dev.	**0.16**	**0.01**

The profile slowly evolved in a localized region surrounding the sand bar. The presence of the sand bar generated a hydrodynamic response from the mildly energetic wave climate, thereby generating the onshore transport of the bar. It appears the simulated hydrodynamics by NPMSE, in combination with the measured currents, generated a similar response by the bathymetry, in which onshore sediment transport was predicted. The predicted profiles compare very well with the observations at the instrument locations. The offshore and shoreline profiles were mostly maintained throughout the simulation, which corresponds to the observations. The bar was qualitatively predicted to move onshore, but the resulting profile is unnatural, and not supported by observations of bar shapes in the field. The trough predicted shorewards of the sand bar is exaggerated compared to typical field observations, but no bathymetry of velocity data is available in this region to improve the model predictions. The overall model series average skill was 0.98, with a standard deviation of 0.01, exemplifying the quality of the predictions at the instrument locations for this onshore bar movement study.

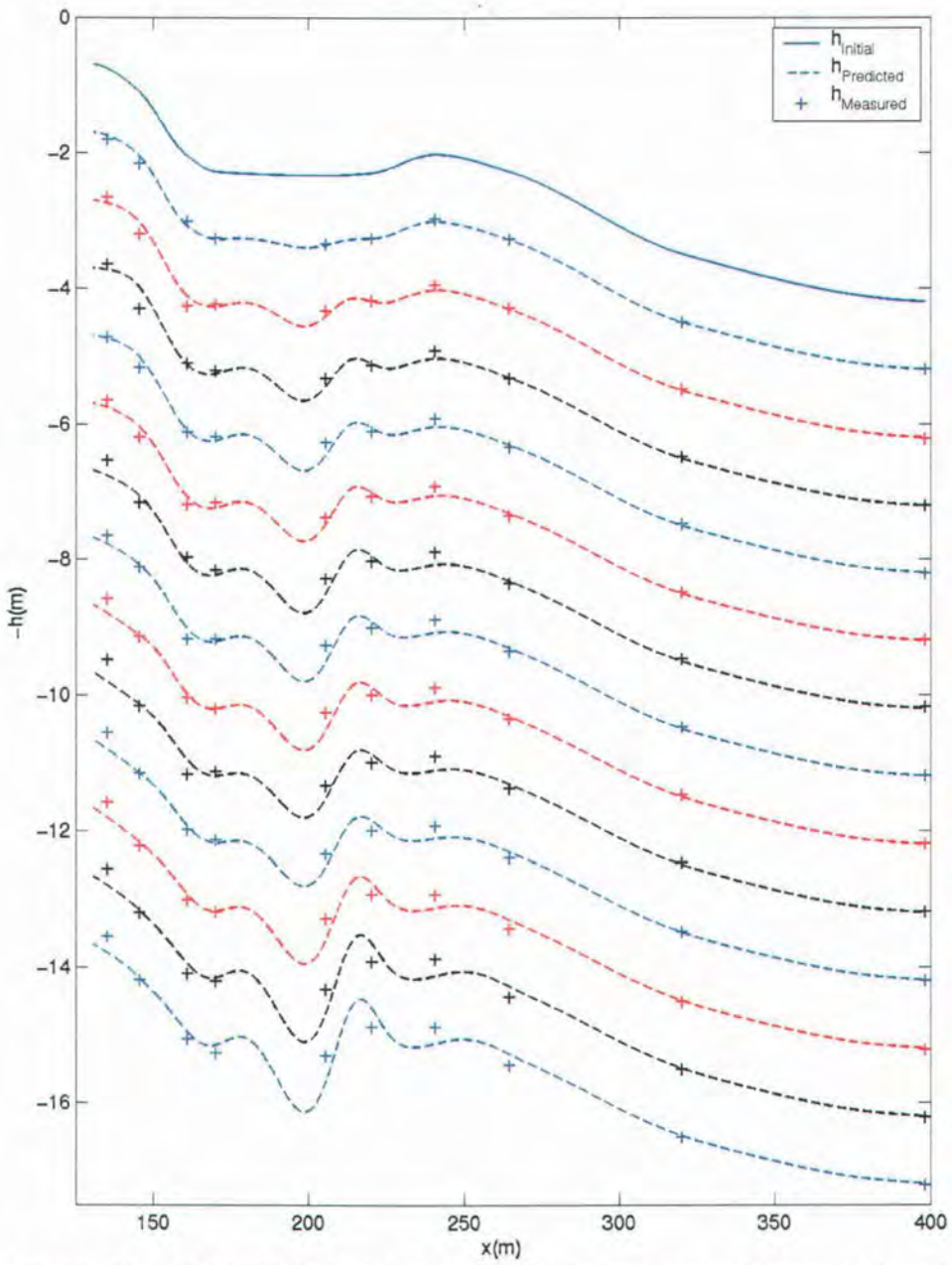

Figure 3.27. DUCK94 September 23rd-27th: Comparisons of measured (+) and predicted (--) bathymetries for the 1st, 10th and 19th hours of Sept. 23rd-26th (top to bottom). The final bathymetry comparison (on the bottom) is for the 22nd hour on the Sept. 26th. The solid line is the initial input measured bathymetry, from the 1st hour on Sept. 23rd, for the 4-day simulation. The total bathymetric predictive skill exhibited by the model series for these particular test hours was (r^2) 0.8342.

A test was performed simulating the onshore bar movement observed between September 23rd and 27th of 1994 at Duck Beach. The test simulation was designed to test the hypothesis that the predicted oscillations of the bathymetry, which tended to grow more unstable with each subsequent test period, are artificial and result from the interpolation routine, 'pchip', utilized consistently throughout this study. A *test model series* was composed NPMSE to predict the wave field, GF2000 to predict the depth-averaged cross-shore return flow, and the Bailard (1981) sediment transport model. Therefore, the contributions by the longshore velocities were taken into consideration by this *test model series*. In the post-processing routine, where Matlab was previously used to smooth and interpolate the predicted bathymetry, the generated bathymetric profiles were smoothed using a 21-point running mean, and the predicted bathymetry of the 10-points adjacent to the onshore/offshore boundaries are retained unprocessed. This particular test case was chosen because onshore bar migration was observed, indicating a weak current system, therefore, the oscillatory wave motions dominated the flow field. As a reminder, one of our main reasons for **not** employing the undertow predictions was the poor quality of the predictions, especially during highly energetic wave conditions. We assumed that during this particular test case, the poor quality undertow predictions would not significantly effect the prediction of the bathymetric evolution because the oscillatory wave motions likely dominated the flow field.

The predicted bathymetries for the 1st, 10th, and 19th hours of each simulated day are compared with the measurements in Figure 3.28. From this visual comparison, it can be seen that the bathymetries are no longer characterized by the unstable oscillations, which were consistently predicted in the previous test cases. Therefore, the interpolation scheme used to generate the smoothed bathymetries in the post-processing routine and to generate the model-input mean current profiles is producing the instabilities observed in the predicted profiles. This finding indicates the need for a new interpolation scheme which does not simply utilize a cubic Hermite interpolant between known locations, as does 'pchip'. Expanding upon this, the new interpolation scheme should have a continuous second derivative. In general, 'pchip' performed well when used to interpolate the bathymetric profile between the instrument locations, but had very negative effects when used to interpolate the mean current profiles.

The interpolated mean current profiles were the most significant contributors to the large oscillations predicted in the bathymetry. A 3rd field model series was previously implemented, which used the wave and sediment transport models consistently utilized by all

the bathymetric evolution studies, but it used the interpolated longshore and cross-shore currents, following the model series described in section 3.4. In the post-processing routine, the bathymetry was smoothed using a running mean, as was done in the *test model series*. The resulting bathymetries were still characterized by the large scale oscillations, implying that the interpolated mean currents were the most significant contributors to the unrealistic bathymetric predictions.

It should be noted that of all the interpolation routines available to us, 'pchip' resulted in the best bathymetric evolution predictions. We tested using a basic linear interpolation routine, a 'splining' routine (which is a cubic spline interpolation scheme that has a continuous second derivative), 'pchip', and multiple combinations of these interpolation routines.

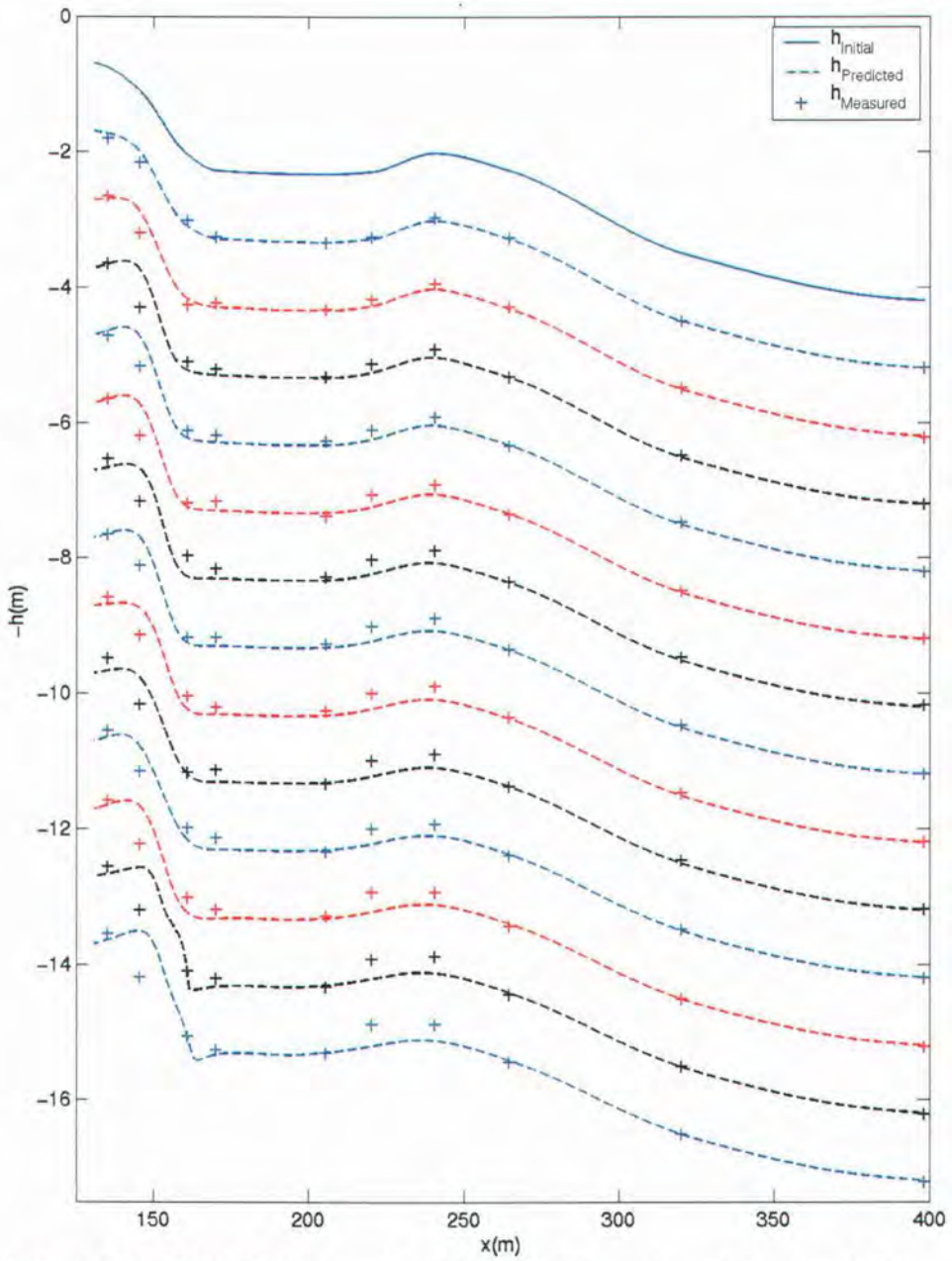

Figure 3.28. DUCK94 September 23rd-27th: Comparisons of measured (+) and predicted (--) bathymetries for the 1st, 10th and 19th hours of Sept. 23rd-26th (top to bottom). This figure follows the same layout of the previous figure. The predicted bathymetries are results of the test model series described above. The total bathymetric predictive skill exhibited by the model series for these particular test hours was (r^2) 0.81.

3.4 Summary of Results

The bar profile predictions of the LIP11D test cases, made by the lab model series, were flattened over the crest. The lab bathymetric simulations also both predicted offshore directed transport of the terrace, which is contrary to the observations. The flattening of the bar crest was found to not be a result of the post-processing smoothing routine performed in Matlab.

We found that the observed large-scale oscillations in the predicted bathymetries were resulting from the interpolation routine, 'pchip', which was used to generate the longshore and cross-shore mean velocity profiles utilized by the field model series. This explained why we did not observe such large scale oscillations in the predicted bathymetries of the LIP11D Test Cases.

In the field morphological evolution study we found that the addition of the longshore velocities improved our predictions. We found through some preliminary simulations that the inclusion of the longshore oscillatory velocities also contributes to the observed sediment transport, likely explaining some of the differences between the measured and predicted bathymetries.

Chapter 4

CONCLUSIONS AND SUGGESTIONS FOR FUTURE WORK

The hydrodynamic testing of the two nonlinear wave models, FUNWAVE and NPMSE, as well as the two empirical models, DB1995 and D2000, provided insight into the strengths and weaknesses of the abilities of the individual models to predict the nonlinear characteristics of the wave field, while propagating through the cross-shore.

For the simulations in this study, the application of the temporal filter every 100 time steps was found to be ideal, for the duration of each test hour/period. Through the hydrodynamic tests in this study, it appears that the results can be fine tuned by changing the slot lengths. This suggests that the slots play a pertinent role in the energy dissipation scheme. The accuracy of the modeled run-up by Boussinesq wave models when employing the slot technique has been shown to have about a 10% error (Madsen *et al.*, 1997). Kennedy *et al* (1999) showed that increasing the slot width resulted in improved hydrodynamic predictions by FUNWAVE for steep beach scenarios, which was found to be true for the LIP11D Test Case 1C and the DUCK94 studies.

A more thorough investigation into the optimization of F, using the predictions of velocity asymmetry and skewness as a gauge, would be very useful to those who are looking to use the predictions to simulate sediment transport. Energetic-type sediment transport models utilize velocity moments to drive the model. These moments are direct functions of velocity skewness, hence, require quality predictions by wave models to potentially make accurate predictions of bathymetric evolution. Bottom boundary layer sediment transport models utilize boundary layer velocities or shear stress, which are both functions of velocity asymmetry and skewness, hence the importance of quality predictions of both nonlinear quantities by the wave models [Trowbridge and Young (1989); Nielsen (2003); Henderson *et al.* (2003)].

In general, the NPMSE dissipation model consistently performed poorly when predicting the evolution of the wave field (primarily the asymmetry of the wave field) within the surfzone. The breaking model of Thornton and Guza (1983) was originally developed to simulate the amount of energy dissipated due to depth-limited wave breaking, therefore, resulting in the wave height decay and potentially breaking-induced longshore current. The evolution of the nonlinear characteristics of the wave field was not intentionally factored into

the wave energy dissipation model, hence the poor quality predictions of wave asymmetry within the surfzone. We are suggesting that a new dissipation model be employed by NPMSE which accounts for the cross-shore evolution of wave skewness and asymmetry.

The bathymetric evolution study was performed to test the ability of a model series to simulate the 1-D evolution of the waves, currents, and subsequent bathymetry in the nearshore system with only knowledge of the initial bathymetry and the periodically updated offshore wave climate. This proved to be a challenge for the field study because the undertow model was incapable of making quality predictions of the cross-shore currents, hence our use of the measured currents. The vertical locations of the predicted and measured velocities used in the lab and field cases were also an issue due to the active debate pertaining to the utilized velocities for sediment transport modeling. Therefore, one potential source of significant error is the vertical location of the velocity predictions for the lab study and utilized total velocity times series (composed of the measured currents and predicted cross-shore wave velocities) for the field study. The Bailard sediment transport model calls for near-bed velocity time series. Recently, in the field of sediment transport modeling, a debate concerning the definition of 'near-bed' velocities has stirred much interest, especially in the context of energetic-type sediment transport models. Historically, 'near-bed' velocities, both time series and time averaged, have been used to predict sediment pick-up, entrainment, transport, and flux in both space and time. One critical issue pertains to the vertical location of the utilized 'near-bed' velocities. Many believe velocity and shear stress from within the bottom boundary layer should be utilized to predict sediment transport (Henderson *et al.*, 2003; Nielsen, 1992, Trowbridge and Madsen, 1984). Others have used velocity time series from outside the bottom boundary layer to successfully predict sediment movement (Gallagher *et al.*, 1998). Still others have used free stream velocity time series in combination with a nonlinear enhancement, such as 'a-spike', to successfully predict cross-shore sand bar movement (Hoefel and Elgar, 2003; Long and Kirby, 2003). Bailard (1981) defined his required near-bed velocities as coming from a vertical location from within the region where the velocity distribution is nearly logarithmic, i.e. the bottom boundary layer. Within the bottom boundary layer, the magnitude and nonlinear characteristics of the velocities change significantly in the vertical. It is also important to understand that the bottom boundary layer is an extremely dynamic region that is small compared to the water column height and it is constantly changing in height as a response to the flow field. All of these factors make it difficult to obtain quality velocity measurements within the bottom boundary layer. With the

improvements to the durability, accuracy and precision of instruments, quality measurements of velocities within this small dynamic region are becoming more readily obtainable and will hopefully lead to advances in the field of sediment transport modeling.

In the field morphological evolution study we found that the addition of the longshore velocities improved our predictions. This is intuitive due to the large magnitudes of the measured longshore currents, which commonly exceed those of the cross-shore currents, and would thereby affect the bathymetry of the domain in question. The simulations of September 1st through the 5th using the approach of Gallagher *et al.* (1998) manifest the importance of the inclusion and prediction of the oscillatory velocities, of which the longshore component was neglected in our model series.

Throughout the bathymetry evolution simulations we utilized the MATLAB routine 'pchip' to interpolate our smoothed, predicted bathymetry (and the measured mean velocity profiles for the field studies) in the processing routine. We hypothesize that this routine, since it uses a series of sinusoidal functions, was a key contributor to the generated oscillations of the bathymetry, which became unstable in the highly energetic offshore bar migration simulations (September 1st-5th, and October 10th–20th). We found that the oscillations were resulting from the interpolation routine, 'pchip', used to generate the longshore and cross-shore mean velocity profiles utilized by the field model series. This explained why we did not observe such large scale oscillations in the predicted bathymetries of the LIP11D Test Cases.

Another explanation for the instability of the bathymetry is the large transport time step utilized in this study. For the lab cases a 1-hour time step was utilized, but for the field cases a 3-hour time step was used. The literature supports using smaller time steps for bathymetric evolution predictions, as done by Long and Kirby (2003), who updated their bathymetry every 0.5s, which was every 5th time step taken by the Boussinesq wave model implemented in their study.

One issue we felt deserved attention was that the efficiency factors have been minimally tested compared to the widespread use of the Bailard sediment transport model. The common values used were tested by Bailard (1981), who found similar results to Bagnold (1966). Thornton *et al.* (1996) again supported the efficiency factor-values proposed by Bailard (1981). These universally applied coefficients were calibrated for two particular field studies, the Nearshore Sediment Transport Study (Torrey Pines, Ca) and DUCK94 (Duck Beach, NC).

In general, there are numerous advances to be made in the field of sediment transport modeling. A more daunting challenge is to develop a model series which can efficiently simulate the nearshore environment with only measurements obtained by offshore recording devices, such as instrumented buoys, or from nearshore image data, such as extracted by Chickadel *et al.* (2003). The future of coastal modeling in the field of engineering is in the development of community models which can provide the flexibility to optimize the computational efficiency and quality of the model predictions required by the application.

REFERENCES

Agnon, Y., P.A. Madsen, and H.A. Schäffer (1999). A new approach to high-order Boussinesq models. *Journal of Fluid Mechanics*, 399, pp. 319-333

Agnon, Y., A. Sheremet, J. Gonsalves, and M. Stiassnie (1993). Nonlinear evolution of a unidirectional shoaling wave field. *Coastal Engineering*, 20, pp. 29-58

Agnon, Y. and A. Sheremet (1997). Stochastic nonlinear shoaling of directional spectra. *Journal of Fluid Mechanics*, 345, pp.79-99

Agnon, Y. and A. Sheremet (2000). Stochastic evolution models for nonlinear gravity waves over uneven topography, In: Lui, P.L.-F. (Editor), Advances in Coastal and Ocean Engineering. World Scientific Publishing Co., Singapore

Arcilla, A.Ś-., J.A. Roelvink, B.A. O'Conner, A. Reniers, and J.A. Jiménez (1994). The Delta Flume'93 Experiment. *Proceedings of the 1st Coastal Dynamics Conference*, pp. 488-502

Bagnold, R.A. (1963). Mechanics of marine sedimentation. *The Sea*, M.N. Hill, ed., Interscience, Vol. 3, pp. 507-528

Bagnold, R.A. (1966). An approach to the sediment transport problem from general physics. *U.S. Geological Survey Prof. Pap. , 422-I*

Bailard, J.A. and D.L. Inman (1981). An energetics bed load model for a plane sloping beach, Part 1: Local transport. *Journal of Geophysical Research*, 86, pp. 2035-2045

Bailard, J.A. (1981). An energetics total load sediment transport model for a plane sloping beach. *Journal of Geophysical Research*, 86, pp. 10,938-10,954

Bailard, J.A. (1982). Modeling on-offshore sediment transport in the surf zone. *Proceedings of the 18th International Conference on Coastal Engineering*, American Society of Civil Engineers, New York, pp. 1419-1438

Bailard, J.A. and D.L. Inman (1981). An energetics bed load sediment transport model for a plane sloping beach: Local transport. *Journal of Geophysical Research*, 86, pp. 2035-2043

Basco, D.R. (1983). Surf zone currents. *Coastal Engineering*, 7, pp. 331-335

Battjes, J.A. and J.P.F.M. Janssen (1978). Energy loss and set-up due to breaking of random waves. *Proceedings of the 16th International Conference on Coastal Engineering,* American Society of Civil Engineers, pp. 569-587

Becq-Girad, F, P. Forget, and M. Benoit (1999). Non-linear propagation of unidirectional wave fields over varying topography. *Coastal Engineering*, 38, pp.91-113

Berkhoff, J.C.W. (1972). Computation of combined refraction-diffraction. *Proceedings 13th International Conference Coastal Engineering*, American Society of Civil Engineers, New

York, pp. 471-490

Booij, N (1981). Gravity waves on water with non-uniform depth and current. *Rep. 81-1*, Department of Civil Engineering, Delft University of Technology, Delft, The Netherlands

Bowen, A.J. (1980). Simple models of nearshore sedimentation: Beach profiles and longshore bars. *The Coastline of Canada*, edited by S.B. McCann, Geological Survey of Canada, Ottawa, pp. 1-11

Bruun, P. (1954). Coast Erosion and the Development of Beach Profiles. U.S. Army Corps of Engineers, Beach Erosion Board, Tech. Memo. No. 44

Bryant, P.J. (1973). Periodic waves in shallow water. *Journal of Fluid Mechanics*, 59, pp.625-644

Bryant, P.J. (1974). Stability of periodic waves in shallow water. *Journal of Fluid Mechanics*, 66, pp. 81-96

Chawla, A, H.T. Özkan-Haller and J.T. Kirby (1998). Spectral model for wave evolution over irregular bathymetry. *Journal of Waterway, Port, Coastal and Ocean Engineering*, 124, pp. 189-198

Chen, Y. and P.L.-F. Lui (1995). Modified Boussinesq equations and associated parabolic models for water wave propagation. *Journal of Fluid Mechanics*, 288, pp. 351-381

Chickadel, C.C., R.A. Holman, and M.H. Freilich(2003). An optical technique for the measurement of longshore currents. *Journal of Geophysical Research*, 108

Church, J.C. and E.B. Thornton (1993). Effects of breaking wave induced turbulence within a longshore current model. *Coastal Engineering*, 20, pp. 1-28

Cox, D.T., H. Kobayashi and H. Mase (1991). Effects of fluid accelerations on sediment transport in surf zones. *Proceedings of Coastal Sediments '91*, American Society of Civil Engineers, pp. 447-461

Cox, D.T. and N. Kobayashi (2000). Identification of intense, intermittent coherent motions under shoaling and breaking waves. *Journal of Geophysical Research*, 105, pp. 14,223-14,236

Dean, R.G. (1977). Equilibrium Beach Profiles: U.S. Atlantic and Gulf Coasts. Department of Civil Engineering, Ocean Engineering Report No. 12, University of Delaware, January

Dean, R.G. and R.A. Dalrymple (1991). Water Wave Mechanics For Engineers and Scientists. World Scientific, Singapore

Dean, R.G. and R.A. Dalrymple (2002). Coastal Processes with Engineering Applications. Cambridge University Press, United Kingdom

Drake, T.G. and J. Calantoni (2001). Discrete particle model for sheet flow sediment

transport in the nearshore. *Journal of Geophysical Research*, 106, pp. 19,859-19,868

Doering, J.C. and A.J. Bowen (1995). Parameterization of orbital velocity asymmetries of shoaling and breaking waves using bispectral analysis. *Coastal Engineering*, 26, pp. 15-33

Doering, J.C., B. Elfrink, D.M. Hanes, and G. Ruessink (2000). Parameterization of velocity skewness under waves and its effects on cross-shore sediment transport. *Coastal Engineering*, ??, pp. 1383-1396

Eldeberky, Y. and J.A. Battjes (1996). Spectral modeling of wave breaking: Application to Boussinesq equations. *Journal of Geophysical Research*, 101, pp.1253-1264

Elgar, S.L. and R.T. Guza (1985). Observations of bispectra of shoaling surface gravity waves. *Journal of Fluid Mechanics*, 161, pp. 425-448

Elgar, S.L., E.L. Gallagher, and R.T. Guza (2001). Nearshore sandbar migration. *Journal of Geophysical Research,* 106, pp. 11,623-11,627

Freilich, M.H. and R.T. Guza (1984). Nonlinear effects on shoaling surface gravity waves. *Philosophical Transactions of the Royal Society of London*, Series A, 311, pp. 1-41

Gallagher, E.L., W. Boyd, S. Elgar, R.T. Guza, and B. Woodward (1996). Performances of a sonar altimeter in the nearshore. *Marine Geology*, 133, pp. 241-248

Gallagher, E.L., S. Elgar, and R.T. Guza (1998). Observations of sand bar evolution on a natural beach. J*ournal of Geophysical Research*, 103, pp. 3203-3215

Garcez Faria, A.F., E.B. Thornton, T.C. Lippmann, and T.P. Stanton (2000). Undertow over a barred beach. *Journal of Geophysical Research, 105, pp. 16999-17010*

Gobbi, M.F. and J.T. Kirby (1999). Wave evolution over submerged sills: Tests of a high-order Boussinesq model. *Coastal Engineering*, 37, pp. 57-96

Gobbi, M.F., J.T. Kirby, and G. Wei (2000). A fully nonlinear Boussinesq model for surface waves. II. Extension to $O(kh^4)$. *Journal of Fluid Mechanics*, 405, pp. 181-210

Grant, W.D. and O.S. Madsen (1979). Combined wave and current interactions with a rough bottom. *Journal of Geophysical Research*, 84, pp. 1797-1808

Guza, R.T. and E.B. Thornton (1980). Local and shoaled comparisons of sea surface elevations, pressures, and velocities. *Journal of Geophysical Research*, 85, pp. 1524-1530

Guza, R.T. and E.B. Thornton (1985). Velocity moments in nearshore. *Journal of Waterway, Port, Coastal, and Ocean Engineering*, 111, pp. 235-256

Hasselmann, K., W. Munk, and G. MacDonald (1963). Bispectra of ocean waves. Time Series Analysis, edited by M. Rosenblatt, Wiley, New York, pp. 125-139

Heitner, K.L. and G.W. Housner (1970). Numerical model for tsunami runup. *Journal of*

Waterway, Port, Coastal and Ocean Engineering, 96, pp. 701-719

Hoefel, F. and S. Elgar (2003). Wave-induced sediment transport and sandbar migration. *Science*, 299, pp. 1885-1887

Holman, R.A. and A.H. Sallenger (1993). Sand bar generation: A discussion of the Duck experiment series. *Journal of Coastal Research*, 15, pp. 76-92

Kaihatu, J.M. (1994). Frequency-domain models for nonlinear finite depth water wave propagation. PhD dissertation in Civil Engineering, University of Delaware

Kaihatu, J.M. and J.T. Kirby (1994). Parabolic and angular spectrum modeling of a fully nonlinear extended Boussinesq Equation. *Proceedings of the International Symposium: Waves-Physical and Numerical Modeling*, pp. 514-523

Kaihatu, J.M. and J.T. Kirby (1995). Nonlinear transformation of waves in finite water depth. *Physics of Fluids*, 7(8), pp. 1903-1914

Kaihatu, J.M, and J.T. Kirby (1998). Two-dimensional parabolic modeling of extended Boussinesq equations. *Journal of Waterway, Port, Coastal and Ocean Engineering*, 124, pp. 57-67

Kaihatu, J.M. (2001). Improvement of parabolic nonlinear fully dispersive wave model. *Journal of Waterway, Port, Coastal, and Ocean Engineering*, March/April, pp. 113-121

Keijzer, M. and V. Babovic (1999). Dimensionally aware genetic programming. *Proceedings of the Genetic and Evolutionary Algorithm Conference*, July 13-17, Orlando, FL, pp.1069-1076

Kennedy, A.B., Q. Chen, J.T. Kirby, and R.A. Dalrymple (2000). Boussinesq modeling of wave transformation, breaking, and runup. I: 1D. *Journal of Waterway, Port, Coastal and Ocean Engineering*, January/February, pp. 39-47

Kirby, J.T. (1986a). Higher-order approximations in the parabolic equation method for water waves. *Journal of Geophysical Research*, 91, pp. 933-952

Kirby, J.T., G. Wei, Q. Chen, A.B. Kennedy, R.A. Dalrymple (1998). FUNWAVE 1.0: Fully Nonlinear Boussinesq Wave Model Documentation and User's Manual. *Research Report* NO. CACR-98-06, Center for Applied Coastal Research, University of Delaware, Newark, DE

Kirby, J.T. (2003). Boussinesq models and applications to nearshore wave propagation, surf zone processes and wave-induced currents. Advances in Coastal Engineering. V.C. Lakhan (ed), Elsevier Oceanography Series, San Francisco, pp. 1-41

Kofoed-Hansen, H. and J.H. Rasmussen (1998). Modelling of nonlinear shoaling based on stochastic evolution equations. *Coastal Engineering*, 33, pp. 203-232

Kraus, N.C., M. Larson, and D. Kriebel (1991). Evaluation of beach erosion and accretion predictors. *Proceedings of Coastal Sediments*, American Society of Civil Engineers, Seattle,

Washington, pp. 572-587

Lee, G. and W.A. Birkemeier (1993). Beach and nearshore survey data: 1985-1991. CERC Field Research Facility, *Tech. Rep.* CERC-93-3, U.S. Army Corp of Engineers, Waterways Exp. Stn., Vicksburg, Mississippi

Lippmann, T.C. and R.A. Holman (1993). Episodic, non-stationary behavior of double bar system at Duck, North Carolina, USA, 1986-1991. *Journal of Coastal Research*, Special Issue No. 15, pp. 49-75

Longuet-Higgins, M. (1953). Mass transport in water waves. *Philosophical Transactions of the Royal Society of London*, A, 245, pp. 535-581

Lozano, C.J. and P.L.-F. Lui (1980). Refraction-diffraction model for linear surface water waves. *Journal of Fluid Mechanics*, 101, pp. 705-720

Madsen, P.A., R. Murray, and O.R. Sorensen (1991). A new form of Boussinesq equations with improved linear dispersion characteristics. Part 1. *Coastal Engineering*, 15, pp.371-388

Madsen, P.A. and H.A. Schäffer (1998). Higher-order Boussinesq-type equations for surface gravity waves: Derivation and analysis. *Philosophical Transactions of the Royal Society of London A*, 356, pp. 3123-3184

Madsen, P.A. and H.A. Schäffer (1999). Review of Boussinesq-type equations for surface gravity waves, In: Liu, P.L.-F. (Editor), Advances in Coastal and Ocean Engineering. World Scientific Publishing Co., Singapore, pp. 1-94

Madsen, P.A. and O.R. Sorensen (1992). A new form of the Boussinesq equations with improved linear dispersion characteristics. Part 2. A slowly varying bathymetry. *Coastal Engineering*, 18, pp. 183-204

Madsen, P.A. and O.R. Sorensen (1993). Bound waves and triad interactions in shallow water. *Ocean Engineering*, 20, pp. 359-388

Madsen, O.R. and W.D. Grant (1976). Quantitative description of sediment transport by waves. *Proceedings of the 15th Coastal Engineering Conference,* American Society of Civil Engineers, New York, pp. 1093-1112

Mase, H. and J.T. Kirby (1992). Hybrid frequency-domain KdV equation for random wave transformation. *Proceedings of the 23rd International Conference on Coastal Engineering*, American Society of Civil Engineers, Venice, Italy, pp.474-487

McCowan, A.D. and D.R. Blackman (1989). *Proceedings of the 9th Australian Conference on Coastal and Ocean Engineering*, pp. 412-416

Mei, C.C. (1983). The Applied Dynamics of Ocean Surface Waves. Wiley, New York

Meyer-Peter, E. and R. Müller (1948). Formulas for bed-load transport. *Prof. 2nd Congress of the International Association of Hydraulic Structures Research*, Stockholm

Mom, Y. and J. Mom (2004). On the degree of orthognality. *Journal of Coastal Imaging Mechanics*, 1, pp. 1

Moore, B.D. (1982). Beach Profile Evolution in Response to Changes in Water Level and Wave Height. MCE Thesis, Department of Civil Engineering, University of Delaware, 164 pp.

Nielsen, P. (1992). Coastal Bottom Boundary Layers and Sediment Transport, World Scientific, River Edge, N.J.

Nielsen, P. (2002). Shear stress and sediment transport calculations for swash zone modeling. *Coastal Engineering*, 45, pp. 255-287

Nielsen, P. and D.P. Callaghan (2003). Shear stress and sediment transport calculations for sheet flow under waves. *Coastal Engineering*, 47, pp. 347-354

Nadaoka, K. and T. Kondoh (1982). Structure of turbulent flow field under breaking waves in surf zone by LDV. *Coastal Engineering of Japan*, 25, pp.125-145

Nwogu, O. (1993). Alternative form of Boussinesq equations for nearshore wave propagation. *Journal of Waterway, Port, Coastal and Ocean Engineering*, American Society of Civil Engineers, 119(6), pp. 618-638

Peregrine, D.H. (1967). Long waves on a beach. *Journal of Fluid Mechanics*, 27, pp.815-827

Phillips, O.M. (1960). On the dynamics of unsteady gravity waves of finite amplitude. *Journal of Fluid Mechanics*, 9, pp. 193-217

Phillips, O.M. (1980). The Dynamics of the Upper Ocean. Cambridge University Press, London

Plant, N.G., K.T. Holland, J.A. Puleo, and E.L. Gallagher (2004). Prediction skill of nearshore profile evolution models. *Journal of Geophysical Research*, 109

Press, W.H., B.P. Flannery, S.A. Teukolsky, and W.T. Vetterling (1992). Numerical Recipes in Fortran (2nd ed.). University Press, Cambridge

Radder, A.C. (1979). On the parabolic equation method for water-wave propagation. *Journal of Fluid Mechanics*, 95, pp. 159-176

Rivero, F.J. and A.S. Arcilla (1995). On the vertical distribution of $\langle \hat{u}\hat{w} \rangle$. *Journal of Coastal Engineering*, 25, pp.137-152

Roelvink, J.A. and A.J.H.M. Reniers (1995). LIP 11D Delta Flume Experiments: A data set for profile model validation. Delft Hydraulics Data Report, H 2130

Roelvink, J.A. and M.J.F. Stive (1989). Bar generating cross shore flow mechanisms on a beach. *J. Geophysical Research*, 94, 4785-4800

Ruessink, B.G., J.R. Miles, F. Feddersen, R.T. Guza, and S. Elgar (2001). Modeling the alongshore current on barred beach. *Journal of Geophysical Research*, 106, pp. 22451-22463

Sancho, F.E., I.A. Svendsen, A.R. Van Dongeren, and U. Petruvu (1995). Longshore nonuniformities of nearshore currents. *Proceedings of Coastal Dynamics '95*, American Society of Civil Engineers, New York, pp. 425-436

Schäffer, H.A. and P.A. Madsen (1995). Further enhancements of Boussinesq-type equations. *Coastal Engineering*, 26, pp.1-14

Shi, F., R.A. Dalrymple, J.T. Kirby, Q. Chen, and A. Kennedy (2001a). A fully nonlinear Boussinesq model in generalized curvilinear coordinates. *Coastal Engineering*, 42, pp. 337-358

Shi, F., R.A. Dalrymple, J.T. Kirby, and Q. Chen (2001b). A curvilinear Boussinesq model and its application. *Proceedings of the 4th International Symposium on Ocean Wave Measurement and Analysis*, Waves'01, American Society of Civil Engineers, pp. 884-853

Smith, R. And T. Sprinks (1975). Scattering of surface waves by a conical island. *Journal of Fluid Mechanics*, Cambridge, U.K., 72, pp. 373-384

Stive, M.J.F. (1986). A model for cross-shore sediment transport. *Proceedings of the 20th Conference on Coastal Engineering*, American Society of Civil Engineers, New York, pp. 1550-1564

Stive, M.J.F. and H.J. De Vriend (1994). Shear stress and mean flow in shoaling and breaking waves. *Proceedings 24th International Coastal Engineering Conference*, American Society of Civil Engineers, New York, pp. 594-608

Stive, M.J.F. and H.G. Wind (1982). A study of radiation stress and set-up in the nearshore region. *Journal of Coastal Engineering*, 6, pp. 1-25

Stive, M.J.F. and H.G. Wind (1986). Cross-shore mean flow in the surf zone. *Journal of Coastal Engineering*, 10, pp. 325-340

Tang, Y. and Y. Ouelette (1997). A new kind of nonlinear mild-slope equation for combined refraction-diffraction of multifrequency waves. *Coastal Engineering*, 31, pp. 3-36

Thornton, E.B. and R.T. Guza (1983). Transformation of wave height distribution. *J. Geophysical Research*, 88, pp. 5925-5938

Thornton, E.B., R.T. Humiston, and W. Birkemeier (1996). Bar-trough generation on a natural beach. *J. Geophysical Research*, 101 pp. 12,097-12,110

Trowbridge, J. and O. Madsen (1984). Turbulent wave boundary layers 2. second-order theory and mass transport. *Journal of Geophysical Research,* 89, pp. 7999-8007

Trowbridge, J. and D. Young (1989). Sand transport by unbroken water waves under sheet

flow conditions. *Journal of Geophysical Research*, 94, pp. 10,971-10,991

Walstra, D.J.R., G.P. Mocke, and F. Smith (1996). Roller contributions as inferred from inverse modeling techniques. *Proceedings 25th International Coastal Engineering Conference*, American Society of Civil Engineers, New York, pp. 1205-1218

Wei, G. and J.T. Kirby (1995). A time-dependant numerical code for extended Boussinesq equations. *Journal of Waterway, Port, Coastal, and Ocean Engineering*, 120, pp.251-261

Wei, G. and J.T. Kirby (1994). A time-dependant numerical code for extended Boussinesq equations. *Research Report* CACR-94-02, Center for Applied Coastal Research, University of Delaware, Newark, DE

Wei, G., J.T. Kirby, S.T. Grilli, and S. Subramanya (1995). A fully nonlinear Boussinesq model for surface waves. *Journal of Fluid Mechanics*, 294, pp. 71-92

Wei, G. and J.T. Kirby (1998). Simulation of water waves by Boussinesq models. *Research Report* CACR-98-02, Center for Applied Coastal Research, University of Delaware, Newark, DE

Zelt, J. (1991). The runup of breaking and non-breaking solitary waves. *Coastal Engineering*, 15, pp. 205-246